ADVANCED MATERIALS
www.advmat.de

Materials as Machines

*Joselle M. McCracken, Brian R. Donovan, and Timothy J. White**

Machines are systems that harness input power to extend or advance function. Fundamentally, machines are based on the integration of materials with mechanisms to accomplish tasks—such as generating motion or lifting an object. An emerging research paradigm is the design, synthesis, and integration of responsive materials within or as machines. Herein, a particular focus is the integration of responsive materials to enable robotic (machine) functions such as gripping, lifting, or motility (walking, crawling, swimming, and flying). Key functional considerations of responsive materials in machine implementations are response time, cyclability (frequency and ruggedness), sizing, payload capacity, amenability to mechanical programming, performance in extreme environments, and autonomy. This review summarizes the material transformation mechanisms, mechanical design, and robotic integration of responsive materials including shape memory alloys (SMAs), piezoelectrics, dielectric elastomer actuators (DEAs), ionic electroactive polymers (IEAPs), pneumatics and hydraulics systems, shape memory polymers (SMPs), hydrogels, and liquid crystalline elastomers (LCEs) and networks (LCNs). Structural and geometrical fabrication of these materials as wires, coils, films, tubes, cones, unimorphs, bimorphs, and printed elements enables differentiated mechanical responses and consistently enables and extends functional use.

1. Introduction

Actuators integrate materials with mechanisms to transduce (convert) energy into motion. Mechanical design principles wellinform approaches that maximize the transduction of energy into force and the efficient conversion of force into motion. End use implementations of actuating systems, for example, in automotive, aerospace, or medical applications, motivate sustained pursuit of performance gains enabled by new mechanical designs, additive manufacturing, or advanced materials.

This review is generally focused on stimuli-responsive materials. The stimuli-response of materials is analogous to a transducing element in that these materials convert input energy into force and in some cases, directly into motion. The profound statement of Bhattacharya and James "the material is the machine"[1] is descriptive to this field of research and is the inspiration for the title of this review. An emerging use of responsive materials as machines is in robotics. The vision, leadership, and research of Bar-Cohen is seminal in both invigorating and focusing current-day research activities to develop responsive materials[2] and implement[3] them as lightweight, dexterous, and gentle (e.g., soft) robotic elements. In this spirit, this review exhaustively details the materials, the nature of their stimuli-response, and discusses considerations for their implementation in robotic systems and subsystems.

Robotics is a well-established but growing field of research. Sustained progress in both performance and functionality continue to be realized in commercial robotic systems largely based on conventional materials and their integration with mechanisms. A recent example is the Atlas robot from Boston Dynamics[4] (**Figure 1**a). The incorporation of stimuli-responsive materials in robotics has largely focused on component-level demonstrations to extend the performance of a subsystem (such as a hand or gripper).

Stimuli-responsive materials, spanning nearly all classes of materials and size scales, are currently subject to widespread examination in corporate, government, and academic research laboratories (Figure 1b–d).[5–7] In some cases, these materials have already found widespread commercial implementation in end use and are comparatively mature. The materials and fundamentals of their responses are summarized in **Figure 2**. Shape memory alloys (SMAs) and ceramic piezoelectric materials are distinctive in that they are hard, stimuli-responsive materials. Deformation of these materials can produce large energy densities due to their inherent stiffness. Electroactive polymers (EAPs) remain a topic of considerable interest, particularly dielectric elastomer actuators (DEAs). Engineered systems are rapidly emerging and enabling performance gains in robotics, largely based on pneumatic or fluidic (such as HASEL[8] actuators) transport processes that localize deformation to generate force or produce motion. Soft materials, such as shape memory polymers (SMPs), hydrogels, and liquid crystalline polymer networks (LCNs) and elastomers (LCEs) may offer distinctive functional performance to robotic systems in allowing local control of deformation without the need for complex interfacing with mechanisms. As will be evident, each of these materials has inherent advantages and performance tradeoffs that must be considered in functional implementations. However, responsive material systems have a common obstacle to widespread use: the performance and

Dr. J. M. McCracken, Dr. B. R. Donovan, Prof. T. J. White
Department of Chemical and Biological Engineering
University of Colorado Boulder
Boulder, CO 80309, USA
E-mail: Timothy.J.White@colorado.edu

The ORCID identification number(s) for the author(s) of this article can be found under https://doi.org/10.1002/adma.201906564.

DOI: 10.1002/adma.201906564

cost of conventional materials and mechanisms. Research and development activities must demonstrate differentiated performance as well as assess potential gains for these materials to truly be considered as technologies in widespread commercial robotic implementations.

This review is scoped to focus on recent advancements in the preparation and mechanical deformation of responsive material systems framed within appropriate historical context. The implications of these materials to machine (robotic) implementations are a continuous thread throughout this contribution. The review is organized by material class and prepared with common subsections describing: (i) the fundamentals of the material and their response, (ii) the transformation mechanism, and (iii) the structural motifs to amplify the stimuli-induced mechanical response common to the particular material system. We conclude with an over-the-horizon outlook of next steps to implement these material machines to enable autonomy in systems that sense, actuate, and compute.

2. Shape Memory Alloys

Metals and metal alloys have enabled robust structural performance as well as functional utility for more than 5000 years. Recent compositional developments as well as processing advances (such as 3D printing) of these materials continue to enable new implementations in aerospace, automotive, architectural, and medical applications.[9–14] This review of responsive material actuators begins with material compositions generally referred to as shape memory alloys (SMAs).[15–18] These materials "memorize" a deformed state and rapidly cycle between shapes when subjected to stimuli.[13,19] A key advance in enabling the widespread implementation of SMAs was the development of equiatomic nickel–titanium (NiTi) alloys, commonly referred to as Nitinol.[20–23] NiTi-based SMA devices are pervasive in end use of these materials due to the rapid transformation with heating, low elastic anisotropy, and high ductility of this composition.[24–27] Other metal alloys exhibit shape memory effects, such as Fe- and Cu-based compositions. These materials are lower cost but are more brittle than Nitinol, limiting performance as well as life cycle in utility.[13,28]

2.1. Materials and Mechanisms of Transformation

SMAs such as NiTi-based alloys have been widely integrated into commercial and industrial end uses, including cardiovascular implants and orthopedic devices, seismic dampening elements in architecture, and morphing wings in aerospace.[12,29–34] In a forward transformation, with cooling, mechanically unloaded SMAs undergo a crystallographic transition from the high-temperature austenite (typically cubic lattices) to the low-temperature twinned martensite structure.[35] Without lattice-distorting force applied, stochastically distributed crystallographically equivalent martensite variants (up to 24 for NiTi-based alloys) develop within the twinned martensite lattice. Accordingly, a fully unloaded SMA does not exhibit significant shape change during a crystallographic phase transformation cycle.[18,29,35]

Joselle M. McCracken received her B.S. degree in chemistry from The College of New Jersey in 2011 before securing a Ph.D. in chemistry at the University of Illinois Urbana-Champaign in 2017 under the advisement of Prof. Ralph G. Nuzzo. Subsequently, she joined the Air Force Research Laboratory as a postdoctoral associate. In March of 2019, she joined the Department of Chemical and Biological Engineering at the University of Colorado Boulder (CU Boulder) as a Senior Research Associate under the advisement of Prof. Timothy J. White. Her research interests include additive manufacturing, tissue engineering, and material actuators.

Brian R. Donovan received his B.S. in chemistry from Canisius College in 2011 before completing a Ph.D. in polymer science and engineering at the University of Southern Mississippi in 2016 with Prof. Derek L. Patton. After graduation, he secured an NRC post-doctoral fellowship at the Air Force Research Laboratory with Dr. Timothy J. White. Subsequently, he worked as a Senior Research Associate in the Department of Chemical and Biological Engineering at CU Boulder. He is currently a Research Chemist at Carbon 3D. His research interests include photopolymerization, photochromics, and liquid crystal elastomers.

Timothy J. White was appointed as the inaugural Gallogly Professor of Engineering at the University of Colorado Boulder in July of 2018. He secured a Ph.D. in chemical and biochemical engineering in 2006 from the University of Iowa. Thereafter, he served for nearly 10 years as a Federal employee at the Air Force Research Laboratory as Technology Advisor of the Photonic Materials Branch. At CU Boulder, he leads the "Responsive and Programmable Materials" Group.

Shape change (one-way shape memory effect, OWSME) of SMAs can occur when these materials are subject to sufficient mechanical load in the low temperature, twinned martensitic

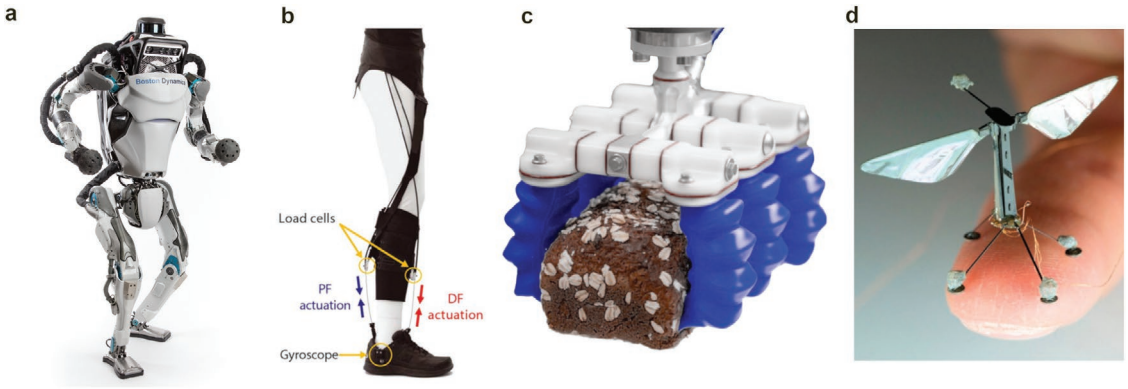

Figure 1. Materials as machines. a) The Atlas robot from Boston Dynamics, Inc. Reproduced with permission.[4] Copyright 2019, Boston Dynamics. b) An exoskeleton can assist motion and enable rehabilitation. Reproduced with permission.[6] Copyright 2017, AAAS. c) The MGrip robot: a soft, pneumatic robotic gripper for delicate object manipulation. Reproduced with permission.[7] Copyright 2019, Soft Robotics Inc. d) The Robo Bee X-Wing is powered by solar energy and based on the response of piezoelectric materials sustain untethered flight. Reproduced with permission.[5] Copyright 2018, IOP Publishing.

phase to reorient the phase variants. The deformation and reorientation of the structure enables the realization of macroscopic shape change through shear lattice distortion.[35] After this detwinning stress is applied, reheating the martensitic structure into the austenite phase results in full shape recovery and the characteristic shape memory cycle of SMAs. During the phase transformation, the austenite-start (A_s) temperature demarcates the beginning of this phase transformation, at which point the SMA begins to recover its lattice structure and shape. Once the material reaches the austenite-finish temperature (A_f), the phase transformation (and mechanical response) is complete.[13,36,37]

Numerous actuation conditions founded on this transformation mechanism have been explored. The martensite-austenite transformation occurs in SMAs even when subject to considerable load, enabling these materials to generate high energy density as actuators. Another mode of actuation utilizes the pseudoelasticity of certain SMAs, in which a very high mechanical load is applied to an austenite lattice structure that is sufficient to deform the SMA into a detwinned martensite lattice without any temperature change. The SMA will spontaneously fully recover its shape as soon as the load is removed.[13,29,38] The OWSME pathway can also be biased to realize a two-way shape memory effect (TWSME) in which the SMA cycles between programmed shapes at both high and low temperatures. This pathway typically requires "training" of the SMA (thermomechanical cycling until the hysteretic response of the material is minimized).[35] Each of the above phase transformation cycles has enabled the development of differentiated material actuators that, when mechanized with geometric motifs, can enable material machines.

2.2. Structural Motifs Enabling Function

The mechanical output of SMAs has already found widespread implementation in end use. SMAs show particular promise as material actuators and have also been examined in robotics.[36] We conclude this discussion of SMAs by describing recent, geometry-dependent (wire, torsional, and film) implementations of SMAs in functional uses in robotics and related technologies.

2.2.1. Wires

SMAs in a wire geometry are particularly suited for tensile actuation due to their comparatively higher efficiency (by weight) and uniformity of generated stress over the cross-sectional area of the device. Numerous wire-based actuators have been described.[36,39–42] For example, Allen et al. employ a Nitinol wire embedded with a polycaprolactone (PCL) rod, both of which are encapsulated in a silicone rubber to form a composite actuator (**Figure 3**a).[43] The PCL is also thermally responsive. Upon heating, the Nitinol wire within the composite actuator transforms between one of three complex states: 1) martensite Nitinol, solid PCL, 2) martensite Nitinol, liquid PCL, or 3) austenite Nitinol, liquid PCL. The temperature dependence of the mechanics of these materials can regulate deformation (Figure 3b). The composite actuator prepared from these materials is shown to emulate finger-like dexterity, realizing six different temperature-governed curvature configurations when subject to 20 N tendon force. Wire SMA actuators have also been utilized to prepare adaptive fabrics. In a recent example, Cherif and co-workers prepare a friction spun hybrid yarn containing SMAs that are integrated into plain, twill, and satin reinforcement fabrics.[44] Similarly, Kang et al. employs an SMA-driven actuator bridge that interfaces with a shape memory polymer to manipulate the fabric curvature over a temperature sweep.[45]

Another implementation of SMA wires as functional material actuators is illustrated in Figure 3c–e. In this example, Majidi and co-workers embed a U-shaped Nitinol wire in a thermally conductive silicone rubber.[46,47] The material composite inherently maintains a strain mismatch between the elastomeric layers (which have been stretched to various extents) that couples with the rigidity differences that exist between the martensite and austenite lattice structures of the SMA wires. This composite system has improved thermal conductivity that enables comparatively fast actuation of the SMA wires (≈3 s transitions) with reduced driving voltage (7.4 V). The authors employ these composite material actuators in robotic implementations including a quadruped, caterpillar, and rolling robot (Figure 3d) that can realize motility (Figure 3e). Ge and co-workers similarly detail the preparation and function of SMA wire actuator composites to fabricate a robotic gripper.[48] These authors prepare slender,

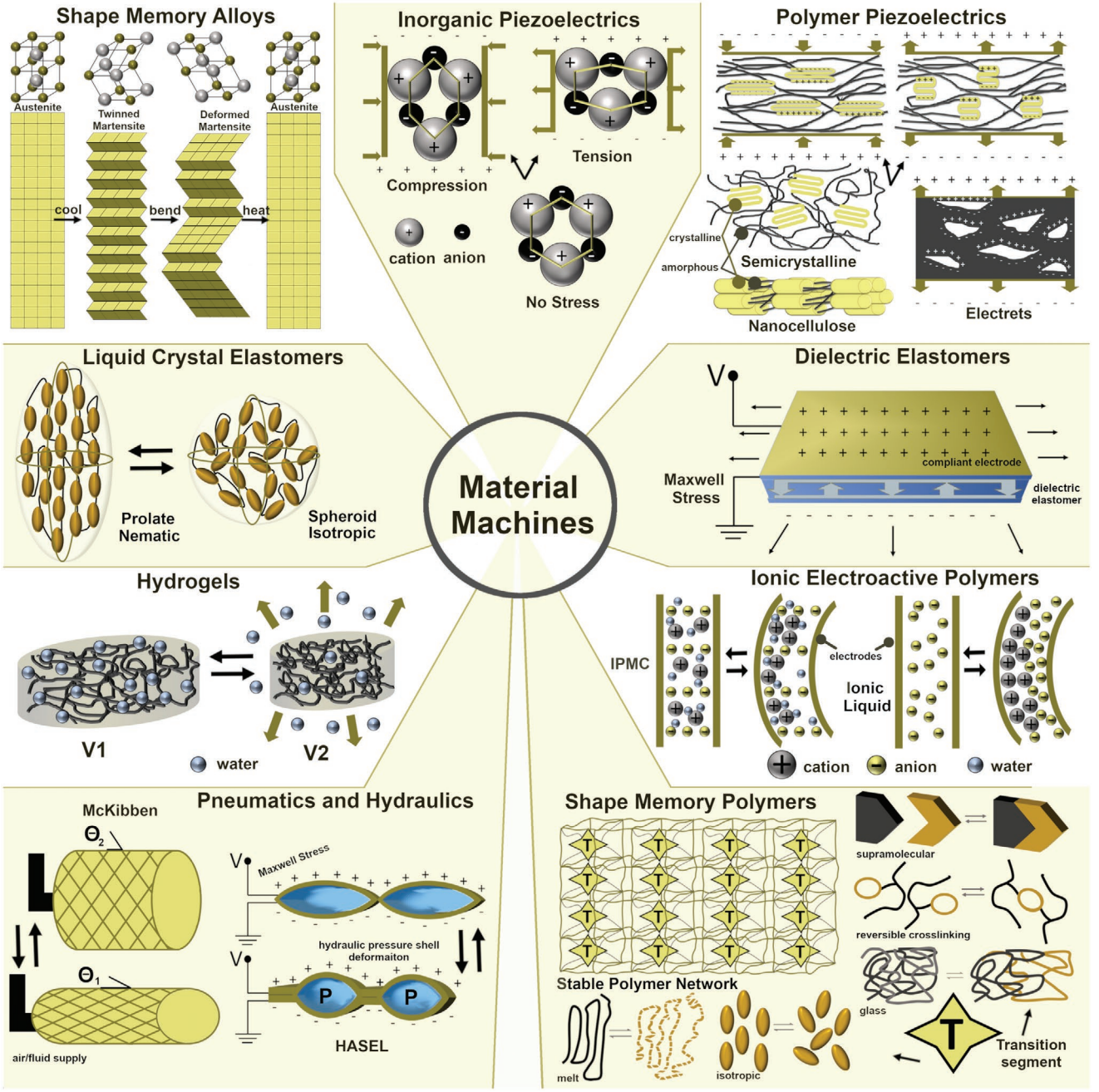

Figure 2. Stimuli-responsive materials: (clockwise from upper left) shape memory alloys (SMAs), inorganic and polymeric piezoelectrics, dielectric elastomer actuators (DEAs), ionic electroactive polymers (IEAPs), shape memory polymers (SMPs), pneumatics and hydraulics, hydrogels, and liquid crystalline elastomers (LCEs). Image for Shape Memory Alloys: Adapted with permission.[594] Copyright 2016, Elsevier. Image for Inorganic Piezoelectrics: Adapted with permission.[593] Copyright 2019, Elsevier. Semicrystalline & electrets image subsets for Polymer Piezoelectrics: Adapted under the terms of the CC-BY Creative Commons Attribution License (http://creativecommons.org/licenses/by/4.0/).[77] Copyright 2018, The Authors, published by MDPI. Nanocellulose image subset for Polymer Piezoelectrics: Adapted with permission.[96] Copyright 2018, The Authors, published by InTech Open. Image for Ionic Electroactive Polymers: Adapted with permission.[217] Copyright 2018, Springer Nature. Image for Shape Memory Polymers: Adapted with permission.[369] Copyright 2013, Elsevier. Image for HASEL image subset for Pneumatics and Hydraulics: Adapted with permission.[8] Copyright 2018, AAAS. Image for McKibben image subset for Pneumatics and Hydraulics: Adapted with permission.[311] Copyright 2018, Taylor & Francis.

bending actuators by 3D printing SMA wires (Figure 3f, left). Subsequently, these elements are embedded between a rigid layer and a soft-matrix layer. The material system is able to realize dexterous motion including twisting, bending, and extension. The concerted effort of multiple finger-like modalities is shown to perform lift-release cycles of 15 g every 15 s (Figure 3f, right).

2.2.2. Twisted Configurations

Twisted SMA geometries (such as coils and springs) can realize comparatively larger strokes than straight wires, enabling differentiated performance in robotics.[36] Twisted SMA configurations (wire coils) have been used by Uchikoba and

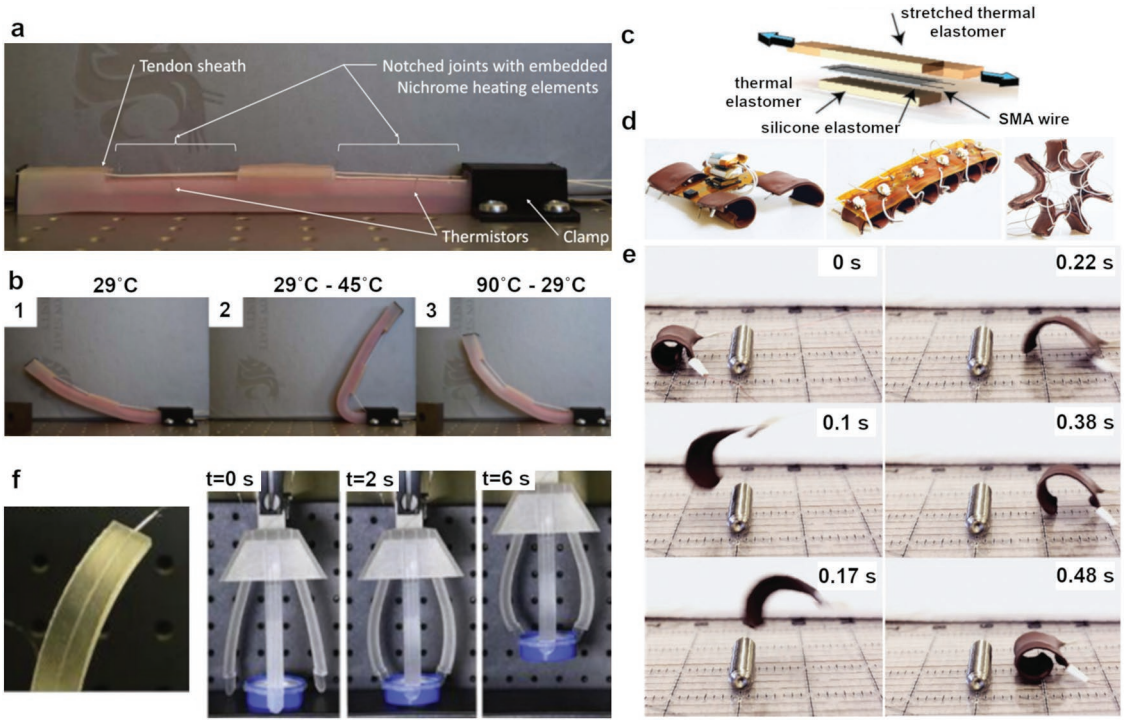

Figure 3. Shape memory alloy (SMA) wire actuators. a,b) The deformation of Nitinol (NiTi) wire embedded into a polycaprolactone (PCL) rod is controlled by temperature. Reproduced with permission.[43] Copyright 2019, IOP Publishing. c) A U-shaped NiTi wire enables motility in d) quadruped (left), caterpillar (center), and rolling (right). Dynamic motion of the robotic element is shown in (e). c–e) Reproduced with permission.[46] Copyright 2019, Wiley-VCH. f) A 3D printed element is prepared from SMA wires. This gripper performs lift-release cycles of 15 g every 15 s. Reproduced with permission.[48] Copyright 2019, Elsevier.

co-workers to control a quadruped MEMS microrobot with four-independent leg locomotors.[49] Meanwhile, the caterpillar-inspired GoQBot achieves near-ballistic motion through SMA coils positioned along its ventral features.[50] Antagonistic torsion springs capable of bidirectional actuation and hollow tube actuators with curved SMA wires have been demonstrated to access torsional modes of motion.[51,52]

Other approaches include origami-inspired designs that integrate twisted SMA actuators. In one instance, Savi and co-workers develop an origami wheel powered by a trained SMA spring coil in a bias system against an elastic spring (**Figure 4**a, left).[53] These authors demonstrate a device that utilizes the martensite-austenite transition of an SMA spring to drive a transformation away from a neutral configuration (P_0) to a compacted configuration when heated (P_1) and a second expanded configuration (P_2) dictated by an orthogonal elastic spring at lower temperatures (Figure 4a, right). Origami-based structures have also been developed that emulate the peristaltic motion of worms in robots prepared from SMA coils (Figure 4b)[54] as well as in active biomedical stents.[55]

Synthetic and natural fabrics have been integrated with SMA structures in other robotic implementations. Park et al. prepare shape memory alloy fabric muscle (SFM) that augments and assist human motion.[56] These actuators are inexpensive, light, flexible, and soft, and are composed of SMA spring bundles fabricated from NiTi wire covered with a soft, light fabric sheath. By incorporating these elements with a wire position encoder in the fabric, the SFMs are shown to lift 2–4 kg barbells to target positions with response times of 1 s or less. Twisted nylon is another synthetic fabric that has been reported by Yin et al. as a responsive material actuation with considerable mechanical performance.[57] These twisted structures are capable of large deformation and power density and are further enhanced by integration of a coiled SMA.

SMA coils have also been examined to enable gripping. Laschi, Trimmer and co-workers have reported on an SMA coil-based robotic arm that mimics the motion of octopus tentacles and functions underwater (Figure 4c).[58–60] SMA coils have also been recently embedded in soft silicone robotic arms functionalized with Hall sensors that provide feedback for self-regulation of deformation and motion.[61] Paik and co-workers describe a device based on SMA coils integrated into an origami-inspired suction gripper composed of silicone, glass fiber, and PET sublayers (Figure 4d).[62] Multiple shape transformation modes (Mode 1–3 in Figure 4d) are realized including the gripping and lifting of flat, cylindrical, triangular, and spherical shaped objects. This device is yet another example of the function that SMA springs can contribute to robotic systems.

2.2.3. Thin Film Structures

Geometric implementations of thin SMA layers have also been employed in robotic applications. Generally, these engineered devices are composite bimorphs based on solid SMA films with localization of other material compositions to adjust or extend mechanical response.[63] These elements can be prepared to achieve comparatively complex geometries that respond dynamically to temperature gradients. In a demonstration by Knick et al.,

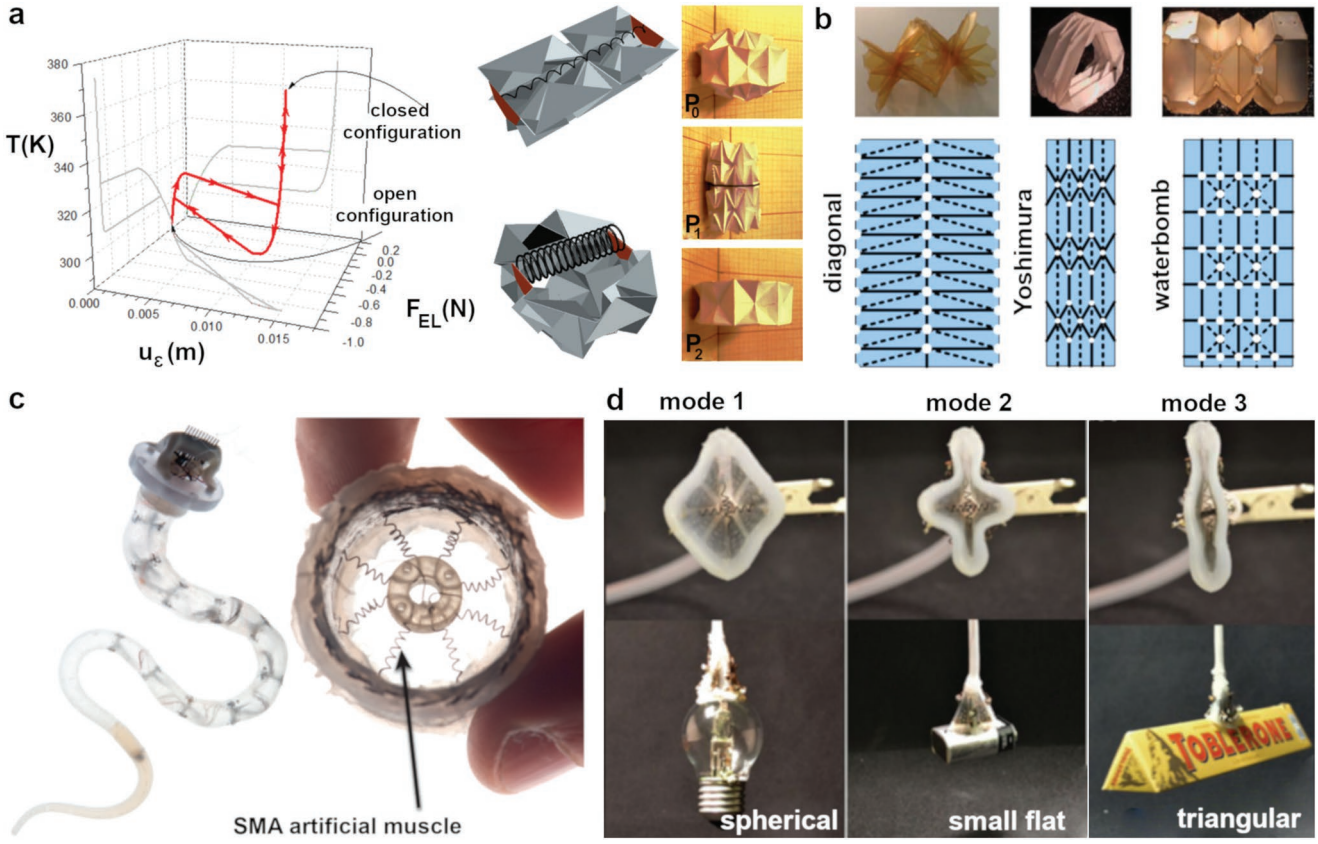

Figure 4. Shape memory alloys (SMAs) in twisted configurations. a) An origami wheel powered by SMA spring coils cycles between open and closed configurations. Reproduced with permission.[53] Copyright 2019, Elsevier. b) The peristaltic motion of worms is replicated with origami-inspired design, powered by SMA spring coils. Reproduced with permission.[54] Copyright 2013, IEEE. c) An aquatic robotic arm based on SMA coil mimics the motion of octopus tentacles. Reproduced with permission.[60] Copyright 2013, Elsevier B.V. d) A suction gripper is prepared from SMA to pick up objects of different geometries. Reproduced with permission.[62] Copyright 2018, IEEE.

a Nitinol film on a Pt-coated silicon wafer is patterned with the photoresist SU8 (AZ 5214e) and dry-etched to release micromachined cantilevers. Upon heating, the bimorphs differentially deflect (**Figure 5**a), and the radius of curvature of the deformed object can be directly correlated to the difference in thermal expansion of the layers. Electrothermal deformation was triggered by heating with applied voltage as low as 0.5 V.[64] Knick et al. have also described a method through which bimorph actuators (Figure 5b) can realize complex deformations in local curvature by spatially patterning the photoresist (SU8) on a Nitinol substrate. The deformation of these structures can occur in under 3 ms when exposed to 14 W cm^{-2} of 532 nm irradiation.[65] Microscale muscles have been prepared by Lee et al. from microscale diamond-shaped frames with focused ion beam (FIB) milling of SMA NiTi wire (Figure 5c–e).[66] Shape transformation of these material systems, again when triggered by a laser, can realize actuation frequencies of 1600 Hz. Curvature control within these microscale devices has also be implemented by Gill et al. for use as grippers in robotic systems.[67]

3. Piezoelectric Ceramics, Polymers, and Composites

Piezoelectric materials release electric charge when subject to mechanical stress. A number of material classes can exhibit piezoelectricity including natural materials, synthetic ceramics, and polymers. Piezoelectricity can occur in crystalline (e.g., quartz), polycrystalline (e.g., $BaTiO_3$), semicrystalline (e.g., polyvinylidene fluoride, PVDF), and even amorphous materials (e.g., electrets). A notable subset of piezoelectric materials are ferroelectric compositions, which are materials that switch different states of electrical polarization based on externally applied electric fields.[68] Ferroelectric ceramics, such as PZT and $BaTiO_3$, are heavily implemented in end-use applications in optics[69–71] and as actuators.[72] Commonly, piezoelectric polymers are loaded with conductive fillers such as graphene, CNTs, and carbon black, as well as other materials such as nanoclay, DNA, and rare-earth salts to improve piezoelectric performance while retaining processability.[73] The high bandwidth, large power density, and amenability to microscaling of piezoelectric materials of all classes are particularly suitable for the preparation of actuators. Accordingly, piezoelectric materials have been widely examined and integrated in robotics.[73]

3.1. Piezoelectrics: Materials, and Mechanisms of Transformation

The mechanism of stimuli-induced deformation of piezoelectric materials is dependent on the class of matter. Generally

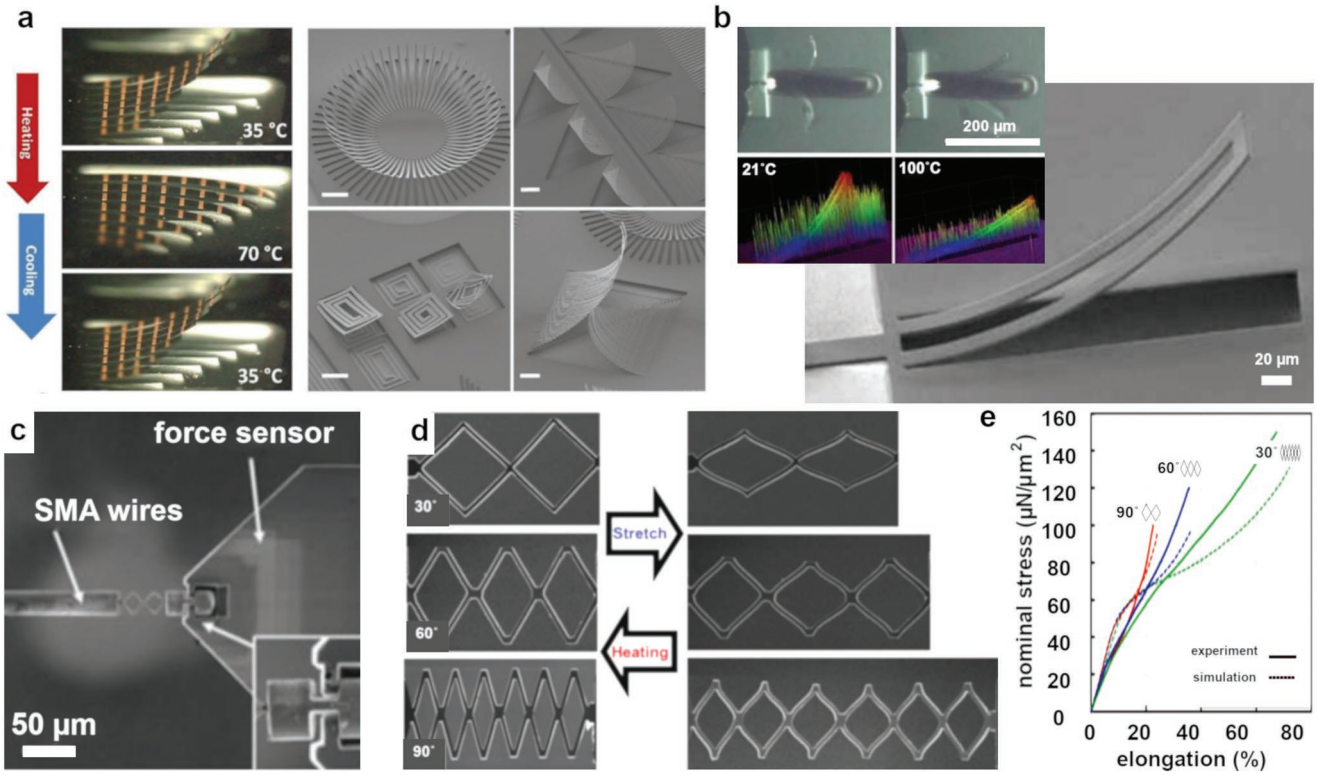

Figure 5. Shape memory alloy (SMA) films and patterned elements. a) Micromachined Nitinol-coated (NiTi) Platinum cantilever arrays actuate in response to thermal stimulus due to the difference in thermal expansion of the metallic layers. Reproduced with permission.[64] Copyright 2019, Elsevier. b) NiTi thin films locally coated with SU8. The composite system responds to low power laser heating due to differences in thermal expansion coefficients. Reproduced with permission.[65] Copyright 2019, IOP Publishing. c) NiTi wires are fabricated using focused ion beam (FIB) milling into geometries that d) deform to different lengths upon stretching and return to their initial lengths with heating back into the austenite lattice structure. e) Stress–elongation curves of these elements as a function of pattern. Reproduced with permission.[66] Copyright 2018, Wiley-VCH.

speaking, piezoelectric actuation in ceramics and composites based on them is associated with the generation of tensile or compressive stress that distorts the distribution of charged atoms within the structure of the material. The heterogeneous charge distribution produces linear mechanical stress at low electrical fields but can become nonlinear when piezoelectric materials are subject to strong electric fields. Threshold fields for nonlinear performance depend on numerous factors[74] but are typically less than 200 V. Current research of piezoelectric materials maintain focus on increasing the piezoelectric charge coefficient (d) as a route to enhance electrical and mechanical performance in devices. This value quantifies the energy conversion efficiency and is the ratio between electric charge generated per unit area and an applied force, described by the equation:

$$d = k\sqrt{\varepsilon_0 k^{\mathrm{T}} s^{\mathrm{E}}} \tag{1}$$

where ε_0 is the permittivity of free space, k is the electromechanical coupling coefficient, k^{T} is the relative dielectric constant when all stresses on the material are constant or not present, and s^{E} is the compliance of the material measured with a closed circuit. The piezoelectric charge coefficient d_{33} is measured when stress or piezoelectrically induced strain is parallel to the piezoelectric poling axis and the electrodes are orthogonally positioned to the poling axis. Piezoelectric ceramics typically have high d_{33} values but the stiffness of these materials limit deformation. Conversely, piezoelectric polymers are comparatively flexible but have order of magnitude lower d_{33} values.[75] For example, a PZT ceramic has a measured d_{33} of 360 $\mathrm{pCN^{-1}}$ as compared to a d_{33} of 33 $\mathrm{pCN^{-1}}$ for a PVDF polymer film under the same conditions. The PZT ceramic, on the other hand, has an elastic modulus of 6.3×10^4 MPa while the PVDF has an elastic modulus of 2×10^3 MPa.[76] Polymer matrix composites of piezoelectric ceramics can retain the high charge coefficient from the ceramic constituents within compliant matrices to blend the responses and enable flexible or wearable devices.[73,77] Suitable polymer matrices for piezoelectric composites require chemical stability, low stiffness, and low acoustic impedance (e.g., soft PZT has a high value of ≈30 MRayl acoustic impedance that originates from the elastic modulus and material density, while PVDF has an acoustic density of ≈3 MRayl).[78,79] Common matrices are poly(dimethylsiloxane) (PDMS), SU8, or poly(vinyl chloride) (PVC).

The piezoelectric response of purely polymeric compositions is the result of molecular-scale transformations. Piezoelectric function in both amorphous and semicrystalline polymeric materials is predicated upon the presence of permanent dipoles. The piezoelectric response in these materials can be strongly affected by how well the molecular dipoles are able to reorient, align, and then maintain their dipole alignment when subject to electrical stimuli. The magnitude of the strain

generated is correlated to composition as well as network structure (crosslinking) of the material.[80] Piezoelectricity in semicrystalline polymers can be enhanced by processing, for example by mechanical alignment of otherwise randomly oriented crystalline regions within the bulk amorphous network[77] or by electric poling.[81]

One of the most common piezoelectric polymers is the ferroelectric semicrystalline polymer, PVDF, and copolymers derived from it. PVDF is known to take on at least four different crystalline forms: α, β, γ, δ. Of these variants, the α phase is the most common but the polar β phase structure exhibits the strongest piezoelectric effect due to the optimal alignment of hydrogen and fluorine atoms along the polymer backbone. Techniques such as phase inversion have been applied to prepare thicker PVDF films that retain the β phase, in which a viscous PVDF solution is immersed in a nonsolvent, causing precipitation of the active polymer phase, but low film reproducibility has been reported.[82,83] Others have reported the inclusion of insulative filler (e.g., MgO) to improve β phase content in PVDF.[84–86] Copolymers, such as PVDF-TrFE (poly vinylidene fluoride trifluoroethylene), have been developed to circumvent limitations associated with PVDF preparation. For example, melt processing of PVDF-TrFE is now accepted as a facile approach to realize good piezoelectric performance while avoiding the mechanical stretching required to prepare piezoelectric PVDF. This is because steric-driven effects lead to the spontaneous crystallization of the active polar β phase in the TrFE copolymer.[87] Still, PVDF-TrFE is outperformed by PVDF, and efforts to incorporate ZnO nanoinclusions have improved the copolymer's d_{33} from 12 to 31 pCN^{-1}, but only at low applied electric field frequencies.[88] Other semicrystalline polymers have also been explored as piezoelectrics, including polyamides,[80,89] liquid crystalline polymers,[90–93] and polyureas,[80,94] each with their own processing, mechanical, and performance trade-offs.

Nanocellulose films are also semicrystalline piezoelectric materials.[95,96] The monoclinic crystal structure of these materials has a natural dipole orientation similar to semicrystalline polymeric piezoelectrics.[77,97] Structurally, nanocellulose piezoelectrics consist of cellulose fiber crystalline domains amidst amorphous (lignin and hemicellulose) regions. Materials processing, for example wet drawing, enables the mechanical alignment of the crystalline domains within the pressed wood fibers and improves the electromechanical output of these materials. The processability of these materials can also tailor other properties such as hydrophilicity, permeability, reactivity, and pulp type composition.[77] Nanocellulose-based piezoelectrics are lightweight, natural, low-cost, respond to low actuation voltages (0.25 V μm^{-1}),[98,99] and can use less power than other piezoelectric polymers.[77]

Fully amorphous polymers do not have an equilibrium polarization state. However, the polarization of these materials can be aligned by poling with mechanical, electrical, or thermal stimuli.[73,77,80] Two common amorphous and piezoelectric polymers are polyimide and polyvinylidene chloride. These materials become piezoelectric when poled near the glass transition temperature (T_g). Generally, the magnitude of the piezoelectric response within these and other amorphous polymeric materials are lower than the other material classes described hereto. Another approach to introduce piezoelectricity to amorphous polymeric materials is to prepare voided charge polymers (VCPs). A common VCP is polypropylene (PP). Gas voids within the polymer network develop space-charge electrets in which there are two near-surface, opposite polarity charge layers in piezoelectric materials (with noncentrosymmetric trapping sites in pyroelectric materials). These materials maintain higher piezoelectric coefficients compared to other polymers but tend to have low Young's moduli that contribute to low coupling coefficients (k values). Processing of these materials, for example by gas injection, can generate microscale, nanoscale, or picoscale voids to further enhance their piezoelectric properties.[77]

3.2. Piezoelectrics: Structural Motifs Enabling Function

The stimuli-response of piezoelectric materials often requires geometric motifs to amplify or extend the deformation of these materials to produced desired outcomes in actuation or robotics. Most simply, piezoelectric materials are sandwiched between electrodes that can either apply voltage across the piezoelectric (inverse piezoelectric effect) or can transmit the voltage supplied by the piezoelectric through the circuit when the material experiences an external stress (direct piezoelectric effect). For inorganic piezoelectric materials, common geometries to enable complex or high performance function include unimorphs, bimorphs, tubes, nanowire (NW) arrays, and simple discs.[100] Multilayer stacking of piezoelectric materials can reduce operating voltage, minimize power consumption, and in some cases enhance stroke length.[101]

3.2.1. Bimorphs and Unimorphs

Robotic designs must balance and optimize the relative economy of scale, mass, and cost. Although more costly and larger, the implementation of actuating elements with multiple piezoelectric actuation enables complex deformation and motion. Robotic systems have extensively integrated piezoelectric materials in unimorphs (one active layer per actuation center) and bimorphs (two active layers per actuation center).

Unimorphs are a common approach to producing piezoelectric actuators. As early as 2001, unimorph piezoelectric actuators enabled insect-like flapping.[102] A notable recent implementation is a legged piezoelectric miniature robot (LPMR) based on active unimorphs that senses vibration mode disparities of the piezoelectric actuators at different driving frequencies to control motion and speed (**Figure 6**a).[103] The kinematic model for a similar piezoelectric miniature robot made from PZT mounted to an elastic beam has been analytically described, extending fundamental understanding and enabling prediction of motility.[104] One such walking robot based on piezoelectric actuation has been demonstrated by Peng et al. by employing second order out-of-plane flexural vibration modes to propel the system at variable and controllable velocities (Figure 6b,c).[105] Other resonant ambulatory microrobots have reported maximum forward velocities of 520 mm s^{-1} at 350 Hz.[106] The leg vibrations that yield bounding gait locomotion modes for piezo unimorph actuators result from the application of alternating

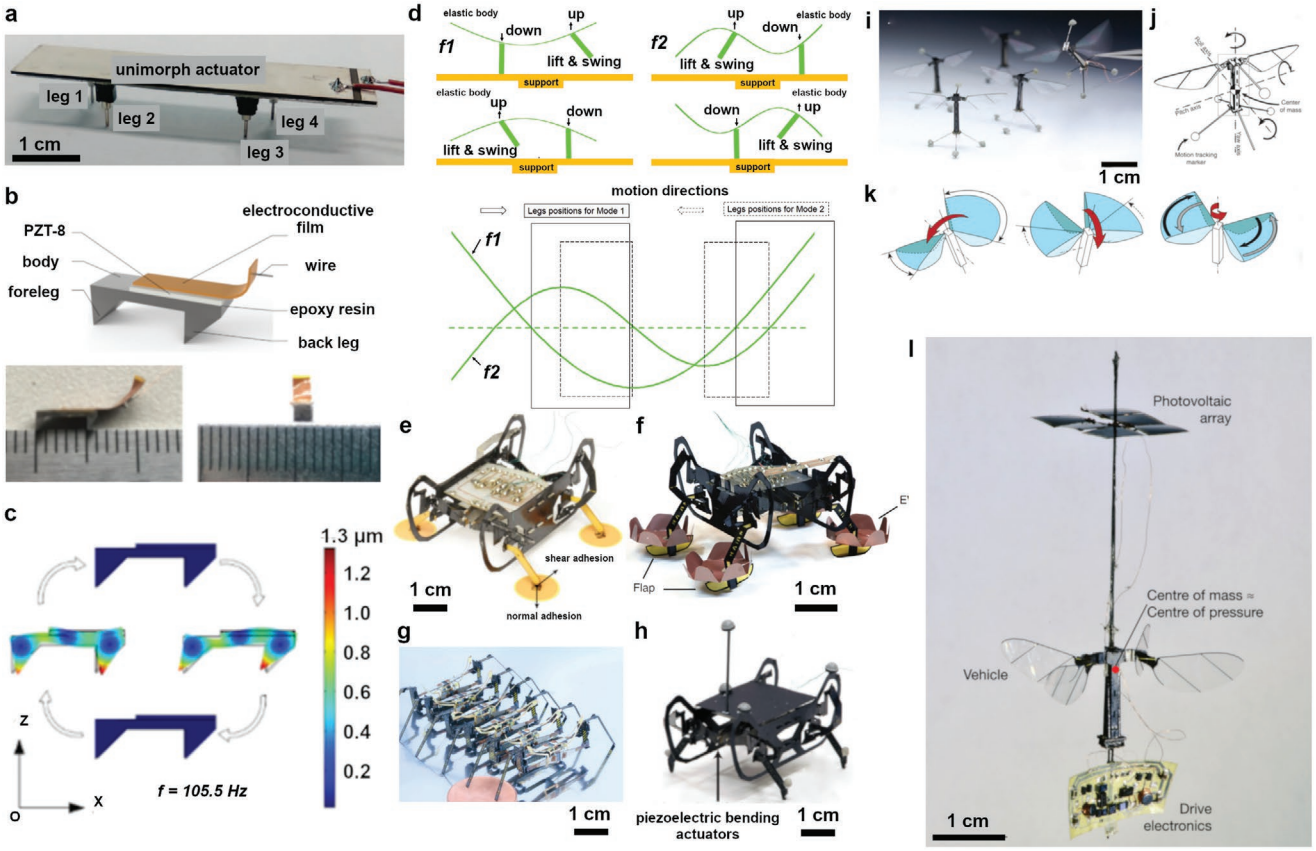

Figure 6. Unimorph and bimorph implementations of piezoelectric materials in robotics. a) A unimorph legged piezoelectric miniature robot (LPMR) microactuator that utilizes a single piezoelectric and steers by exploiting vibration mode disparities. Adapted with permission.[103] Copyright 2017, IEEE. b) A lightweight surface milli-walker based on piezoelectric actuation uses second order out-of-plane flexural vibration modes to propel the 135 mg walker up to 200 mm s^{-1}. c) Displacement per cycle is modeled with finite element modeling (FEM) for the milliwalker. b,c) Reproduced with permission.[103] Copyright 2019, IEEE. d) Motion modes f1 and f2 for an LPMR piezo unimorph actuator. Reproduced with permission.[103] Copyright 2016, IEEE. e) An 8 degree-of-freedom climbing quadrupedal robot locomotes with piezoelectric bending bimorph actuators. Reproduced with permission.[103] Copyright 2018, The Authors, published by AAAS. f) The Harvard Ambulatory Micro-Robot (HAMR) is a high-speed quadrupedal microrobot. Reproduced under the terms of the CC-BY Creative Commons Attribution License (http://creativecommons.org/licenses/by/4.0/).[103] Copyright 2018, The Authors, published by Springer Nature. g) A piezoelectric centipede-inspired segmented microrobot ambulator. Reproduced with permission.[103] Copyright 2011, AAAS. h) A proprioceptive high-speed quadrupedal locomotor robot. Reproduced with permission.[103] Copyright 2019, IOP Publishing. i,j) A microrobotic fly based on flapping wing flight is shown schematically. k) Roll torque (left), pitch torque (center), and yaw torques (right) are generated by different wing thrust forces. i–k) Reproduced with permission.[103] Copyright 2013, AAAS. l) Untethered flight of a microscale aerial vehicle, the RoboBee X-Wing, facilitated by a microphotovoltaic array. Reproduced with permission.[103] Copyright 2019, Springer Nature.

sinusoidal voltage and were described in the context of an LPMR by Hariri et al. in 2016 (Figure 6d).[122] A four-bar mechanism was later integrated with the unimorph form factor by Dharmawan et al. that facilitates locomotion with payload transport.[108]

Bimorph actuators are commonly used in microscale machines as well as robotic systems.[109–118] These elements are particularly advantageous due to their amenability to electronic integration. Bimorph actuators can function independently and do not require other mechanical components, which can also reduce weight penalties. As an example, an articulated finger driven by three discrete single-mode piezoelectric actuators bridged by two interconnecting elements has been prepared by Chen et al. within a compact structure by eliminating design challenges associated with coincidence of modal frequencies.[119] Bimorph elements have also been employed in robotics to generate complex and diverse modes of locomotion. Wood and co-workers commonly utilize bimorph piezoelectric elements to realize complex motion, including flight (linear, bending, rotary).[120] Demonstrations include climbing microrobots (Figure 6e),[121] microaerial vehicles, high speed microrobots such as the Harvard Ambulatory MicroRobot (HAMR-VP) (Figure 6f),[122] insect robots[123] such as the centipede-inspired robot in Figure 6g,[124] proprioceptive, high speed quadrupedal robots (Figure 6h),[125] and mini resonant ambulatory robots.[106,118,126,127] The piezoelectric actuators in the HAMR, the centipede, and the RoboBee (Figure 6i–k) are composite laminates of two piezoelectric ceramic layers (PZT-5H) with nickel electrodes bonded to a central conductive carbon fiber layer tipped with aluminum.[5,123] The RoboBee X-Wing (Figure 1d) utilizes PZT actuators with an alumina bridge along with a photovoltaic array to achieve untethered flight at insect-size scales with a flapping wing mechanism (Figure 6l).[128]

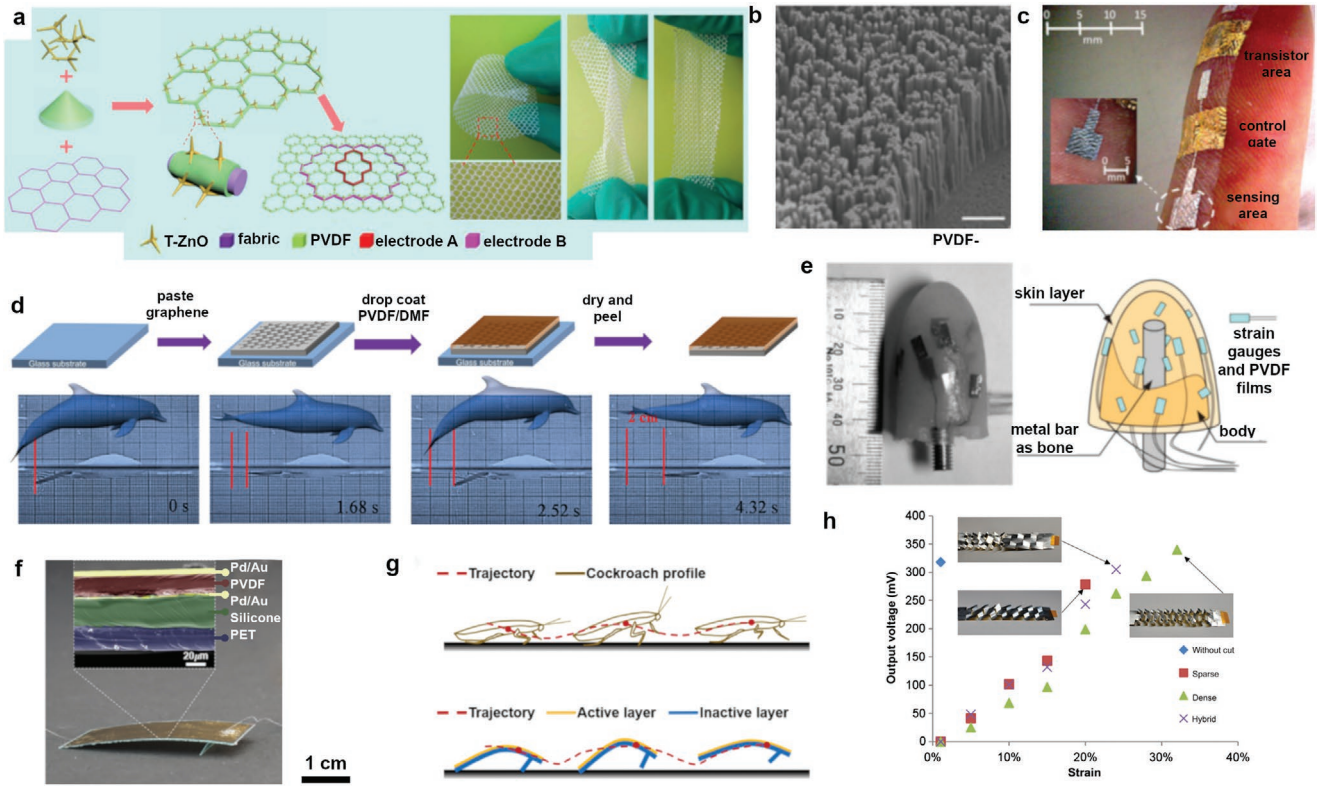

Figure 7. Nanowire arrays and piezoelectric films for actuators and robotics-integrated sensors. a) Poly(vinylidene fluoride) (PVDF)/T-ZnO Electronic E-skin. Adapted with permission.[136] Copyright 2017, Elsevier. b) PVDF-TrFE templated into nanofiber arrays. Reproduced with permission.[138] Copyright 2015, RSC. c) Ultrathin, flexible sensors use organic field-effect transistors (OCMFETs) and commercial PVDF piezoelectric films for temperature sensing on skin. Reproduced under the terms of the CC-BY Creative Commons Attribution License (http://creativecommons.org/licenses/by/4.0/).[139] Copyright 2018, The Authors, published by Springer Nature. d) A PVDF/DMF drop-coated graphene film integrated into a fish-like robot that propels locomotion of 5 mm s^{-1}. Reproduced under the terms of the CC-BY Creative Commons Attribution License (http://creativecommons.org/licenses/by/4.0/).[140] Copyright 2016, The Authors, published by Wiley-VCH. e) An artificial fingertip integrates a series of spatially and depth-distributed PVDF films and strain gauges. Reproduced with permission.[143] Copyright 2006, Elsevier. f) Cockroach locomotion mimicked with a Pd/Au electrode sandwiched with a piezoelectric. Adapted with permission.[146] Copyright 2019, The Authors, published by AAAS. g) These function as actuators that use a large vibration amplitude and a bouncing gait mechanism to achieve wavelike locomotion near their resonant frequency. Applied voltages of only 8 V are required. Reproduced with permission.[146] Copyright 2019, The Authors, published by AAAS. h) Kirigami PVDF outputs voltage variably with strain depending on configuration. Reproduced with permission.[148] Copyright 2018, APS.

3.2.2. Nanowire Arrays

Arrays of piezoelectric nanowires enable information feedback loops as sensing elements. Most commonly, nanowire arrays are prepared from piezoelectric polymer composites to assimilate the high performance of ceramic piezoelectrics with the toughness and flexibility of polymers to enable the ruggedness needed for sensing and wearables applications. Four sensing mechanisms—piezoelectric, piezoresistive, piezocapacitive, and triboelectric—are commonly used and are described in detail in a review of tactile sensors.[75] For piezoelectric sensors in particular, nanowire (NW) arrays are a recurrent motif that achieves high-impact performance. They have been prepared by Ha et al. utilizing ZnO NWs dip-coated and annealed onto metal-coated PDMS micropillars,[129] as PMMA-supported ZnO NWs layered with an ITO electrode by Pan et al.,[130] and as $BaTiO_3$ NWs distributed within a PVDF-TrFE piezoelectric polymer on a PET electrode substrate by Jeong et al..[131] Other sensing platforms have been demonstrated using micropatterned PVDF-TrFEs[132,133] as well as with perovskite ($PbTiO_3$, PTO) nanotube matrices coating titanium fibers[134] and piezoelectric nanofiber mats sandwiched between PDMS/Au electrodes.[135] A unique extrapolation of the coated pillar array motif is one described by He et al. that structures the pillars laterally into a macroporous, flexible piezoelectric composite "e-skin." E-skin is based on PVDF in conjunction with (tetrapod) T-ZnO nanostructures and PET fabric to prepare a flexible composite capable of tactile-perception and even gas-sensing. The composites can adhere to skin and remain attached during complex motion (**Figure 7**a).[136] Similar to NW arrays, active nanofibers can also be integrated into PVDF systems. Graphene oxide nanofibers interlaced with PVDF nanofibers that are sandwiched between PDMS/Cu electrodes have been reported by Lou et al.[137] PVDF-TrFE itself is also amenable to templating into nanofiber arrays that do not require further loading with inorganic piezoceramic domains or NW arrays (Figure 7b).[138]

3.2.3. Films

A number of notable recent examples detail the incorporation of film-based piezoelectric sensing elements into robotics

applications. For example, Cosseddu and co-workers describe film-based structural motifs to prepare ultrathin, flexible sensors that combine charge-modulated field-effect transistors (OCMFETs) with commercial films of PVDF for temperature sensing on skin (Figure 7c).[139] Previously, Chen and co-workers reported preparing a graphene film drop-coated with PVDF/DMF solution to prepare flexible piezoelectric composite sensors capable of 14 mm deformation and that generate stresses above 312 MPa g^{-1}. When integrated into a fish-like robot, the PVDF piezoelectric actuators are capable of propelling locomotion of 5 mm s^{-1} (Figure 7d).[140] Nanocellulose piezoelectric films also show promise as actuators. Zheng et al. prepared actuators from porous, flexible nanofibril cellulose sheets in a PDMS aerogel.[141] Additionally, film-based electret piezoelectric polymers have been prepared that are composed of polytetrafluoroethylene (PTFE) and fluorinated ethylene propylene (FEP). When heat-pressed into cellular structures, these materials become corona charged and also realize piezoelectric activity.[142]

Piezoelectric films are integrated into robotic devices to perform crucial roles in feedback and sensing. In 2006, Asada and co-workers describe an artificial fingertip capable of distinguishing multiple material types by combining an artificial skin layer, structural support, and an embedded series of depth-distributed PVDF films and strain gauges (Figure 7e).[143] In another instance, Tian reported the integration of PVDF films into a multilayer sensor in which the piezoelectric active layer facilitates the smart-manipulation of different object types when mounted into a traditional hard-robotics gripping chassis.[144] In 2018, Yen and Guo reported a PVDF sensor that is applied to an oscillating robotic fish to monitor pressure fluctuations as it locomotes.[145] Soft robotics with complex motion profiles utilizing PVDF/Silicone multilayers have also recently been demonstrated by Wu et al.[146] In these robots, Pd/Au electrodes sandwich the piezoelectric PVDF film that is then mounted to a silicone/PET bilayer in order to mimic cockroach locomotion (Figure 7f). The actuators use large vibration amplitude and a bouncing gait mechanism to achieve wavelike locomotion near their resonant frequency, but only consist of soft and compliant materials to do so (Figure 7g). Stimuli-response of this material system only require an 8 V supply. PVDF-based films integrated into mechanical designs structures have also been demonstrated in functional and robotics applications, including flapping wings of an origami butterfly (Ahmed an co-workers),[147] catapulting weights (Ahmed and co-workers),[147] and stretchable Kirigami elements (Figure 7h) (Hu and co-workers).[148]

4. Dielectric Elastomers

Electroactive polymers (EAPs) are responsive materials of considerable relevance to emerging end use in actuating systems and robotic devices. EAPs are divided into two subclassifications: electronic EAPs and ionic EAPs.[149] By far the most common and widely used EAP are dielectric elastomer actuators (DEAs). DEAs are elastomeric materials that have been conditioned to be electrically active.[150–152] A seminal contribution, from Pelrine et al. at the Stanford Research Institute, demonstrated that applied voltages to conventional, commercially available materials (such as 3M VHB 4910) can electrically generate strains as large as 380%.[153] DEAs are sensitized to electric stimuli in two ways: i) by surface coating ionic charges or ii) by deposition of compliant electrodes that sandwich the elastomeric film.[150] The latter geometry can be modeled as a compliant variable capacitor if the electrodes are more flexible than the elastomeric material.[150,154,155] DEAs are lightweight and soft materials capable of large deformations as well as high specific elastic energy density and fast response.[150,156]

4.1. DEAs: Materials and Mechanisms of Transformation

Electronic EAPs are particularly appealing for integration in actuating systems and robotics due to the similarity of the mechanical properties of these materials to natural muscles as well as the nascent benefits of reconfiguration by electrical field.[150] The stimuli-induced mechanical response of DEAs is caused by the application of DC field across the material system. The actuating material system is simply a compliant capacitor. The surfaces of the DEA (either charged surfaces or coated with compliant electrodes) attract to each other upon application of an electric field. This attraction subjects the elastomeric material to Maxwell stress resulting in tensile strain (e.g., a reduction in the material thickness). The elastomeric nature of the DEA (an incompressible solid) dictates concurrent lateral expansion of the film in orthogonal vectors to the field application.[150,156] The mechanical response of DEAs is commonly referred to as electrostriction. Applied voltages are large (kV range). Equations (2) and (3) define the electromechanical output of DEAs to applied field and material properties:

$$\sigma_{\mathrm{M}} = \varepsilon_0 \varepsilon \frac{V^2}{z^2} \tag{2}$$

$$u = \varepsilon_0 \varepsilon \frac{V^2}{E z^2} \tag{3}$$

where σ_{M} is the Maxwell stress, u is the strain, ε_0 is the permittivity of free space, ε is the dielectric constant of the material, E is the Young's modulus, V is the applied voltage, and z is the material thickness. Informed by these relations, considerable research continues to develop and characterize the electromechanical response of new material systems focused on reducing the voltage requirements by increasing the dielectric constant of the material system concurrently to decreasing the modulus, reducing the material thickness, and improving electrode robustness.

A critical design consideration of DEAs is the compliance of the electrode layers. Carbon grease, graphite, and carbon powder, among others,[157] are commonly utilized as electrodes for DEAs. Carbon grease is simple and cost-effective but is not robust. Solids such as graphite and carbon powder are comparatively robust but are prone to lose electrical contact with the DEA films at higher operating temperatures.[150] Encapsulation of carbon grease electrodes has been described by La and Lau as a method to improve the contact and thermal stability of carbon grease electrodes.[158] Optically transparent electrodes have also been a topic of interest, most notably the use of ionogels.[159–161]

Another consideration with DEAs is the dielectric breakdown of the materials. Due to the high voltages associated with their operation, risk of dielectric breakdown of DEAs is not

inconsiderable in these devices. Stark-Garton theory describes how a polymer at elevated temperature may mechanically collapse under electrical stress, and is particularly relevant to predict the critical dielectric strength required of a DEA.[162] Effects such as thermal runaway, electronic avalanche, and increased leakage current have been used to describe the failure modes possible with these devices.[158,163,164] To counteract this, prestretch of DEAs has been widely used to increase the dielectric strength of these soft actuators. For instance, a standard DEA—the commercial acrylic foam tape VHB 4905—has a dielectric strength go from 34 MV m^{-1} without strain up to ≈400 MV m^{-1} after stretching that is attributed to suppression of air voids and reduced electromechanical instability.[165] Immersion in dielectric silicone oil is another strategy shown by La and Lau to increase the breakdown of VHB tape from 11 up to 18 kV.[165] Accounting for mechanisms of failure due to dielectric breakdown are particularly important when designing DEA geometries and selecting materials for them.

The polymer network and associated material properties of the elastomeric compositions to form DEAs differentiate the mechanical response. From Equations (2) and (3), the dielectric constant is a critical material parameter. The Young's modulus of the elastomer is also an important consideration, particularly relating to the electrically generated strain. Not surprisingly, numerous material systems have been examined in implementations as DEAs, including polyurethanes (PUs), acrylics, and silicones.[166] Each of these material chemistries offers relative advantages and disadvantages. For example, the seminal report of Pelrine et al. was based on acrylic DEA matrices.[153] However, subsequent study has shown that viscoelastic nonlinearities in acrylic material compositions can affect their overall performance and repeatability in DEA implementers.[167,168] Further, acrylics are not as thermally robust as silicones.[169] Conversely, acrylics are mechanically robust and can withstand elongations of more than 800%, with commercial materials available (such as 3M VHB 4910 and other compositions).

PUs generally produce larger force outputs due to the comparative increase in dielectric constant in these material systems. However, PU-based DEAs generate less strain.[150] Compositional development and advances continue to improve DEA performance. For example, Jomaa et al. describe how the microphase separation that is predominant in PUs can be exploited to improve electrostriction by adjusting the electrical properties of the hard and soft domains (which have different dielectric constants).[170] In other words, the phase separation of the two domain types in PUs leads to heterogeneities of both elastic and dielectric constants which contribute to the performance of the DEA.

Silicone-based DEAs are also common. Silicone-based DEAs comparatively exhibit strain values that exceed PUs but are less than acrylates (largely due to the smaller dielectric constant for silicones). Detailed characterization of DEAs prepared from a series of silicones with different cross-linking hardeners with equivalent dielectric constants has detailed that maximum strain (deformation) for a given field strength was increased at lower crosslink densities. However, the reduction in crosslinking introduced a commensurate decrease in the threshold for dielectric breakdown.[156]

One approach to concurrently maintain optimal material properties and enhance electric field susceptibility is by preparing composites. Examples include the preparation of PU composites with carbon black or other conductive fillers that increase the dielectric constant in comparison to pure PU and make them well suited for low frequency electric field actuation (e.g., 0.1 Hz).[170–172] A three-phase PU-based composition, combining graphene sheets and polyaniline powder within the PU, was recently reported as an approach to realize comparative increases in electrostriction,[173] Silicone composites with titanium oxide can be prepared to reduce the modulus while increasing the dielectric constant.[174] Fiber reinforced silicones have recently been described with enhanced dielectric properties,[175] and core–shell calcium copper titanate nanoparticles have been incorporated in silicon composites and shown to contribute to a 10% increase in strain at lower field strengths.[176]

4.2. DEAs: Structural Motifs Enabling Function

DEAs have been incorporated into robotics as actuating systems, including as grippers, flexible gear motors, a spring roll walking robot, miniaturized pumps, and even parts of arms that have participated in arm wrestling competitions.[177] The use of DEAs in robotics has been recently reviewed.[150] DEAs have been implemented in planar conformations such as extenders and diaphragms as well as in multilayers, cylindrical and pyramidal rolls and tubes, and hybrids of these mechanical conformations.[150] Other approaches use origami principles to fold DEA sheets to achieve complex function.

4.2.1. Plates and Membranes

DEA membranes (and stacks of them) are widely applied in robotics and actuator systems. Evident in **Figure 8**a,b, a stack of commercial silicone-based DEA plates developed by Jung et al. realizes a worm-like motility with three degrees of motion.[178] Another multistack quadruped robot developed by Nguyen et al. uses DEA stacks in each leg to undertake locomotion.[179] Others have prepared related devices.[180] 3D printed stacks of DEAs from silicone-base dielectric layers and ionic hydrogel electrodes have also shown promise for use in self-sensing or multifunctional devices.[181]

Frame-mounted DEA membranes and membrane stacks are geometries often explored as actuator types due to their conferral of prestrain into the materials. Evident in Figure 8c, Rothemund et al. have reported the use of commercial DEAs integrated with stretchable, transparent ionic conductors based on polyacrylamide hydrogel with NaCl electrolyte for noise cancellation devices (Figure 8d).[160] This work is an extension from the fabrication of a transparent speaker (from DEA by Keplinger et al.).[161] Maeda and co-workers described a balloon acrylic DEA that functions as a speaker as well.[182] Another example of a frame-mounted disc-shape DEA robot was one developed by Qin et al. by mounting the DEA into the center of a wheel that interacts and guides electro-adhesion actuators around its perimeter.[183] These enable the robot to move

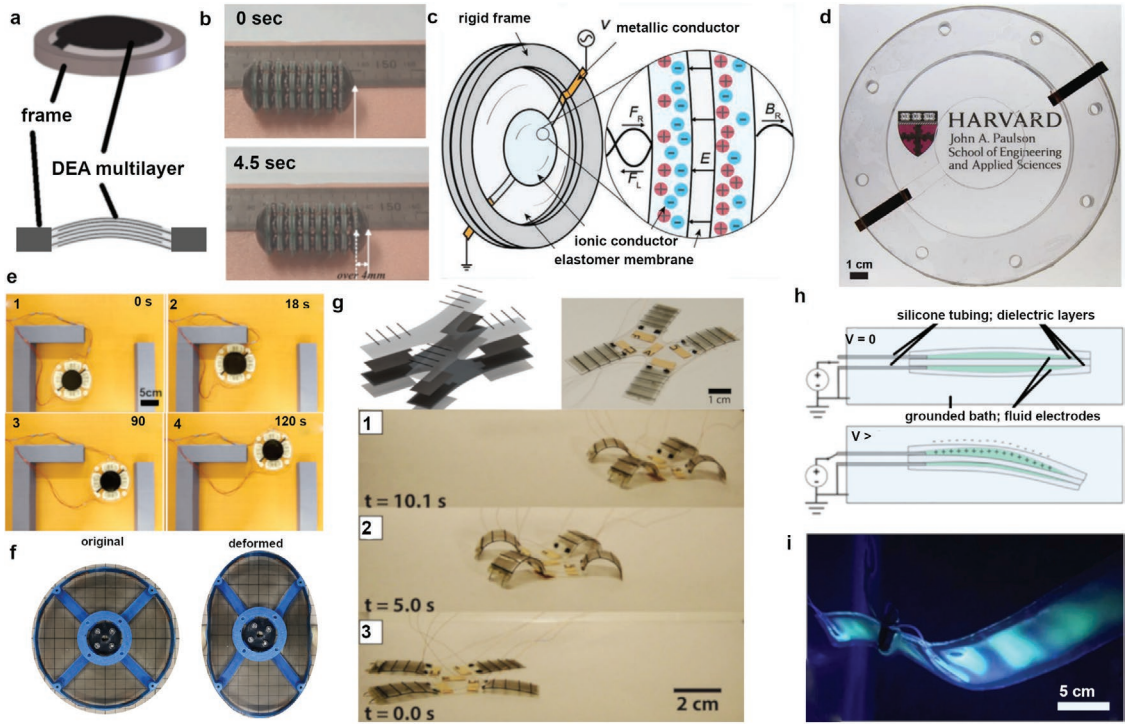

Figure 8. Dielectric elastomer actuators (DEAs) plate and membrane elements. a) A multilayer DEA membrane is embedded in a frame. b) Stacks of DEA multilayers combine into an annelid-mimetic locomotor. Reproduced under the terms of the CC-BY Creative Commons Attribution License (http://creativecommons.org/licenses/by/4.0/).[178] Copyright 2007, The Authors, published by Europe PMC. c) A rigid frame around a transparent DEA membrane with a transparent compliant ionic conductor electrode produces a d) fully transparent noise cancellation membrane. c,d) Reproduced with permission.[160] Copyright 2018, Wiley-VCH. e) A soft frame-mounted DEA actuator disc is used to locally manipulate adhesion to move around obstacles. Reproduced with permission.[183] Copyright 2018, IOP Publishing. f) A deformable DEA motor. Reproduced under the terms of the CC-BY Creative Commons Attribution License (http://creativecommons.org/licenses/by/4.0/).[185] Copyright 2019, SPIE. g) Locomoting multilayer DEA soft actuators without the need for prestretch and rigid frames. Reproduced with permission.[192] Copyright 2017, IEEE. h) A translucent, DEA trilayer stack forms two internal fluid-electrode chambers resulting in a i) transparent, fluorescent aquatic DEA swimming actuator. h,i) Reproduced with permission.[193] Copyright 2018, The Authors, published by AAAS.

around complex geometric barriers as it locomotes along the floor (Figure 8e). In 2019, Minaminosono et al. described a deformable motor that built upon a DEA crank mechanism first proposed by Anderson et al. as a thin membrane artificial muscle rotary motor (Figure 8f).[184,185] Meanwhile, other robots systems such as FLEX 2 and Skitter have used DEAs to perform complex locomotion.[186]

Prestrained (framed) DEAs have been incorporated in robotics and motion assistive implementations such as wearables and tactiles. For example, an annular DEA has been used in conjunction with a fluid filled lens as an artificial eye. Other tactile devices have been designed to mount onto or interact with fingertips using hydrostatically coupled DEAs or DEA sensor arrays.[187–189]

Frame-mounted DEA locomotors have also been developed for aerospace applications. Recently, Anderson and co-workers described a DEA made from a 100 µm, inflatable silicone membrane with segmented embedded electrodes—effectively prestraining the membrane (associated with higher performance)—in order to prepare a multidirectional inflatable dome actuator (or MIDA), as well as a phased inflatable locomotory actuator (the PILA) that mimics earthworm locomotion through sinusoidal activation of an elongated, segmented body form. This type of motion is triggered by 90° out-of-phase electrode activation but does not result in directional locomotion. Instead, 180° out of phase motion is used to drive directional locomotion in the PILA.[190]

Frameless DEAs have some advantages from a design perspective as they can enable access to a wider array of robotic form factors and achieve actuation modes and motility not possible in frame-confined devices. One such dynamic, frameless DEA was described in 2017 by Henke et al. that uses a soft silicone skeleton bonded to a DEA that changes its curvature with applied voltage.[191] The same year, Wood and co-workers reported a urethane acrylic copolymer multilayer sheet-style robot that stacks elastomers, carbon fiber stiffeners, and compliant electrodes together to make multigait capable crawlers (five-layer inchworms and four-legged crawling robots) that do not require prestretching and thereby eliminate the need for rigid components commonly used in more traditional DEA robot designs (Figure 8g).[192]

Dynamic actuation modes have been achieved in aquatic, biomimetic robotics systems as well. For instance, a prestrain-free DEA robot designed by Christianson et al. took the form of a translucent, DEA trilayer stack.[193] Instead of traditional electrodes sandwiching the DEAs, the trilayer stack is formed from two internal fluid-electrode chambers capable of actuating the device when voltage is applied to the internal fluid through

the use of a grounded, polar aqueous environment as a second electrode (Figure 8h). Designed in this way, the DEA-based device is capable of continuous deformation without the need for rigid guidance frames, and therefore can actuate flexibly and controllably underwater (Figure 8i). In 2019, Zhu and co-workers reported the use of transparent DEAs that are sandwiched between three layers of compliant conductive polymer (CP) electrodes to create a camouflaged swimming robot with multimodal forms of swimming locomotion.[194] Floreano and co-workers prepared sheet-based DEAs by laminating soft silicone layers around compliant electrodes to prepare an artificial swimming fish robot as well as an underwater soft gripper robot.[195]

4.2.2. Cones and Cylinders

Conical and rolled DEAs have also been integrated into an array of functional devices and robots. An impactful demonstration of rolled DEA geometries was reported by Pelrine and co-workers.[196] Here, a MERbot locomotor, a six-legged robot with two DOFs per leg, was developed (**Figure 9**a) using the actuation of electroelastomer rolls that perform axial extension (Figure 9b) and bending (Figure 9c). These were then integrated into arrays to engineer the MERbot. Relatedly, Meng and co-workers have developed tube-based DEA actuators by rolling a sheet with soft, segmented DEAs that locomotes through a rolling mechanism.[197] Carbon-fiber cross-ply reinforced frames that are pre-stretched in rolled silicone tubes and sandwiched with graphene electrodes to function as lightweight, high-speed DEA-based wing flapper-type devices have also been demonstrated.[198] Cylindrical and tube-shaped DEA actuators were further demonstrated by Anderson and co-workers, who utilized pre-straining through inflation to achieve function, with actuator geometries specifically formed into cylinders to increase their length and curvature under applied field.[190] Wood, Clarke, and co-workers have also used an electrode-sandwiched dielectric roll actuator with concentric rings to operate at up to 200 Hz with 1 N of blocked force.[199]

Conical geometries have also been used in compelling DEA-based robotics and actuator demonstrations. Voltage-controlled

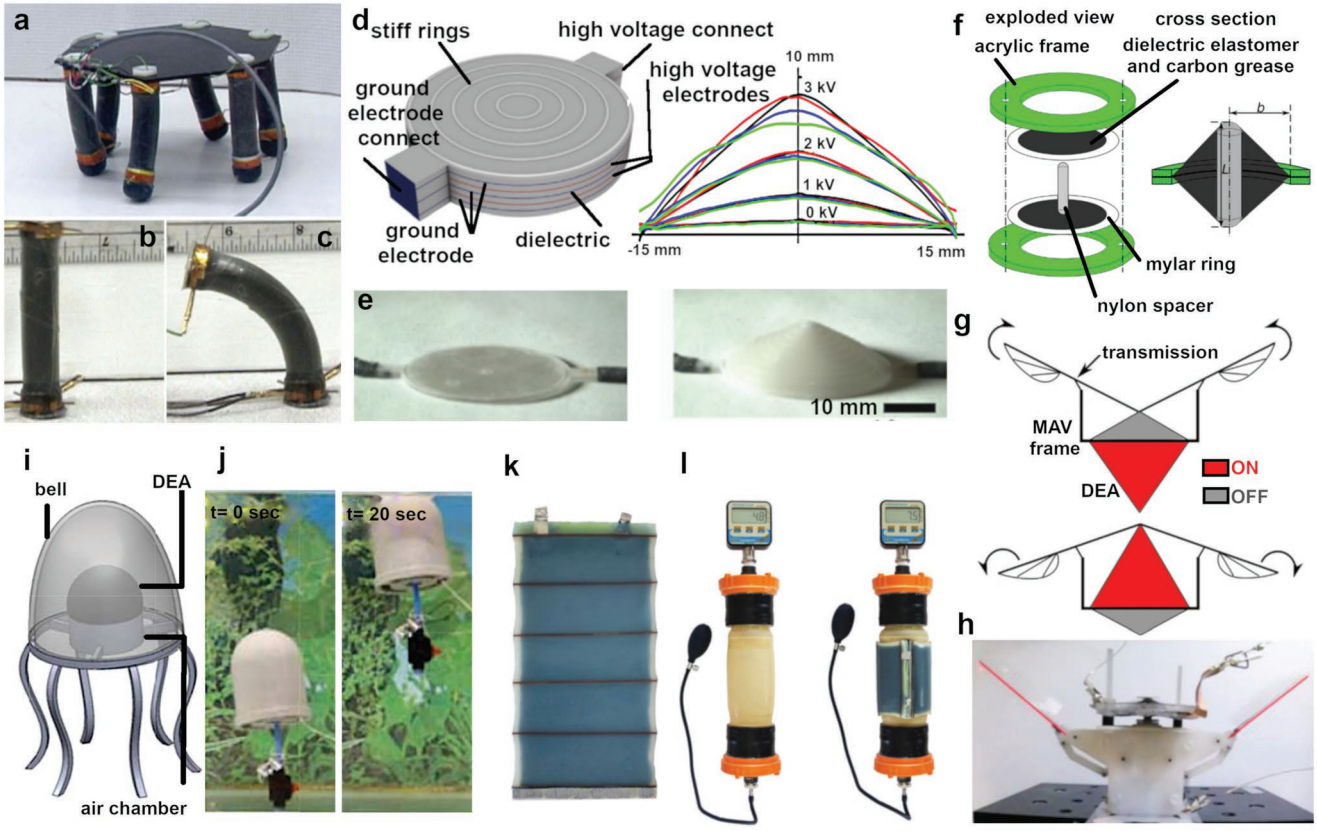

Figure 9. Deformation of dielectric elastomer actuators (DEAs). a) The MERbot locomotes using six electroelastomer roll actuators. Each roll actuator demonstrates multiple degrees of freedom including b) axial extension and c) bending. a–c) Reproduced with permission.[196] Copyright 2004, IOP Publishing. d) Schematic of 3D printed multilayer DEA stacks (left). Actuation is quantified (right). e) The concentric DEA rings actuate from flat to out-of-plane conical structures. d,e) Reproduced under the terms of the CC-BY Creative Commons Attribution License (http://creativecommons.org/licenses/by/4.0/).[200] Copyright 2019, The Authors, published by Elsevier. f) A micro-air vehicle (MAV) has dual eight-layer DEA films stretched into two symmetric conical actuators that use a g) two-state flapping wing design to operate. h) The MAV demonstrates a peak flapping stroke of 63° at 18 Hz. f–h) Reproduced under the terms of the CC-BY Creative Commons Attribution License (http://creativecommons.org/licenses/by/4.0/).[201] Copyright 2019, The Authors, published by Frontiers Media S.A. i) A bell-shaped silicone DEA cone with air chamber mimics a jellyfish that j) expels water as a mechanism of propulsion. i,j) Reproduced with permission.[202] Copyright 2016, IEEE. k) Multistacks of DEAs are applied to end use applications such as l) compression bandages. Reproduced with permission.[203] Copyright 2018, IEEE.

morphing of 3D printed DEA multilayer sheets with embedded and localized electrodes (Figure 9d, left) deform into a cone (Figure 9d, right). The cone forms from strain gradients within the printed concentric circles that are interlayered with alternating high voltage electrodes to realize deformation from flat into a conical conformation (Figure 9e). The multilayer DEA material systems generate structures with vertical displacement approximately ten times the disc thickness.[200] Another conical deformation of DEA has been detailed that utilized a dual eight-layer DEA multilayer made from polyacrylate tape, silicone elastomers, and a nylon spacer dowel to stretch the DEA films into two symmetric conical actuators (Figure 9f) enabling the flight of a micro aerial vehicle (MAV) with a flapping wing mechanism (Figure 9g). The MAV demonstrates a 209 mW mechanical power output, 108.9 W kg^{-1} mass-specific mechanical power density, and a peak flapping stroke of 63° at 18 Hz (Figure 9h).[201] Another illustration of bioinspired implementation of DEA has been reported by Godaba et al. who prepare a bell-shaped cone from commercial silicone DEA to prepare an air chamber to mimic a jellyfish (Figure 9i).[202] By applying field to the DEA membrane, the entire chamber contracts and expels water out of the jellyfish as a form of propulsion; a process that inverses upon field removal (Figure 9j). Both rolled tubes and conical DEA geometries are amenable to scaling and stacking to achieve end-use function. Multilayer stacks using dual acrylic/silicone elastomer layers (Figure 9k) have been suggested for end utility as compression bandages in wound healing (Figure 9l).[203] Variants of these foldable, rollable, compressive mechanical elements could be readily applied to assistive and wearable robotics technologies as well.

5. Ionic Electroactive Polymers

A distinct attribute of ionic electroactive polymers (IEAPs) when compared to other electroactive polymers (such as DEAs) is that the material itself is inherently sensitive to electric fields and accordingly, actuation is observed when these materials are subjected to only a few volts.[204] The reduced power requirements uniquely position these materials for uses in wearables and medical devices[205] and have motivated their consideration and implementation in robotics.[204] However, the implementation of IEAPSs in robotics is subject to limitations, including slow response times.[150] Coupling efficiency (k^2, energy converted into mechanical work per cycle/electrical energy applied) can be comparatively low as well. For instance, the conductive material polyaniline has a $k^2 < 1$ in contrast to PU DEAs where $k^2 = 21$ or silicone DEAs with $k^2 = 54$.[206,207] Further, the electrochemical nature of the response mechanism in IEAPs can result in device degradation (in water and air) and in some instances, inability to sustain constant strain to extended application of electric field.[208,209] Similar to other EAPs, such as DEAs, large area electrodes are required.[204,205]

5.1. Ionic EAPs: Materials and Mechanisms of Transformation

Many of the early examinations of the electromechanical response of IEAPs focused on deformation of IEAPs in a cantilever geometry. Upon application of an electric field, a bias-dependent strain gradient can develop. Reversing the polarity of the bias voltage has been shown as a means to induce bidirectional deformation of IEAPs.[209] IEAPs are electrochemical systems and accordingly, the mechanical response of these materials is strongly correlated to the nature of the ionic constituents and their integration into the insulating medium. Common subclassifications of IEAPs are ionic gels (IGs), conjugated polymers (CPs), ionic polymer–metal composites (IPMCs), CNT–electrolyte suspensions, and bucky gels that utilize CNT/ionic liquid (IL) electrodes sandwiching an IG electrolyte layer.[209,210] Electrorheological (ER) fluids can also be considered a subclass of IEAPs.

An ionic gel (IG) is an IEAP in which a polymer matrix is swollen with ionic or ion-containing solutions. This material system is then sandwiched within surface electrodes. Some IGs, such as polyacrylonitrile, are aqueous and rely on electrochemical reactions to locally change the pH and ion concentrations within the gel.[211] Upon application of a bias voltage, ion migration generates osmotic pressures and directs anisotropic swelling. The reliance on ion diffusion in IGs as the mechanism of transformation dictates limited response speeds relative to other IEAP material systems. Nonaqueous IGs have been prepared by embedding organic electrolyte and/or ionic liquid (IL) solutions within a polymer matrix.[212]

Conductive polymers (CPs) are organic compositions that conduct electrons through conjugated electron orbitals. Certain CPs are mechanically responsive to stimuli and are a subclass of IEAPS. Electromechanical response in CPs are typically induced by reversible counter-ion diffusion during oxidation/reduction reactions. Mechanistically, application of an electric field reversibly cycles expulsion and inclusion of ions into the polymer matrix. CPs can be paired with electrolyte separation layers. When this geometry is sandwiched between electrodes, application of an electric field generates imbalances in charges within the electrolyte polymer matrix that trigger swelling (expansion) or deswelling (contraction).[213] CP actuators are fast (>30 Hz).[209] In one recent illustration, ultrathin poly (3,4-ethylenedioxythiophene) (PEDOT) CP electrodes were synthesized using vapor phase polymerization with promising performance outcomes of curvature change up to 50% strain at frequencies below 10 Hz, but with measurable strains persisting up to 30 Hz at 3 V peak-to-peak.[159]

IPMCs have been prepared and examined as IEAPS for nearly 30 years.[214,215] Application of an electric field to hydrated IPMCs causes deformation (most commonly bending) by inducing transport of hydrated cations and water molecules within the membrane.[214,216] In IPMCs, upon exposure to an electric field, solvated cations move freely through channels in the immobilized anionic polymer network of the actuator. The asymmetry in the distribution of solvated cations as they flow toward the cathode induces anisotropic swelling and subsequent bending of these materials toward the anode due to the asymmetric water distribution through the thickness of the IPMC membrane.[217] These actuator types typically contain a thin ion exchange membrane made from a wet electroactive polymer (commonly Nafion or Flemion) that has been chemically plated on both faces with metal (such as gold or platinum).[210] Other IPMCs are simply sandwiched between inert metal electrodes.[218] Efforts to

produce stronger force and high powered outputs at lower cost than possible with pure Nafion have included increasing the size and stiffness of those electrolyte layers, while others have doped Nafion with silica particles or montmorillonite flakes to improve their stiffness.[219–225] Recent work reported the effect of the thickness of Au electrodes on Nafion-based IPMCs and found that blocking force of the IPMCs increases from 10 to 45 nm electrode thicknesses and begins to decrease again as thickness is ramped up from 45 to 80 nm.[226] Like other IEAPs, electric fields less than 10 V are needed to achieve functional outcomes.

IPMC systems have been fabricated in more complex geometries, for instance to realize material state awareness and feedback of coupled IPMC-sensor-actuators in robotics implementations.[216] Other work has focused on improving IPMCs by diversifying their electrolyte film chemistries. Recently, a polyvinyl pyrrolidone-modified PVDF composition was reported by Guo et al. that incorporates ionic liquids (ILs) to prepare bending cantilevers capable of 75° deformation in response to less than 10 V.[227] Other reports document the use of imidazolium cations, among others, and anions such as trifluoromethane sulfonate (TfO) to prepare PVDF-based IPMCs.[214,228–232] Modifying PVDF with polar groups such as sulfonated poly(ether ether ketone) or sulfonic grafts has been shown by Panwar et al. and others to increase the hydrophilicity of the networks and improve ion intercalation.[233–239]

Another class of IEAPs is CNT-electrolyte suspensions. Electric field application to these compositions creates an electric double layer at the networked CNT/electrolyte interfaces, which allows for charge injections that affect the entire CNT molecular network, causing uniform bond lengthening throughout and subsequent dimensional changes. A common approach to prepare IEAPs from these materials is to separate two CNT-electrolyte sheets with an insulating layer and subsequently immerse the multilayer element in an electrolyte solution. Bucky gels are a specific class of IEAPS that integrate CNTs with ILs and polymer layers in a three-layer construct with exterior CNT/IL/polymer blends and an intermediate IL/polymer layer.[213,217,240,241] Fabrication of these IEAPs is often done via layer-by-layer casting in sometimes dry conditions and does not necessitate the electroplating utilized in IPMC systems.[241] The typical mechanical response is illustrated in a recent effort that prepared a bucky gel with a PVDF-based polymer (poly[(vinylidene difluoride)-*co*-hexafluoropropylene) and an ionic liquid, EMIBF4 (1-ethyl-3-methylimidazolium tetrafluoroborate). This material system was functionalized with custom electrode layers containing the IL as well as single-walled nanotubes (SWNTs). Application of 3 V induces charge separation of the ionic liquid and causes anisotropic swelling through the thickness of the gel. Deformation is induced by swelling associated with the cationic domain of the material system due to the comparative ion size.[213]

Electrorheological (ER) fluids can also be considered as IEAPs in certain implementations. ER fluids are colloidal dispersions that when subject to an electric field, undergo considerable increase in viscosity. Oil dispersions of fine powders were described as early as the 1940s, and can be useful for certain actuation systems.[242] One of the key properties of ER fluids is the speed of response to the actuating force that has led to applied research in automotive mechanics as well as with medical devices and instruments.[243] The locking mechanism enabled by ER fluids makes them particularly useful for joint-based actuators. ER fluids have been demonstrated in multiple compelling robotics and actuation applications as well, including demonstrations in orthopedic devices,[244] haptic masters for robotics-assisted surgery,[245,246] and braille readers.[243,247]

5.2. Ionic EAPs: Structural Motifs Enabling Function

IEAPs have been widely integrated into adaptive systems. These implementations have extended upon the fundamental advances in material compositions detailed in Section 5.1 to enable functional output in robotic systems. IEAPs have been integrated as active mechanical elements to enable swimming, dexterous gripping, integrated sensing, or to facilitate adaption in wearables. The amenability of these materials to advanced manufacturing, such as 3D printing, has been exploited to prepare geometrically complex IEAP material actuators.

5.2.1. Films and Paper

IEAPs have been widely prepared as conductive papers and films that function as sensors within robotic systems. These implementations of IEAPs have used a variety of techniques and materials[247] including CPs, CNTs, graphene, metallic particles, NWs, microplates, and mixtures thereof.[248–261] A recent review by Peng and co-workers has directly compared aqueous and nonaqueous ionic gels scoped to applications in stretchable electronics.[212] Wearable technology using IEAPS was demonstrated by Ming et al. by embedding IPMC sensors in a smart glove (shown schematically in **Figure 10**a).[262] This glove can sense, pulse, braille, and enable human computer interactions (Figure 10b).

As material machines, geometrically simple IPMC films have been reported in numerous contexts as responsive linkages between structural plastic and functional components. In one implementation, ionic gel actuators containing P(VDF-HFP) polymer and IL was placed in between copper electrodes to function as microgrippers.[263] Porfiri and co-workers prepared a swimming robot using a strip of IPMC actuator in the tail that propels itself directionally and rapidly in water, with surge speeds up to 12 mm s^{-1} (Figure 10c,d).[265] Remote control of the IPMC-actuated biomimetic vehicle enables the device to actively engage with a shoal of golden shiners (Figure 10e). Previously, Yeom et al. had reported a jellyfish robot with tentacles made from IPMC membranes directed by a floating control head and an electrode driving component (Figure 10f).[266] In 2015, Yue et al. developed an 8-arm IPMC robot for underwater manipulation tasks that includes gripping rectangular, spherical, and cylindrical objects (Figure 10g,h).[267] An IPMC joint was also demonstrated more recently by Chen et al. to propel 2D maneuvering of a fish-like robot.[264]

5.2.2. Multilayer Laminates

Functional outcomes realized by IPMCs have been extended by stacking them into laminate structures, with several reports

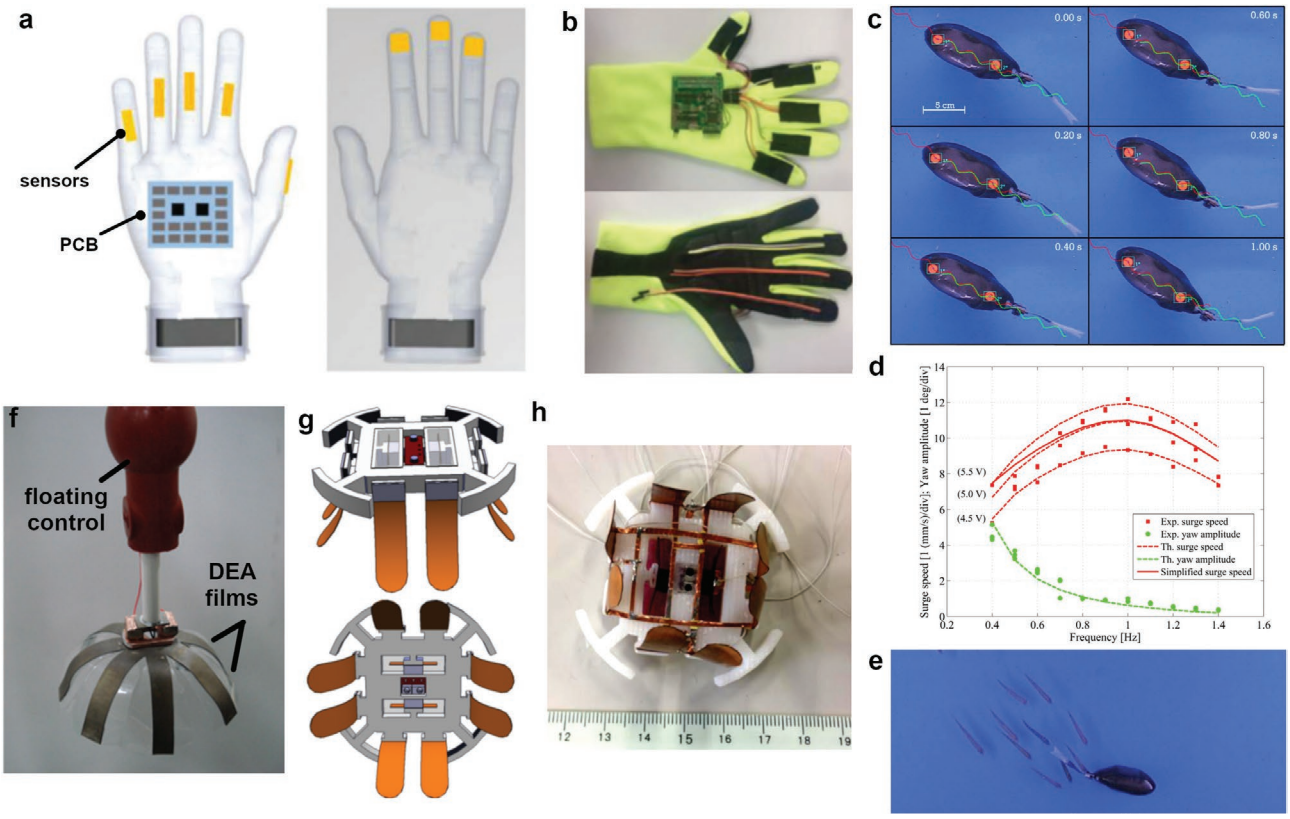

Figure 10. Ionic electroactive polymer (IEAP) film actuators and sensors. a) Schematic of ionic polymer–metal composite (IPMC) sensors integrated in a smart glove. b) Smart glove used for pulse diagnosis and braille recognition. a,b) Reproduced with permission.[262] Copyright 2018, Wiley-VCH. c) IPMC fish-like swimming robot using a strip of IPMCS actuator in the tail. d) Surge speeds of the IPMC fish-mimetic robot are up to 12 mm s^{-1}. e) Romote control of the robot allows it to interact with living fish shoals. c–e) Reproduced with permission.[265] Copyright 2010, IEEE. f) Jellyfish robot with tentacles made from IPMC membranes with a floating control head and an electrode driving component. Reproduced with permission.[266] Copyright 2009, IOP Publishing. g) Schematic of IPMC actuator array integrated into an aquatic robot with an underwater launching/grasping system using its IPMC grippers. h) Underwater launching/grasping IPMC robot. g,h) Reproduced with permission.[267] Copyright 2015, IEEE.

documenting their preparation and performance. In one instance, Wang et al. reported that stacked Nafion membranes can be heat-pressed together, swollen in alcohol solution to achieve ion exchange, and then processed with electroless plating to yield ultrathick IPMCs containing nanodispersed electrodes (**Figure 11**a).[221] The force displacement, or "weight lifting," demonstrated by a laminate prepared with this method is capable of lifting 124 g with only 4 V (DC) applied (Figure 11b). The charge and structural distribution of metal electrode–polymer interfaces present in the stacked Nafion membranes are depicted in Figure 11c. In another report by Suzumori and co-workers in 2019, a multilayer casting process is used to prepare geometrically biomimetic IPMC actuators while also eliminating cracking or other functionality-limiting fabrication artifacts in the devices.[268] After multilayer casting and drying of the Nafion dispersion, the device forms are immersed in Au (aq) solution and reduced electrochemically to plate their surfaces with gold electrodes. Due to the differential depths used during the casting process, these IPMCs exhibit spatially localized responses to different resonance frequencies that correspond to the local Nafion membrane thickness. When activated, these soft IPMC actuators can perform flapping and swimming-type dynamic actuation (Figure 11d).

5.2.3. Additive Manufacturing of IEAP Actuators

In addition to film-based IEAPs, more work has been done on integrating these materials into additive manufacturing contexts with form factors derived therefrom. Device outcomes in this space have included diverse IEAP material systems, including IPMCs, bucky gels, and ionogels. For instance, in 2017 Leang and co-workers reported an IPMC that is fabricated using a fused deposition modeling (FDM) additive manufacturing technique.[269] To prepare this device, a sulfonyl fluoride precursor of Nafion polymer is printed into the desired geometric form before undergoing base hydrolysis and plating via an impregnation reduction method. By fabricating body sections designed for linear extension as well as leg structures that function as grippers (**Figure 12**a), they demonstrate a fully 3D printed IPMC soft crawling robot that is structurally inspired by the locomotion of caterpillars (Figure 12b). To electrically isolate and independently actuate different portions of the devices, the electrode plating is selectively segmented. The result is a multigait-capable robot that can travel up to ≈20 cm in 10 s.

Bucky gel devices have also been developed with additive manufacturing techniques. In 2010, Kamamichi et al. described

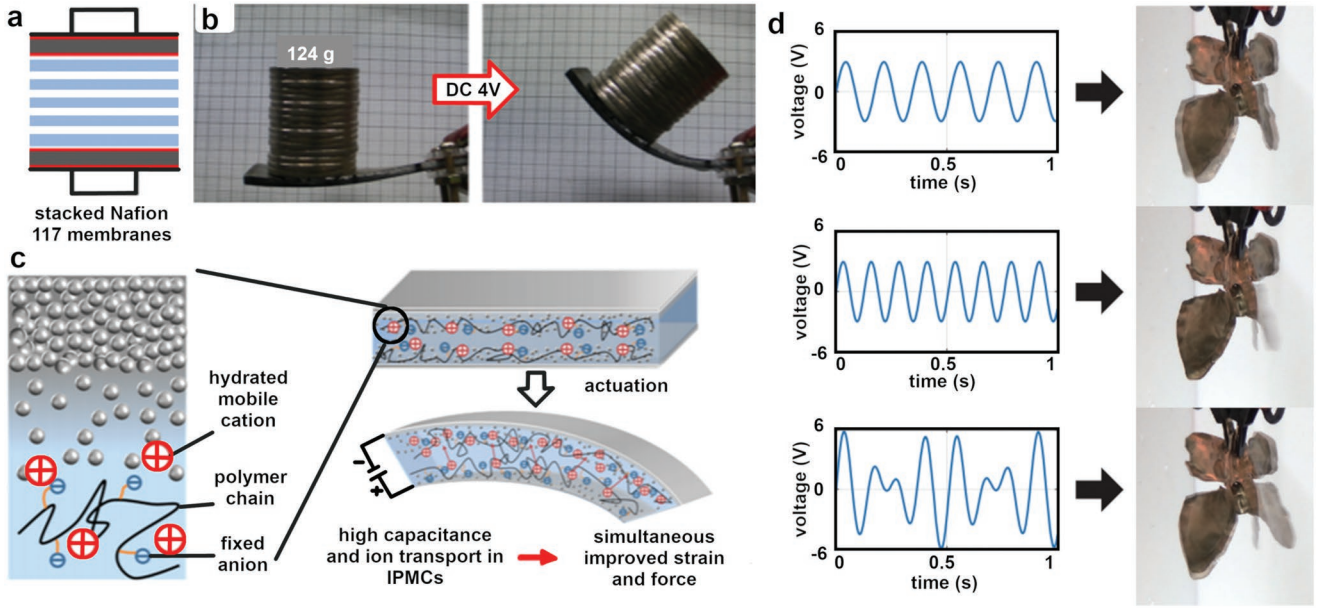

Figure 11. Multilayer assemblies of ionic electroactive polymers (IEAPs). a) Plated Nafion membranes are stacked to realize b) thick ionic polymermetal composite (IPMC) actuators. c) Charge and structural distribution of metal electrode–polymer interfaces in stacked Nafion membranes. a–c) Reproduced with permission.[221] Copyright 2017, American Chemical Society. d) Multilayer casting process of IPMC have different spatial thickness that responds differently to applied resonance frequencies, providing flapping and swimming actuators. Reproduced with permission.[268] Copyright 2019, IEEE.

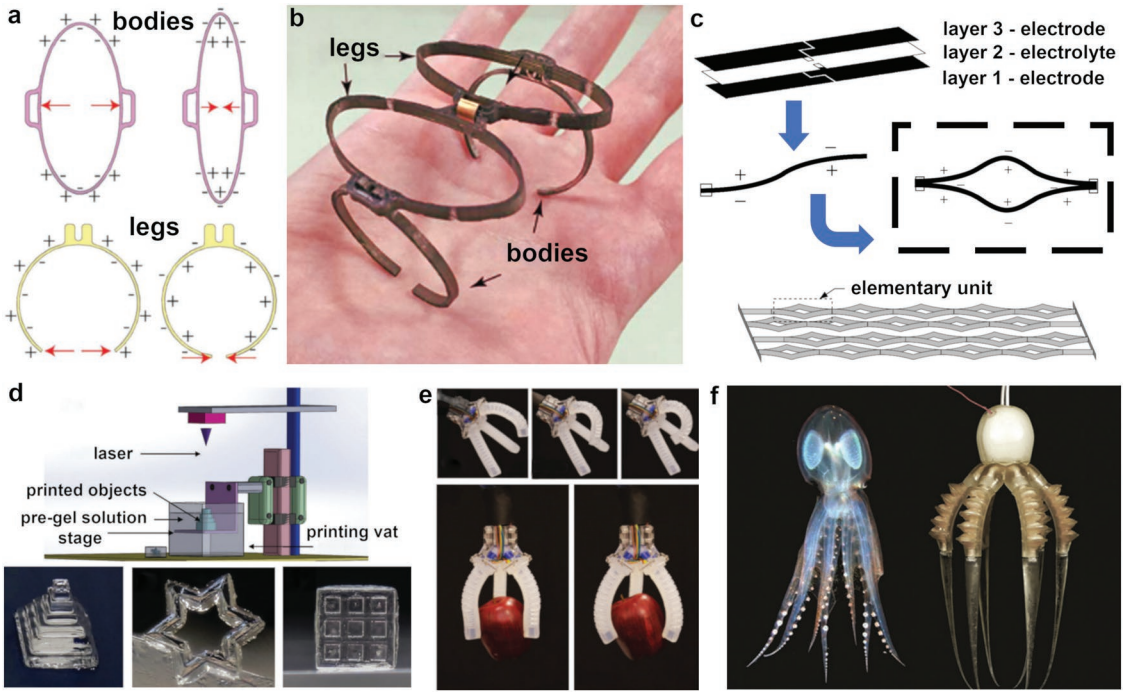

Figure 12. Additive manufacturing of ionic electroactive polymer (IEAP) and rheological fluid (RF) actuators. a) Fused deposition modeling (FDM) used to fabricate ionic polymer–metal composite (IPMC) body and leg structures. b) Connected IPMC segments form a soft crawling robot inspired by the locomotion of caterpillars. a,b) Reproduced with permission.[269] Copyright 2017, IEEE. c) Direct ink writing (DIW) used to fabricate bucky gel units cells (electrode–electrolyte–electrode trilayers) that form elementary units in actuator arrays. Adapted with permission.[240] Copyright 2010, Taylor & Francis. d) Stereolithographically patterned scaffolds of polymer/ionic liquid mixtures are resolved into diverse geometries. Reproduced with permission.[271] Copyright 2018, Wiley-VCH. e) 3D printed pneumatically actuated robotic grippers with integrated, printed ionogel sensors. Reproduced with permission.[272] Copyright 2019, IEEE. f) a fully 3D printed soft jellyfish mimetic robot actuates through voltage application to rheological fluid in its joints and cavities. Reproduced with permission.[275] Copyright 2018, Mary Ann Liebert Inc.

a bucky gel type IEAP that is 3D patterned into functional devices using direct ink writing (DIW).[241] Through combination of the solvent methyl pentanone, CNTs, PVDF-*co*-hexafluoropropylene, and the ionic liquid 1-ethyl-3-methyl-imidazolium, a printable bucky gel electrode solution is used to sandwich a printable electrolyte layer (a composition that excludes the CNTs but includes a significant weight fraction of the solvent methyl pentanone) to prepare the characteristic three-layer bucky gel structure. These trilayers are prepared into repeating elementary bilayer units that are connected at their ends and function as linear actuators when printed into an array (Figure 12c). These devices respond at low voltages (±2 V at 0.2 Hz) but are reported to have low force outputs that are attributable to the stiffness of the material.

Ionogels have also been prepared through additive manufacturing techniques. One such effort was described by He et al.[270] using a roll-to-plate fabrication method for the development of conductive ionogel-type paper. This strategy was used to periodically deposit a mixture of methyl methacrylate (MMA) monomers as well as ionic liquids onto paper substrates. In 2018, Furakawa and co-workers also prepared an ionogel that may be relevant to future actuators through the use of stereolithographic printing (SLA).[271] In this demonstration, the researchers described a range of prepolymer solutions that use thiol-ene/IL formulations and can be polymerized into diverse scaffold geometries with photopatterning (Figure 12d). Though not yet incorporated into contexts that achieve locomotion or actuation, these active material constructs show promise for integration into soft robotics or sensing devices that may rely upon functional ionogel components to achieve motion or motion feedback. Meanwhile, a compelling demonstration of ionogel sensors based on ILs and fumed silica particles has been reported by Truby et al., in which these material sensors are embedded (via the EMB3D technique) in 3D printed pneumatically actuated robotic grippers to complete the signal feedback loop needed for somatosensitive manipulation (Figure 12e).[272]

5.2.4. Fluids

ER fluids are a particularly unique class of actuator, since robotics and actuators that utilize them are inherently hydraulic systems. Yet, as will be detailed later sections, more typical fluids selected for hydraulic devices are used due to their passive and/or unreactive flow dynamics, with certain notable exceptions of which ER fluids are one. Due to the specifically electroactive response of ER fluids, we describe some of the recent and compelling uses for them in robotics systems here. In particular, ER fluids have been used to realize elastohydrodynamic lubricated spherical joints that better mimic human locomotion.[273] Home-based rehabilitation robots have also been proposed with ER fluid-based clutches.[274] A recent report documented the development of a fully 3D printed soft ER fluidic valve that was incorporated into hydraulic robots that mimic jellyfish (Figure 12f).[275] This device functions by transitioning between three states: 1) pump off/valve off, at which the tentacles are in their most extended conformation; 2) pump on/valve off, at which the tentacles contract inward into an intermediate actuated state; and 3) pump on/valve on, at which the tentacles contract to their maximum. The entire robot weighs less than 10 g, has onboard actuation control, and possesses a maximum holding pressure of 264 kPa with 5 kV applied across its electrodes. More traditional hydraulic and pneumatic devices, focusing on the geometric motifs of the constitutive elastomers that achieve performative function, will be discussed in the sections that follow.

6. Pneumatics and Hydraulics

An emerging class of stimuli-responsive material systems are based on dynamic reconfiguration of fluid (gas or liquid) within engineered material constructs. Compelling implementations have been reported, including the use of these responsive actuators in assistive devices, exoskeleton robots, and wearables.[276–281] Pneumatic and hydraulic actuating elements have high power-to-weight ratios,[282] maintain compliance at cold temperatures,[283] and are potentially low cost.[284] An inherent limitation of this approach in certain applications is response time. However, actuators and robots prepared from these materials are particularly suited for end uses that manipulate or handle soft or delicate objects.[283,285]

6.1. Materials and Mechanisms of Transformation

A key consideration in the design and fabrication of pneumatic and hydraulic-type actuators is the mechanical properties of the enclosing material, in particular the rigidity, stretchability, and durability.[286] Two commercially available silicones that are widely used in this context include EcoFlex (Smooth-On, USA) and Dragonskin.[287] Latex is also reported in pneumatic actuators,[288] as are polyurethanes, polyacrylates, and block copolymers.[289] Electrical charges, chemical reactions, shape memory polymers (SMPs), vacuum, and hydraulic components have been incorporated into pneumatics to achieve complex or unique functionalities.[290]

The dynamic reconfiguration of these material systems is induced by fluid transport (gas or liquid). Pumps valves and hinge joints are common, well-established components used within pneumatic systems to generate pressure, to induce localized fluid transport, and to cause mechanical reconfiguration. Notably, this approach is particularly relevant to applications in health sciences, such as for wearables or assistive technologies.[276] Comparatively, pneumatic or hydraulic actuators have higher load capacity, are potentially sterile, and operate athermally. Some of the most critical challenges in enabling the integration of these approaches for end uses such as microrobotics, is to scale these components to appropriate size.[291] An emerging opportunity is the assimilation of pneumatic or hydraulic devices with fluids such as ILs, ERs, magnetorheological fluids, metal liquid-like films, solvents of varying polarity, liquid metals, and other active material suspensions.[292] Pressurization of pneumatics via on-board gas production, for example through combustion reactions or platinum catalyzed decomposition of peroxides, have been of recent interest.[289,293,294]

Considerable research has and continues to demonstrate advanced robotics function derived from pneumatic or hydraulic actuators that utilize inert fluid content such as mineral oils or silicone oils. Other materials used in these contexts include carbon grease, water, and oxygen or atmospheric gas.[289] These systems are advantageous as chemically inert and environmentally friendly actuating systems for operations in extreme environments (high temperature). Incompressibility, low foaming, low vapor pressure, shear stability, and low toxicity are key considerations in the identification and incorporation of fluids in many hydraulic machines.[295] The hydrostatic pressure of these fluids is a critical performance indicator, since the Gibbs free energy of the fluid must be included when considering the maximum stress applied from the surrounding elastomer.[289] Rheologically driven fluid selection is also a consideration, but in practice does not play as large a role in performance since typical actuation occurs at slow shear rates where fluid shear stresses contribute negligibly.

6.2. Structural Motifs Enabling Function

Enabled by the comparative maturity of the pumping components, the long-established understanding of fluid dynamics, and the design criteria of pneumatic and hydraulic systems, recent research activity regarding actuators has focused on the construction of the elastomeric materials to localize deformation and to ultimately generate force and motion. These stratified elastomers have been prepared with processing methods including molding, layer-by-layer, and 3D printing. A review of pneumatic and hydraulic actuators by De Volder et al. differentiates the structural motifs as membrane-, balloon-, bellow-, and artificial muscle-type constructs.[296]

6.2.1. McKibben Actuators and Tensegrity Structures

First designed and fabricated in the 1950s, McKibben actuators rely on an internal bladder such as a tube or balloon that is wrapped in a braided mesh shell of threads that are inextensible but flexible.[297,298] A valve is mounted on one end of the actuator and the chamber is pressurized with air. The inextensible threads move in a scissor-like motion relative to each other to resolve the radial expansion. This results in a contraction in length of the McKibben actuator.[297] Artificial muscles have also been designed using a distinct construct.[285] Proportional integral derivative (PID) sliding mode, adaptive, and model-based control systems have all been employed to control antagonistic pairs of McKibben actuators for soft robotic joints.[282,284,299–304] Despite the compelling performance metrics associated with these actuators, low force outputs, nonlinear motion, and range of motion limitations remain as challenges for the implementation of this structural motif in certain robotics challenges.

Fiber-reinforced McKibben actuators were described by Liu and Rahn in 2003.[305] They reported a key threshold braided sleeve angle of 54.7° that shifts contractor pneumatic artificial muscles (PAMs) into extensor PAMs.[306] Variation of fiber angles or selective fiber re-enforcement have also been used to achieve expansion, bending, and twisting motion.[307] For example, Nefti-Meziani and co-workers harnessed McKibben muscles to create soft exoskeletons that perform bending motions (extensor bending pneumatic artificial muscles; EBPAMs) by converting radial pressure inside the elastomeric tube via one-sided re-enforcement of the actuator tube to selectively constrain its length (**Figure 13**a).[285]

Addition of other functional materials has also led to useful feedback mechanisms and modes of motion in McKibben-type PAMs. Conductive, insulated wires wound on McKibben actuators were recently used by Remy and co-workers (shown schematically in Figure 13b) to measure contraction based on induction changes. Using solenoid woven wire patterns, they achieved better sensing without cumbersome component add-ons.[308] SMPs have been integrated into McKibben actuators for sensing applications, for instance coupling glass transition temperature changes with pneumatic actuation mechanisms.[297] In 2016, thermally activated paraffin-filled McKibben actuators were described by Spinks and co-workers.[309] In 2017, they described an evolution of this design in the form of an electrothermally actuated McKibben.[310] This latter work expanded upon the paraffin-based McKibben actuator design and uses conductive filaments woven into the fiber structure of the device for rapid heating of the actuator (Figure 13c).[310] Suzumori and co-workers recently described another hydraulic McKibben actuator design that undergoes rotational modes of actuation.[311] Though McKibben actuators are a well-established technology, to date, modeling and implementation of McKibben actuators remains an active area of research, such as with work done to model McKibben actuators in hydraulic systems by Thomalla and Van de Ven in 2018.[298]

Other recent implementations of this approach have explored introducing motility into robots. McKibben actuators were integrated by Faudzi et al. into a long legged hexapod robot based on a "Giacometti" style gait that locomotes well on uneven surfaces (Figure 13d).[312] More traditional McKibben actuators have been utilized elsewhere. For example, a one-legged jumping robot was functionalized by Yamamoto et al. with McKibben actuators to output 1200 N of force (Figure 13e).[313] Other variants of fibrous woven pneumatic actuators have been described. For instance, Takamizawa and co-workers prepared "18 weave" muscles as an adaptive wearable (Figure 13f).[314] Coiled fiber pneumatic actuators were described by Singh et al. as parts of an assistive device for walking with crutches (Figure 13g).[315]

6.2.2. Bellow Geometries

Bellow-type actuators have attracted considerable attention for pneumatic-based robotics. Straight fiber, PneuNet, SLiT, and Peano-HASEL actuators all utilize bellow geometries to achieve function. Straight fiber actuators consist of elastomeric tubes that are banded by fibers or reinforcement in the axial direction. These then resist expansion forces when air is pumped into the elastomeric tube, pinching the tube at specific points as it expands into an actuated state.[316] PneuNet actuators are constructed quite differently, often from molding processes, but are also axially segmented at specific intervals. First described

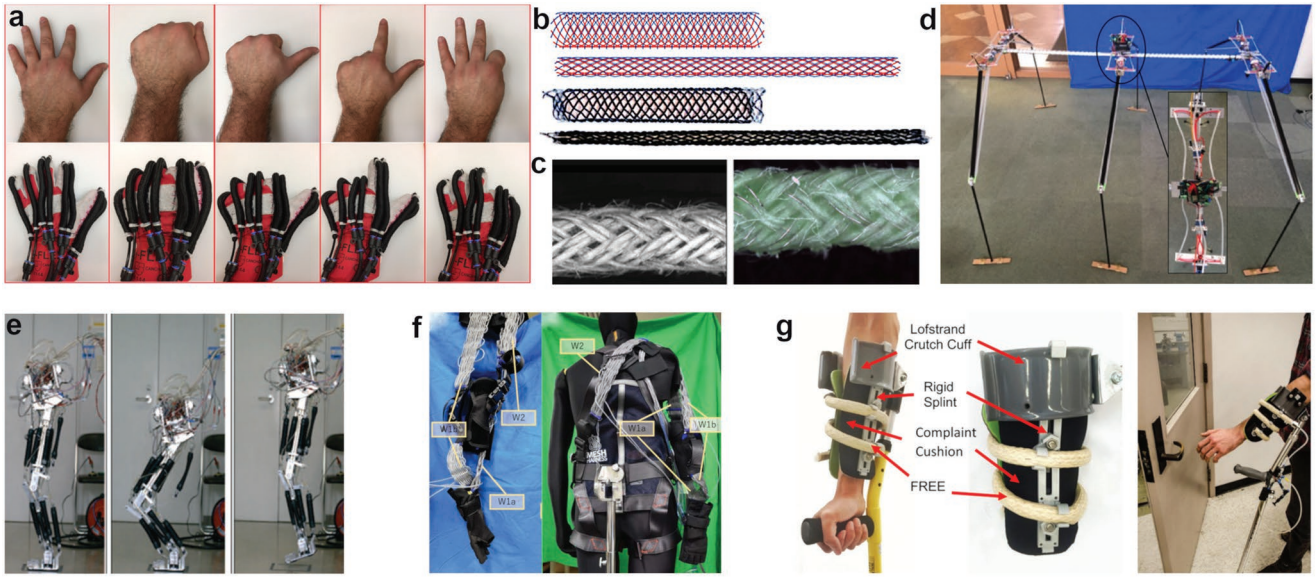

Figure 13. McKibben-type pneumatic actuators and robotic implementations. McKibben actuators have been implemented as soft exoskeletons. a) A McKibben actuator converts radial pressure to one-sided actuation via selective re-enforcement of the actuator tube. Reproduced with permission.[285] Copyright 2018, Elsevier. b) Schematic showing contraction based on induction changes from solenoid woven wire patterns for better, compact sensing. Reproduced with permission.[308] Copyright 2016,IEEE. c) Electrothermally actuated paraffin-filled McKibben actuators. Reproduced with permission.[310] Copyright 2017, IOP Publishing. d) Soft McKibben actuators integrated into a long-legged hexapod robot using a "Giacometti" style gait for uneven surface locomotion. Reproduced with permission.[312] Copyright 2018, IEEE. e) One-legged jumping robot outputs 1200 N of force. Reproduced with permission.[313] Copyright 2016, IEEE. f) 18 weave muscles provide soft power support to a suit-type wearable. Reproduced with permission.[314] Copyright 2019, IEEE. g) Assistive walking device prepared from coiled fiber pneumatic actuators. Reproduced with permission.[315] Copyright 2018, IOP Publishing.

by Whitesides and co-workers, PneuNets are elastomeric materials with embedded channel networks that localize pneumatic pressure (**Figure 14**a).[317] In one illustration, these authors power actuators and robots with on-board chemical reactions.[318,319] Later, a soft pneumatic glove was prepared with PneuNets to assist with hand rehabilitation (Figure 14b).[320] The fabrication of local structure in PneuNets has been widely shown to be a facile means of directing and controlling actuation. One recent report by Gu and co-workers detailed the correlation of chamber angle and twisting actuation of PneuNets (Figure 14c).[307] Ongoing efforts continue to predict and accurately control soft pneumatic actuators, which includes incorporating sensors to enable feedback loops as described by Truby et al. and Elgeneidy et al.[272,321] Belding et al. described a related approach, SLiT actuators, that also rely on axial banding but are prepared by selectively cutting slits into the walls of the elastomeric actuator.[322] With this differentiated approach, these authors realize rounded, right-angle, zigzag and twisting motions. Accordingly, SLiT actuators are able to perform complex motions such as screwing in a light bulb (Figure 14d). Other fluidic actuators that employ slit-based motifs harness snap-through instabilities, as have been reported by Overvelde et al., to reduce volumetric requirements to efficiently realize large scale actuators (Figure 14e).[288] Microactuators have also been prepared by Sinatra et al. from slit-type striations within PDMS/nanofiber composites.[323]

Large contractive forces have been reported by Keplinger and co-workers using Peano-HASELs (hydraulically amplified self-healing electrostatic actuators).[324] This class of devices integrates DEA substrates (with compliant electrodes) to prepare arrays of fluid-filled bellows. Application of electric field generates Maxwell forces which compress and subsequently displace the fluid within the HASEL pouches. Correspondingly, the length of the bellows reduces, generating a net contraction of the actuating system. Subsequent study by Keplinger and co-workers at the University of Colorado has demonstrated stackable HASEL actuators and manipulation of delicate objects such as eggs and raspberries (Figure 14f).[324]

Other axially reinforced pneumatic actuating systems have been described over the past decade. For example, a distinctive pneumatic actuator tube has been prepared by Shapiro et al. from two concentric tubes. The outer tubed is slotted selectively on one side of the actuator tube, leading to bending modes.[325] Later, a multimaterial actuator was designed by Calderon et al. with front and rear radial actuator domains and an axially constricted central actuator (Figure 14g).[326] Forward and reverse worm-like motility was later demonstrated by Ge et al. by 3D-printing hard casings on both of the locomotor ends.[327] Verma et al. has described a vacuum-actuated muscle-inspired pneumatic structure (VAMP) made from an open cellular elastomer construction that is able to navigate inside tubes with various turns, inclines, and diameters.[287] More recently, a VAMP-type actuator was prepared by Yang et al. to realize reversible buckling via arrays of elastomer beams to generate motions emulating skeletal muscle.[328]

6.2.3. Balloon Actuators

Balloon actuators have been widely used in pneumatic actuator designs. An early, compelling example reported by Morin et al.

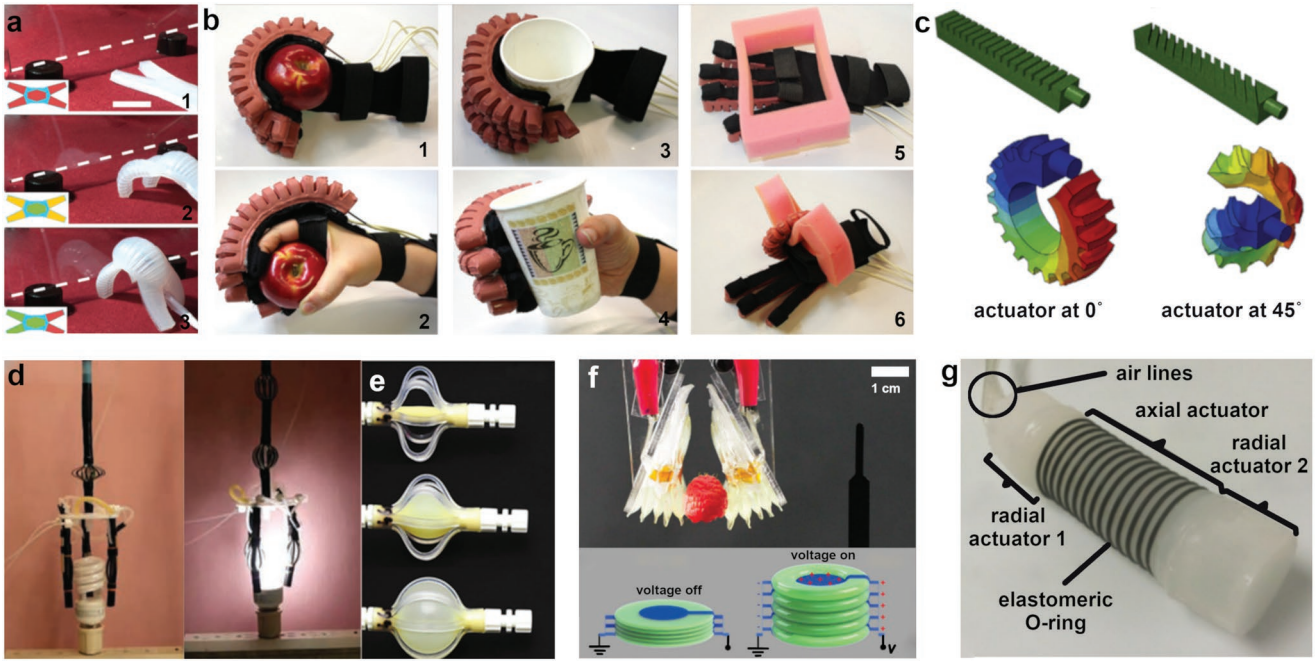

Figure 14. Pneumatic actuators from bellow-type architectures. a) Multi-gait robots prepared from a PneuNet pneumatic actuator designed to achieve locomotion. Reproduced with permission.[317] Copyright 2011, Wiley-VCH. b) Soft pneumatic glove, based on PneuNets.[320] Copyright 2013, IEEE. c) Chamber angles in PneuNets directs actuation modalities. Reproduced with permission.[307] Copyright 2018, Elsevier. d) SLiT actuators with slits cut into the elastomer walls screw in a light bulb. Reproduced with permission.[322] Copyright 2018, Wiley-VCH. e) Fluidic actuators use slit-based motifs to harness snap-through instabilities to efficiently realize larger scale actuation. Reproduced with permission.[288] Copyright 2015, NAS. f) Stackable circular HASEL actuators assemble into arrays that grasp extremely delicate objects such as eggs and raspberries. Reproduced with permission.[324] Copyright 2018, The Authors, published by AAAS. g) Multimaterial–multiactuator robot inspired by worm locomotion combines front and rear radial actuator domains with an axial central actuator. Reproduced with permission.[326] Copyright 2016, IEEE.

of balloon actuators used in robotics took the form of cube-based locomotors. Locomotor cubes are prepared by dovetailing soft joints of PDMS or Ecoflex polymer tiles such that different cube faces consist of disparate modulus polymers while the entire structure remains airtight (**Figure 15**a, top).[329] When supplied with air, the cubes actuate selectively depending on the location of the most compliant tiles. The softest modulus materials inflate like a balloon, while other cube faces remain unchanged. The anisotropic inflation induces rotation and locomotion. These multi-material cubes are stackable and connectable via luer lock adaptors to prepare highly modular pneumatic actuators and locomotors (Figure 15a, bottom).

Another example of balloon-based robots used them in joints during locomotion. Nemiroski et al. reported on arthrobots prepared from thin polymeric tubes that are low cost, simple to make, and exhibit mechanical compliance.[330] These systems derived inspiration from the hydrostatic joints of spiders and the inflation of the elastomeric tubes enable active control of limb extension while an opposing elastic tendon enables passive retraction (Figure 15b). Asymmetric extension at the pneumatic joints of the elastomeric balloon contributes to bending locomotion. Unlike other elastomeric pneumatic actuators detailed hereto, arthrobots (shown schematically in Figure 15c) are capable of linear motion instead of buckling motion. Discrete locomotor arthrobot architectures and size regimes can be prepared using this joint structure (Figure 15d,e). Locomotion of an arthrobot is shown in Figure 15f. Most recently, a soft ring pneumatic oscillator has been prepared by Preston et al. that temporally coordinates periodic motion in soft actuators using a single, constant-pressure source, without hard valves or electronic controls (Figure 15g, top). The fundamental unit of this ring oscillator is a soft, pneumatic inverter based on instabilities in elastomeric structures. These include buckling of internal tubing and snap-through of hemispherical membranes (Figure 15g, bottom).[331]

An eversion-based pneumatic robot was described by Okamura and co-workers that performs not through locomotion but through growth.[332] Asymmetric lengthening of the tip of this extending device allows it to traverse through extremely confined geometries and functionally interact with its environment. For example, these elements can turn off valves behind a closed door (Figure 15h, left), put out fires in enclosed volumes (Figure 15h, center), or extend outward as a radio antenna (Figure 15h, right). More recently, a report by Baydere et al. detailed an extensible pneumatic actuator based on a dual tube construct with pinch-roller mechanisms. These function to retract slack on the tubes and trigger contraction or increase slack in the tubes to generate expansion (Figure 15i).[333] A rolling, untethered, ballooning, intelligent (RUBIC) cube was reported by Chen et al. that is comprised of four selectively inflatable elastomer actuators (one on each cube face) is yet another route to generate a rolling motion (Figure 15j).[334] The RUBIC cube is powered internally by an on-board lithium polymer battery capable of powering 1 h of locomotion for

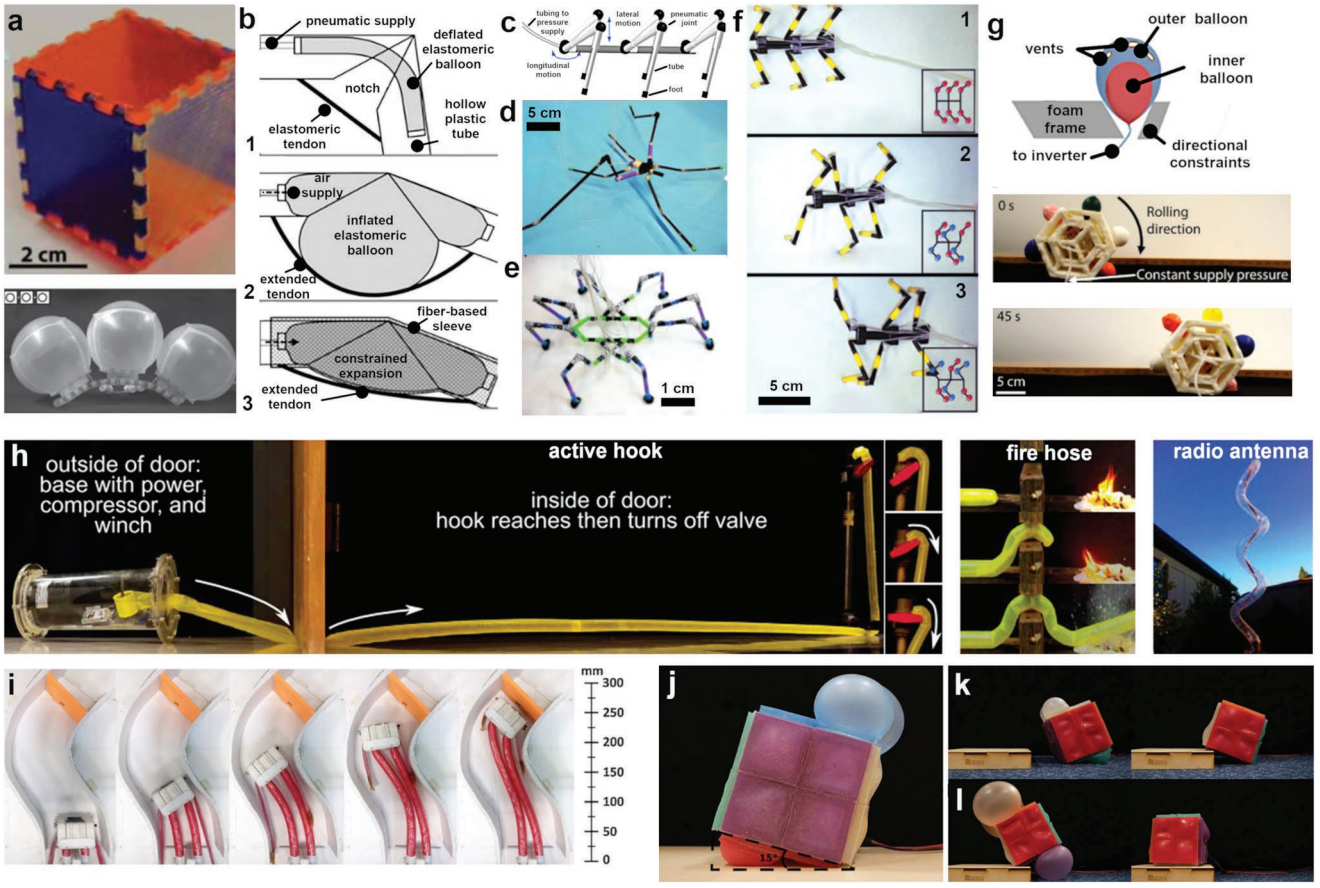

Figure 15. Balloon-type pneumatic actuators and robotic systems. a) Dovetailed soft joints using PDMS or Ecoflex polymer tiles actuate depending on the location of the more compliant tile moduli. Reproduced with permission.[329] Copyright 2014, Wiley-VCH. b) Arthrobots use a partially confined, hydrostatic balloon-based pneumatic joints. c) One arthrobot architecture shown schematically. d) A smaller scale arthobot architecture. e) Mini arthobot architecture. f) An arthobot locomoting. b–f) Reproduced with permission.[330] Copyright 2017, Springer Nature. g) Soft ring pneumatic oscillators uses balloon pneumatic to propel rolling locomotion. Reproduced with permission.[331] Copyright 2019, AAAS. h) Eversion-based pneumatic robot performs not through locomotion but through controlled asymmetric tip lengthening of the tip to traverse through extremely confined geometries: turning off valves behind doors (left), putting out fires in enclosed volumes (center) or extending outward as a radio antenna (right). Reproduced with permission.[332] Copyright 2017, The Authors, published by AAAS. i) Extensible pneumatic actuator using a dual tube construct with pinch-roller mechanisms in the head to locomote within tubes of arbitrary geometries. Reproduced with permission.[333] Copyright 2018, Elsevier. j) Rolling, untethered, ballooning, intelligent (RUBIC) cube comprises four fluidic elastomer actuators on each face of the cube that are selectively inflated to generate a rolling motion capable of k) locomoting over obstacles and l) repositioning. j–l) Reproduced under the terms of the CC-BY Creative Commons Attribution License (http://creativecommons.org/licenses/by/4.0/).[334] Copyright 2019 The Authors, published by Frontiers Media S.A.

every charge (Figure 15k). The RUBIC is capable of traversing over obstacles and (Figure 15l) repositioning.

6.2.4. Additive Manufacturing

While many examples of pneumatic or hydraulic actuators described here integrate 3D printed of components or segmenting of compartments, a recent trend is direct additive manufacturing of the pneumatic devices themselves. A number of these studies target 3D printing of soft grippers. For example, Wang and Hirai used an Objet260 printer to fabricate soft object grippers by combining TangoBlack+, a standard rubber for 3D components, with a hard polypropylene-based material, VeroWhite (also a standard plastic used for 3D components) (**Figure 16**a).[335] Maccurdy et al. have prepared printable hydraulic actuators by coprinting solids and liquids within a single device (Figure 16b).[336] In this examination, a commercial elastomer, 28 Shore A, is printed with a noncuring poly(ethylene glycol) liquid into a soft gripper capable of holding delicate objects such as eggs. In another compelling demonstration by Ge et al., a quarter-sized PneuNet-type three-legged gripper was prepared by 3D printing (Figure 16c).[337] More recently, Yi et al. 3D printed origami soft robot that contains pneumatic chambers capable of carrying a payload (18.5 N m at 180 kPa actuation pressure), and that maintains performance linearity and variable stiffness (Figure 16d).[338] Whitesides, Lewis, Wood, and co-workers fabricated a unique, complex soft robotic device in which direct ink writing (DIW) manufacturing allows for the integration—at the point of printing—of an array of microfluidic hydraulic chambers for platinum-catalyzed locomotion within a silicone octobot actuator (Figure 16e).[293] Studart and

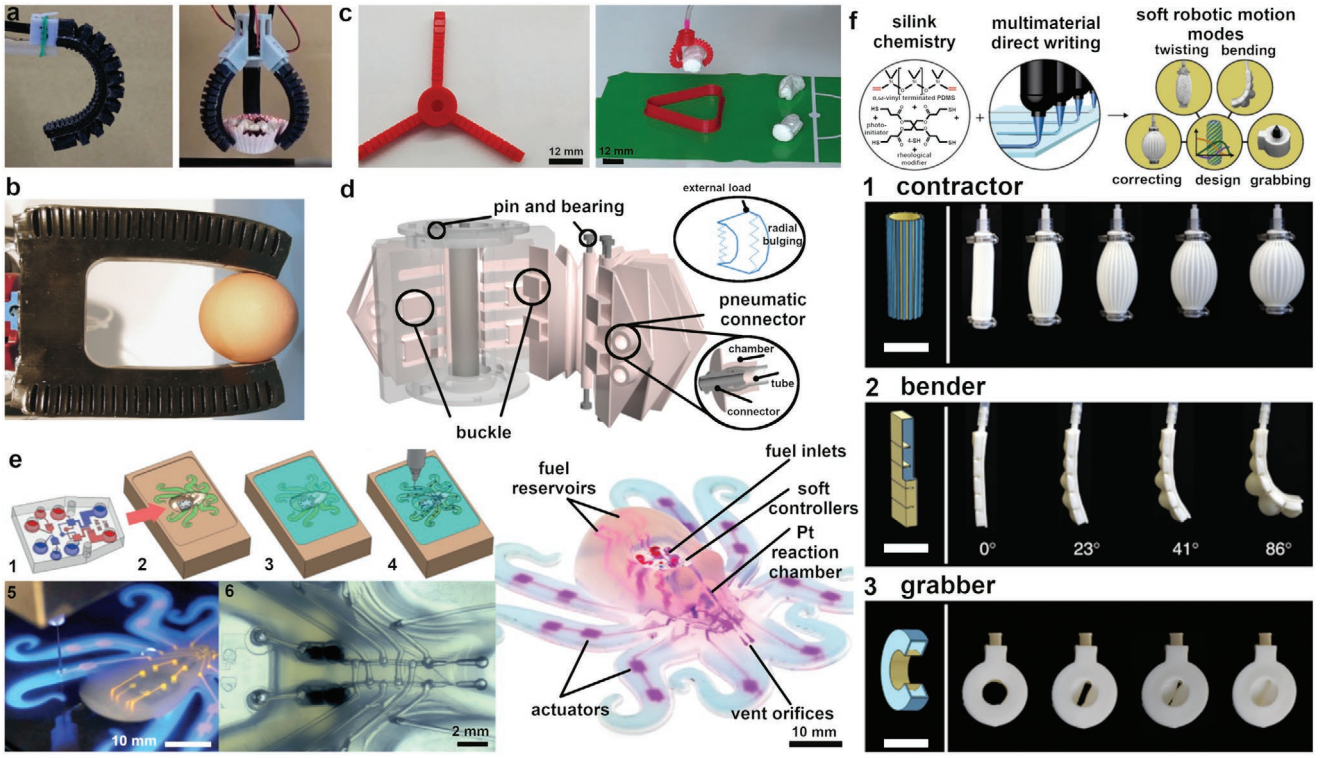

Figure 16. Pneumatic actuators prepared by 3D printing. a) 3D printed soft pneumatic grippers with commercial printable resins, TangoBlack+ and VeroWhite. Reproduced with permission.[335] Copyright 2017, IEEE. b) Commercial elastomer, 28 Shore A, printed with a noncuring poly(ethylene glycol) liquid into a soft hydraulic gripper form is capable of holding delicate objects such as eggs. Reproduced with permission.[336] Copyright 2016, IEEE. c) Digital light processing (DLP)-printed PneuNet-type three legged gripper. Adapted with permission.[307] Copyright 2018, Elsevier. d) 3D printed origami robotic joint containing pneumatic chambers for robust payload and performance linearity of the actuator. Reproduced with permission.[338] Copyright 2019, IEEE. e) Direct ink writing (DIW) manufacturing integrates an array of microfluidic hydraulic chambers that allow for platinum-catalyzed locomotion within a silicone octobot actuator. Reproduced with permission.[293] Copyright 2016, Springer Nature. f) Robotic soft actuators printed using a multimaterial printhead. Chemistries used include vinyl-terminated polydimethyl siloxane, a tetra-thiol crosslinker, and fumed silica to prepare actuators capable of twisting, bending, and grabbing. Reproduced under the terms of the CC-BY Creative Commons Attribution License (http://creativecommons.org/licenses/by/4.0/).[339] Copyright 2018, The Authors, published by Springer Nature.

co-workers directly printed robotic soft actuators with programmable, bioinspired actuators using a multimaterial printhead (Figure 16f).[339] Vinyl-terminated PDMS, a tetra-thiol crosslinker, and fumed silica were rheologically optimized for extrusion and printed with support material. With this strategy, twisting, bending, and grabbing motions (Figure 16f 1–3) were achieved by printing stiff stripes along different axes of a soft silicone tube elastomer bladder.

7. Shape Memory Polymers

Shape memory effects (SMEs) can also be realized in polymers. As detailed in Section 2, SME in metal alloys is heavily dependent on compositional and morphological considerations. Comparatively, shape memory processes in polymers are limitless—although the term "shape memory polymer" (SMP) is common to the vernacular used by scientists and even in commercial marketing, it can be argued that all polymers are SMPs (beneath their T_g). However, while any polymer can be programmed with an SME process, the quality of shape fixing and retention are indeed closely associated with compositional and structural considerations. Hayashi is commonly credited with the targeted synthesis of a polyurethane (PU) thermoplastic SMP that is amenable to diverse processing (as through injection molding, extrusion, dip coating, spin coating) across a wide range of temperatures.[340] The processability of this PU SMP formulation enables its straightforward reconfiguration into numerous form factors, which, at the time opened up new opportunities for SMPs.[341,342] Today, countless reports detail the integration of SMPs of a range of compositions and network chemistries into end uses spanning from deployable space structures[343–345] to medical implants[346–349]

While SMPs are not competitive with the energy densities achievable with SMA actuators, these materials have other distinct attributes: compositional variation, processability, and morphological diversity that differentiate their use and motivate integration in robotic devices. Foremost of these benefits is the considerable weight savings associated with the density of SMPs (polyurethanes—1.25 g cm^{-3}) when compared to SMAs (Nitinol—6.4 g cm^{-3}).[349,351] Another key advantage of SMPs in robotics is their tolerance of large deformations during shape memory cycling. Compared to SMAs, the soft and elastomeric nature of thermo-responsive SMPs allows for a considerable increase in fully recoverable (reversible)

strain during the shape memory process—as much as 800% has been reported.[347,350,352–356] SMPs have other notable benefits including chemical stability,[357] biocompatibility,[347] damping,[343] transparency, and stimuli-response (optical, magnetic, electrical).[29,358,359]

7.1. Materials and Mechanisms of Transformation

SMPs are programmed into temporary shapes (bends, creases, twists, or folds) by processing a polymer above a transition temperature. Most commonly, shape fixing of SMPs uses a physical transition (glass (T_g) or melt transition (T_m))[350,360] although chemical transitions via dynamic covalent chemistry[361,364–366] are an increasingly popular approach. Other physical transitions can enable shape memory effects in polymers including liquid crystallinity[365–368] and supramolecular bonds.[369–371] After shape programming, the material is cooled back through this transition with sustained deformation (load) to arrest the temporary shape. For one-way shape memory effects (OWSME), subsequent heating through the transition temperature (such as T_g or T_m) unlocks the temporary shape and the material recovers the permanent shape (usually a sheet or rod). These SMPs are also described as dual-shape memory polymers (dual-SMPs) because of their simple transitions between two shape states, with only one "memorized" temporary shape.[372] Although OWSME can be observed in any polymer, some materials are either naturally, synthetically, or structurally advantageous to SME processing. Specific material considerations are triggering temperature (e.g., tailoring to physiological conditions), shape fixity, shape recovery,[350] and amenability to multi-state programming.

Multistate thermal programming of SMPs is particularly promising for robotic implementations because of their potential to perform complex functions or reversibly cycle their actuation and be able to self-locomote. Over the past decade, the multishape memory effect (MSME) and the two-way shape memory effect (TWSME) have been subjects of significant study to expand upon the capabilities afforded by the OWSME.[372] Cross-talk between mechanisms within a single material system is also becoming increasingly common for advanced materials of complex form and function.[373–375] In particular, multishape memory polymers (MSMPs) are materials that can "memorize" two or more temporary shapes. Triple-,[376–378] quadruple-,[379] and quintuple-[380] SMPs have each been described. Multishape programming of SME in polymers is enabled by the preparation of materials with multiple transitions. Accordingly, the materials can be programmed at specific temperatures and undergo multistate shape transformation when heated. Common MSMP materials include poly(ε-caprolactone) (PCL) copolymers,[378] polyurethanes,[378] liquid crystal elastomers,[381] and polyethylene copolymers.[372]

Despite the distinctive function and shape control enabled by MSMPs, many of these systems need to be reprogrammed through loading after a transformation has completed. This limits their integration in robotics. However, a subclass of MSMPs that allow TWSME has found use in robotics in that a material can cycle between two states without a reprogramming step. A number of TWSME compositions have been explored.[372,377,382,383] Recovery within TWSME is a critical performance parameter for robotic and actuator implementation, since complete recovery is essential. A locomotive SMP harnessing this principle was demonstrated in a photothermally triggered PCL copolymer system by Wang and Zhu.[384] The photothermally driven locomotion of the TWSME occurs because a film programmed to the correct bent angle can recover and self-locomote directionally along an anisotropic ridged surface.

Thermal programming of SMPs has been the most widely utilized approach in actuation and robotics. Light can be used to globally or locally heat polymeric materials or composites.[385–393] Photothermal programming is distinctive in enabling remote (wireless) triggering as well as spatio-temporal control. SMP processes in composites can differentiate mechanical performance (such as anisotropic moduli) or be an approach to sensitize the material system to light (typically through nanoinclusions).[369] For example, silica and Celite (a mixture of silica and alumina) reinforce polyurethane SMPs and improve the shape fixity and recovery of these materials.[394,395]

Electrothermal responses have also been explored to realize SME in polymers. SMP nanocomposites based on nanoinclusions including graphene[396,397] self-assembled silver nanowires,[398] carbon nanofibers,[399] siloxane-modified alumina powders with carbon fibers,[400] nanoporous gold,[401] and CNTs[402,403] enable electrothermal deformation and shape programming. Similarly, including carbon black in polymeric materials is a facile route to enabling either photothermal or electrothermal responses.[404] The incorporation of 2D materials such as graphene and transition metal dichalcogenides into diverse polymer networks that include brush polymers, PDMS elastomers, acrylamide copolymers, pH responsive matrices, as well as the SWNT incorporation into PVA polymer to prepare nanoyarns, have all been applied in compelling actuators that also demonstrate, to an extent, the SME.[405,406]

An emerging approach to realizing SME in polymers is via dynamic covalent chemistry. So-called covalent adaptive networks are crosslinked polymer networks prepared with dynamic covalent bonds. Bond breaking and reforming can be induced thermally, photothermally, or by photoinduced reactions that ideally proceed without any unwanted side reactions. The thermally reversible Diels-Alder (DA) reaction is uniquely suited for use in thermoresponsive SMPs.[407] At low temperatures, the material is a stable covalent thermoset via the cycloaddition of a conjugated diene and an alkene (a dienophile). Heating the material triggers reconfiguration of the network. 3D printing of DA material system has been shown to allow local control of shape via a photothermal shape programming to local laser exposure.[341]

Lendlein and co-workers first reported an approach to realize "light-activated" shape memory processes.[364] Regulating shape with light has some advantages in the potential for remote, wireless control as well as local manipulation. This initial approach detailed a light-activated SMP subject to photoinduced changes in the crosslink density of the network as a means to program and release a desired shape.[364] These authors prepared an interpenetrating network containing up to 10 mol% of cinnamic acid groups, which photocrosslink when subjected to UV light >260 nm for one hour to "photo-fix" a mechanically elongated shape. Subsequent irradiation with UV

light <260 nm for 1 h decrosslinks and releases the fixed shape. Fixity, a measure of shape retention, was reported in the range of 0.3–0.5, with others focusing on related approaches.[408] White and co-workers have demonstrated shape fixing in azobenzene-functionalized polymer networks (both liquid crystalline networks and amorphous polyimides) from irradiation with blue light capable of inducing reorientation of these photochromes in the glassy material.[366,409] Other groups have also reported SMEs in azobenzene compositions with photoinduced trans–cis isomerization.[410,411] PU networks have been prepared with pendant azo groups to access this type of shape memory functionality.[412] When combined with nanoparticle fillers that are responsive to various wavelengths of light, azo-PUs assembled into bilayers have demonstrated selective curling based on the exposure wavelength.[413] In addition to azobenzene, light-activated shape memory in which crosslinking is reversibly modified via photocrosslinking and photocleaving, generates a transition state and allows shape programming.[408] Stage-responsive shape memory properties of PSMPU–azom composites, prepared by incorporating 4-(4-oxyalkyl chain carbonyl) azodi-benzoic acid (Azo11) into the PCL-based SMPs were developed by Zhuo and co-workers.[414] These materials display a unique combination of light- and thermal-responsiveness, permitting instantaneous shape-deformation under UV irradiation, but also demonstrating the capability to be temporarily fixed in arbitrary shapes once the UV irradiation is halted at room temperature conditions.

Another approach to reconfiguring SMPs is by exposing programmed shapes to water or other liquids. The hygroscopic nature of PU materials (programmed by thermal or other means) can be utilized to introduce shape reconfiguration. As the PU absorbs water, the glass transition of these materials can change over time and in some cases, allow for shape transformation.[415] Water sensitivity has been explored in numerous copolymers and compositions. For instance, polyurethane block copolymers modified with polyhedral oligomeric silsesquioxane exhibit 70% shape recovery when subjected to water.[416] Others have prepared a polyurethane–collagen composite in which the hydrogen bonds within the collagen fiber serve as a water-sensitive "switch" to trigger shape deformation. Water exposure softens the material, and the elastic recovery of the polyurethane drives shape recovery of the material. Other SMPs in aqueous environments have been shown to be pH responsive.[417]

7.2. Structural Motifs Enabling Function

The diversity of material compositions, structures, and processability afforded to SME processing of polymers has enabled distinctive functional benefits to both actuators and robotics. A common implementation of SMPs in robotics has been to program temporary states in polymers to act as grippers. More complex shapes, such as origami patterns, have been programmed and explored as actuating elements and in robotics. The amenability of SMP compositions to additive manufacturing is a particularly compelling opportunity to prepare 3D printed structural elements capable of reconfiguration.

7.2.1. Films

SMP-based film geometries that emulate grippers or respond intelligently to environmental cues are a promising approach to enable robotic utility and performance. Lendlein and co-workers described an SMP-based gripper prepared using a multiphase copolyester urethane networks with two discrete crystallizable domains/segments (**Figure 17**a). SME programming of these materials enables demonstrations including self-sufficient grippers or reversible fastening devices that can lift objects as diverse as pennies or dowels.[418]

A recent review details SMPs and other active materials in the context of origami and kirigami approaches to shape programming.[419] Origami design principles have been employed by Chen et al. in the extraterrestrial and autonomous deployment of a solar panel enabled by SMPs (Figure 17b–e).[420] 3D printed origami structures have been prepared by Teoh et al. with SMPs that enable reconfiguration.[421] Others have employed processes to lock origami folds in SMPs. Air Force Research Laboratory researchers prepared a chemically sensitive polyimide material and demonstrated self-folding cubes, tubes, and flowers (Figure 17f).[422] Liu et al. have shown that Miura ori tessellations can exhibit shape memory behavior under compressive loading to access dynamic and structural geometries.[423] Suppression of strain relaxation reported by Zhao and co-workers allowed for 2D to 3D transformations of poly(ethylene oxide) and poly(acrylic acid) SMPs through a multistep exposure to heat and light stimuli (Figure 17g).[424] Their results confirmed the accessibility of geometries as diverse as latches, airplanes, flowers, and coils that can be cycled through different form factors going from room temperature to heated conditions, then alternating thermal and light stimuli. Wang et al. have also reported twistable origami and kirigami SMP structures for applications in mechanical energy storage,[425] and Bowman and co-workers reported thermoreversible origami folding of SMPs in ductile polymer networks (Figure 17h).[426] Arguably the first SMP, a heat shrink polymer, was recently conjoined by Cui et al. into a bilayer with a high modulus thin film to enable self-folding origami when the devices are heated.[427]

7.2.2. Additive Manufacturing-Based Filaments and Fibers

SMPs of various chemistries have been incorporated into smart fabrics, extruded with 3D printing techniques, electrospun into fiber mats, and otherwise integrated into functional and complex systems in filament-form. Additive manufacturing strategies have enabled SMP-type materials to be applied in direct ink writing (DIW), digital light processing (DLP), stereolithography (SLM), and fused deposition modeling (FDM) to prepare complex and responsive devices. For example, in 2019, Lendlein and co-workers described highly-crosslinked electrospun fiber mats made from PCL blended with triallyl isocyanurate and benzophenone that perform as reversible, bidirectional SMPs with temperature-responsive pore sizes.[428] Additionally, shape memory behavior and recovery force of 3D-printed circular braided tube preforms have been demonstrated by Mather and co-workers.[429] Zhang et al. used FDM-printed, SMP polylactic acid (PLA) to show the effects of braiding angle, tube wall

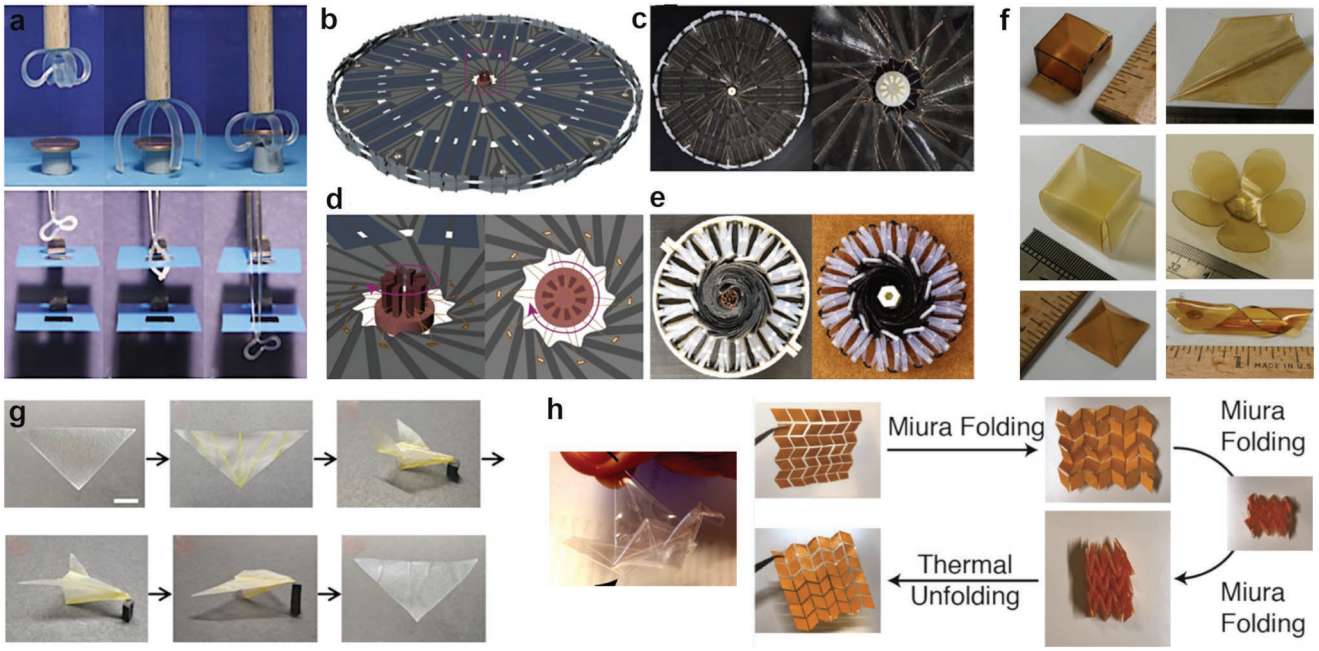

Figure 17. Mechanical response of shape memory polymer (SMP) films. a) SMP-based gripper with reversible and bidirectional SMPs using multiphase copolyester urethane networks. Reproduced with permission.[418] Copyright 2013, Wiley-VCH. b) Extraterrestial deployment of solar panels employing an origami design and SMPs. c) In a deployed configuration, flexible wires are installed along with d) a panel core. e) When heated (left), the panel fits into a cylindrical mold, then is cooled and released (right). b–e) Reproduced under the terms of the CC-BY Creative Commons Attribution License (http://creativecommons.org/licenses/by/4.0/).[420] Copyright 2019, The Authors, published by APS. f) Origami-inspired self-unfolding polyimide SMPs crosslinked with phosphine oxidecontaining triamine (POTAm) or a trianhydride (POTAn) to prepare self-folding cubes, tubes, and flowers. Reproduced with permission.[422] Copyright 2019, American Chemical Society. g) 2D to 3D transformations of poly(ethylene oxide) and poly(acrylic acid) SMPs through a multi-step exposure to heat and light stimuli produces latches, airplanes, flowers, and coils. Reproduced with permission.[424] Copyright 2018, Elsevier. h) Thermoreversible Miura origami folding of SMPs in ductile polymer networks. Reproduced with permission.[426] Copyright 2018, AAAS.

thickness, and shape recovery temperature on 3D printed fiber preforms and their silicone elastomer matrix composites.[423]

Therriault and co-workers demonstrated a family of highly conductive multimaterial composites that can be directly printed into multifunctional electrical devices using a flexible solvent-cast 3D printing technique (**Figure 18**a).[430] The materials leverage the high aspect ratio and low contact resistance of hybrid silver coated carbon nanofibers to prepare rapid and low-voltage-triggered electrical-responsive shape memory behavior. In 3D printed devices, gripper-like actuation was realized to lift and release objects on command. Lee and co-workers also used FDM in order to fabricate shape memory polymer composites that combine SMAs with SMPs (Figure 18b).[45] The SMA contributes to a thermal SME due to a phase change between its martensite and austenite phases, while the SMP domains undergo a glass transition in their transition segments. The SMP's SME induces a change in the proportion of hard and soft segments, resulting in the shape change cycles. Bodaghi and co-workers demonstrated how FDM can be used to functionally program the self-folding of extruded filaments due to changes in fabrication parameters like printing-speed and liquefier-temperature.[376,431,432] 3D printing techniques have been used to prepare SMP actuator units, and ultimately SMP meta-material lattices, for self-expanding and shape-changing structures, along with actuating geometries such as hinges and coils. Chen and co-workers described work on PU-based, SMP flower-mimetic 3D structures built with FDM that exhibit phototriggered shape memory behavior (Figure 18c). Time-lapse images show the opening and closing cycles of the flower (Figure 18d) before (Figure 18e) and after light stimulus sufficiently heats the SMPs to return it to its original (open) conformation (Figure 18f).[404]

SLM has been employed to prepare sequentially self-folding structures with different glass transition temperatures into geometries such as hinges, ladders, shape-changing rings, periodic macrostructures, folding hinge sheets, and grippers. These printed compositions are based on SME in polymers as well as active hydrogel elements to realize complex reconfiguration.[433] A micro-SLM print of a methacrylate copolymer prepared by Ge et al. was subject to SME to enable shape transformation and reconfiguration with temperature cycling (Figure 18g).[434] Printing allows the preparation of a complex "permanent" shape that the programmed elements can return to upon heating (Figure 18h). DLP, closely related to SLM methods, has been used by Suriano et al. to prepare and pattern ureidopyrimidinone (UPy) methacrylate monomer into a polycaprolactone SMP matrix capable of shape programming, reconfiguration, and self-healing.[435] DIW has also been an approach to print SMPs and enable implementations in robotics.[436] A recent report by Qi and co-workers documented the use of DIW to print an epoxy composite that is further processed to adopt temporary shapes. Leng and co-workers have used DIW to print SMP based on crosslinked polylactic acid to demonstrate 1D, 2D, and 3D shape transformations.[437]

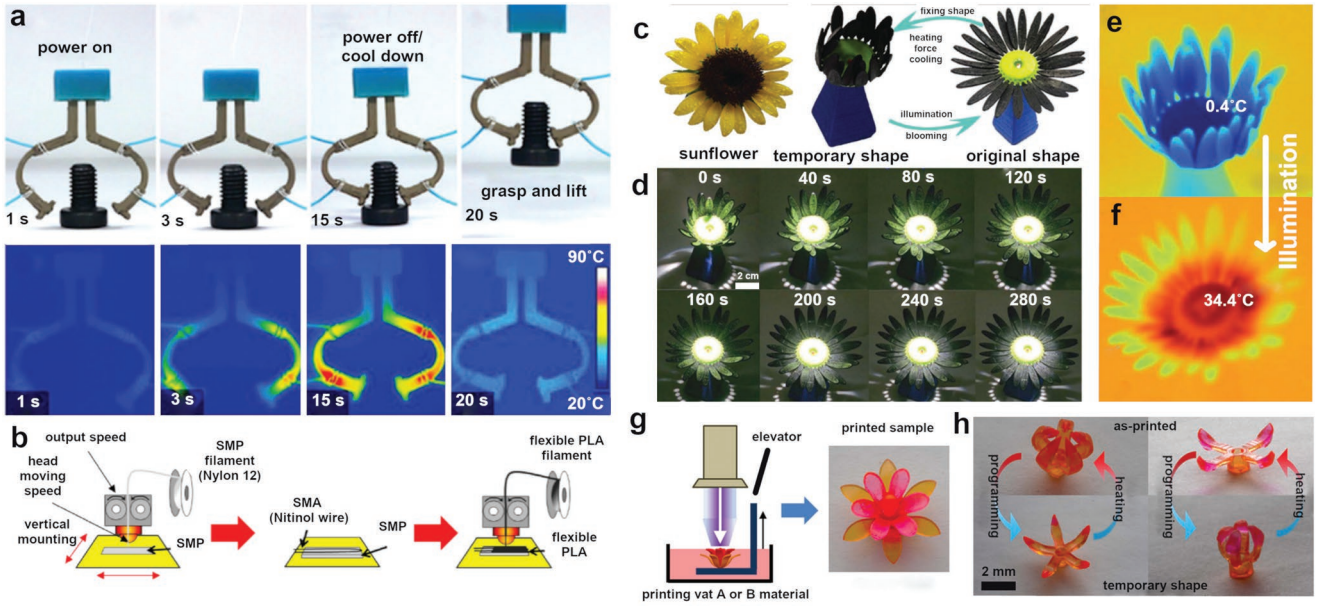

Figure 18. Shape memory polymer (SMP) elements prepared by additive manufacturing techniques. a) A family of highly conductive multimaterial composites are 3D printed into multifunctional electrical devices with flexible solvent-casting. 3D printed devices from these materials function as grippers to lift and release objects on command. Reproduced with permission.[430] Copyright 2019, American Chemical Society. b) Fused deposition modeling (FDM) fabricates SMP composites (SMPCs) that combine shape memory alloys (SMAs) with SMPs. The SMA contributes to a thermal shape memory effect due to a phase change between martensite and austenite phases, while the SMP domains undergo a glass transition in their transition segments. Reproduced with permission.[45] Copyright 2018, Elsevier. c) Polyurethane (PU)-based SMP flower-mimetic 3D structures built with FDM manifests phototriggered shape memory behavior. d) Timelapse of opening and closing cycles of the flower after light stimulus sufficiently e) heats the SMPs to return it to f) its original (open) conformation. c–f) Reproduced with permission.[404] Copyright 2017, Wiley-VCH. g) A micro-SLA printing bath is used to prepare multi-material SMPs into flower-mimetic structures. h) The thermal transition between the printed SMP shape and the temporary shape of the grippers allows it to grip objects or release them, depending on the printed "original" conformation. g,h) Reproduced under the terms of the CC-BY Creative Commons Attribution License (http://creativecommons.org/licenses/by/4.0/).[434] Copyright 2016, The Authors, published by Springer Nature.

8. Hydrogels

Stimuli-responsive hydrogels are particularly relevant to robotic implementations targeted for physiological environments.[438–440] These material systems are prepared from hydrophilic polymers and copolymers and swell when placed in aqueous media.[441–444] Covalent bonds within the polymer network of these materials prevent dissolution. When subjected to an external stimuli (most frequently temperature), hydrogels undergo a reversible swelling–deswelling process referred to as a volume phase transition.[445] Conventional hydrogels are isotropic and undergo a homogenous volume phase transition. Recent reviews detail the synthesis, mechanism, and utility of hydrogel actuators.[446–452] Of relevance to this review, demonstrations focused on the preparation of anisotropic hydrogels and programming of the mechanical response are presented as an emerging area of research with increasing relevance to robotic implementations.

8.1. Materials and Mechanisms of Transformations

Hydrogel actuators are most frequently comprised of thermally responsive polymers that display a lower critical solution temperature (LCST) or an upper critical solution temperature (UCST). A polymer with an LCST is soluble in water at low or room temperatures due to hydrogen bonding between the water molecules and the polar functional groups of the polymer backbone. As the solution is heated, the entropy of the system increases, and hydrogen-bound water is released. The polymer correspondingly deswells and contracts, forming agglomerates in solution and decreasing the macroscopic volume of the hydrogel.[453] The volume decrease can be reversed by placing the hydrogel in cool water where the material reswells. The most widely utilized LCST-containing polymer is poly(*N*-isopropylacrylamide) (PNIPAm). The LCST of PNIPAm is near physiologically relevant temperatures (≈32 °C).[454] A UCST-containing hydrogel is one that is insoluble at room temperature but that, when heated, begins to swell due to hydrogen bonding between water and the polar functional groups of the polymeric backbone. These interactions solubilize the polymer chains in a process described as volumetric expansion. Common examples of UCST polymers are poly(acrylic acid) (PAAc) and polyacrylamide (PAAm). The LCST and UCST of a hydrogel can be selectively tuned through the inclusion of copolymers of varied hydrophilicity and hydrophobicity.

Thermal transitions are the most widely employed transformation mechanism in generating mechanical responses in hydrogel actuators. However, deformation of hydrogels can also be triggered by changes in ion concentration, pH, light exposure,[455,456] and electric field.[452,457,458] Of particular relevance to robotics are electromechanical effects realized in

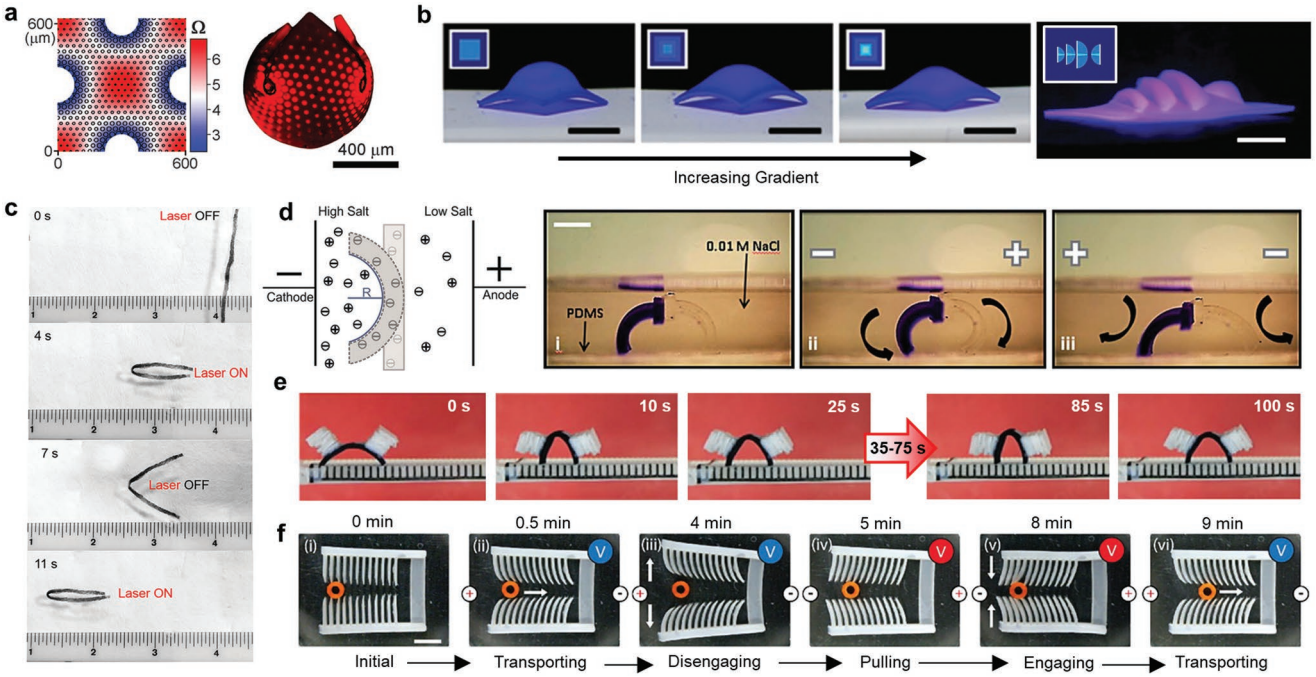

Figure 19. Mechanical deformation enabled by chemical and stimuli gradients in hydrogels. a) Programmed swelling ratios (Ω) prepared via modulated photoinduced crosslinking densities generating 3D Gaussian curvature deformation. Reproduced with permission.[461] Copyright 2012, AAAS. b) Digital light processing (DLP) rapidly prepares spatially modulated swell ratios in 2D hydrogel sheets that develop complex curvature. Reproduced with permission.[464] Copyright 2017, Wiley-VCH. c) Photothermally induced swimming in a poly(N-isopropylacrylamide) hydrogel. Reproduced with permission.[465] Copyright 2015, Wiley-VCH. d) Osmotic pressure walker anionic hydrogel displaying concerted motion under application of an E field. Reproduced with permission.[458] Copyright 2014, RSC. e) Anionic hydrogel transporting a load over time. Reproduced under the terms of the CC-BY Creative Commons Attribution License (https://creativecommons.org/licenses/by/4.0/).[467] Copyright 2015, The Authors, published by Springer Nature. f) DLP of electrically active hydrogel capable of sequential motion. Reproduced with permission.[468] Copyright 2018, American Chemical Society.

ionic hydrogels, most frequently prepared from poly(2-acryloylamido-2-methyl propane sulfonic acid) (PAMPS). PAMPS hydrogels are anionic (the covalently bound ions are anionic and the mobile counterions are cationic) and when placed in an ionic media and subjected to an electric field, cations migrate towards the cathode. The covalent incorporation of anionic groups within the polymer network limits their mobility. Consequently, the heterogeneous distribution of ions results in an osmotic pressure gradient within the hydrogel. Mechanically, the heterogeneous distribution of osmotic pressure generates asymmetric swelling on the anode side of the hydrogel, which causes the material to deflect.[455,456]

8.2. Structural Motifs Enabling Function

8.2.1. Crosslinking and Stimuli Gradients in Homogenous Materials

Fundamentally, shape change in hydrogels requires anisotropic (e.g., local) swelling/deswelling. A common method to program deformations in hydrogel actuators is to generate gradients through the thickness of the material. Two primary approaches have been utilized: 1) the intentional preparation of spatial or through-thickness heterogeneity in crosslink density and 2) spatial or through-thickness variation in stimuli response.

The mechanics governing the formation of a 3D shape from 2D programming in hydrogel materials has been described in detail.[446,459–461] Generally, crosslinking gradients in swollen hydrogels generate in-plane stresses that are compensated for via out-of-plane bending. Consequently, 3D shape transformation can be realized by precise patterning of hydrogel swelling ratios. Kim and Hayward published an impactful approach to spatially pattern swelling in hydrogels by synthesizing benzophenone-modified poly(NIPAm-*co*-AAc).[461] The benzophenone moieties in the hydrogel sensitize the gel to light processing via a method referred to as halftone lithography. The hydrogel shape is first fixed via a low dose UV light. A second, high dose, patterned UV light exposure allows programming of the material by locally increasing the crosslink density. Accordingly, upon exposure to thermal stimuli, axisymmetric and nonaxisymmetric Gaussian curvature can be achieved, plainly evident in a hydrogel that swells to a near spherical shape (**Figure 19**a). Yum and co-workers have since demonstrated that the formation of Gaussian curvature is dynamic and may be programmed by controlling the rate at which given regions of a hydrogel swell, resulting in spatially controlled, sequential deformation in a thermoresponsive hydrogel.[463]

Other authors have employed higher fidelity methods such as digital light processing (DLP) to prepare hydrogels with fine control (resolution in xy plane = 0.01 mm^2) of local swelling ratio.[464] Xie and co-workers examined hydrogels composed of hydroxyethyl (meth)acrylate and potassium 3-sulfopropyl-methacrylate monomers in which the local swelling ratio is precisely tuned through exposure time. The spatial control over the

swelling ratios allows for facile tuning of the radius of curvature in a deformed hydrogel sheet by transitioning from discrete to gradient crosslinking densities (Figure 19b). Further, exposure of these materials to patterned light as a stimulus allows for the generation of complex shapes, including the Sydney Opera House.

Motility in hydrogel actuators can also be realized by preparing hydrogels with crosslink density gradients. A recent report by Luo et al. demonstrated motility in a hydrogel prepared with a porosity gradient through a two-step PNIPAm polymerization.[465] Accordingly, the top surface of the hydrogel consists of a highly porous, loosely crosslinked network while the bottom surface consists of a lower porosity, more densely crosslinked network.[465] Homogenous distribution of polypyrrole (PPy) nanoparticles in the hydrogel sensitizes the material to near infrared light exposure, enabling a photothermal mechanism. Under uniform light exposure, the degree of deswelling (as the PNIPAm collapses) is greater at the highly porous hydrogel surface causing the material to rapidly bend toward the light source, mimicking the motion of an octopus arm. This deformation propels the gel in an aqueous environment (Figure 19c). Relatedly, Emrick and Hayward used light as a means to generate a graded response in Au-nanoparticle patterned hydrogel disks. The variation in absorption across the material thickness generates motion and self-assembly in a group of hydrogel disks under white light exposure.[466] The photothermal gradient emanating radially out from the centrally patterned nanoparticle region results in a large degree of deswelling close to the nanoparticle interface, and a low degree of deswelling at the edges of the hydrogel disk. The swelling mismatch causes the material to deform with negative Gaussian curvature azimuthally along the hydrogel. Hydrogel deformation consequently deforms the surrounding air–water interface upward or downward to match the shape of the hydrogel. The variation in shape of the air–water interface generates capillary attraction or repulsion between the hydrogel disks.

Electromechanical effects in hydrogels can be realized through local variation in stimuli-response, most frequently employed in ionic hydrogels. Velev and co-workers utilized this motif to electrically regulate walking in a hydrogel.[458] Anionic and cationic legs prepared from an acrylamide/sodium acrylate copolymer and an acrylamide/quaternized dimethylaminoethyl methacrylate, respectively, can be bound via polyion complexation under an applied electric field. When a field is applied such that the cathode and anode face the cationic and anionic legs of the walker, respectively, an osmotic pressure difference between the walker legs and the surrounding solution induces a bend in the cationic leg toward the anode and a simultaneous bend in the anionic leg toward the cathode. By mechanically tuning the friction of the cationic leg and the dimensions of the anionic leg, the walker "steps" toward the anode in the absence of a ratcheted substrate (Figure 19d). When the field is reversed, the deformation of the legs reverses and the walker takes a step. Repeatably reversing the polarity of the applied field is shown to generate sustained motion, the magnitude of which is highly dependent on both the concentration of fixed ions in the hydrogel and the mobile ions in the solution. Chu and co-workers have synthesized a similar anionic hydrogel walker using attenuation-based UV photopolymerization.[467] Here, a ratcheted surface is used to propel the walker under the application of an electric field. Further, their work demonstrates the potential of electroactive walkers for remote cargo transport, presenting a hydrogel that can displace a load up to 125% its own weight (Figure 19e).

The electromechanical response of ionic hydrogels has more recently been 3D printed to localize function. For example, Lee and co-workers utilized an osmotic pressure gradient in a monolithic, 3D printed, anionic hydrogel to generate precise architectures displaying sequential deformation.[468] They prepared a mechanical system containing thin, hair-like structures connected by a thicker bridge capable of transporting an object. When a current is applied, the hairs quickly deform towards the cathode, propelling an object towards the bridge (Figure 19f). The thicker bridge displays the same macroscopic response, but on a longer length scale due to its increased thickness. Under a continuous current, the bridge eventually bends, allowing the field to be reversed and the direction of hairs to be switched without pushing the transported object backwards. Over time, the bridge closes, and the transportation process can be repeated.

8.2.2. Composite Bilayers

As discussed hereto, a common approach to realizing local deformation is in the preparation of bimorphs. Comparatively, bilayer hydrogel material systems lack the spatial resolution and local control of shape change when compared to the techniques described in Section 8.2.1. However, the modulus contrast between two distinct hydrogel layers can enable larger magnitude deformations, as well as leverage other response mechanisms that are relevant for implementations in robotics.

A recent example of a composite bilayer actuator was presented by Chen and co-workers who prepared a hydrogel containing a poly(acrylic acid-*co*-acrylamide) (p(AAc-*co*-AAm)) layer with a UCST of 37.5 °C, and a poly(*N*-isopropylacrylamide) (PNIPAm) layer with an LCST of 33.5 °C.[469] At low temperatures, the PNIPAm layer is swollen, which causes the hydrogel bimorph to deflect towards the p(AAc-*co*-AAm) layer. When heated above the UCST of the p(AAc-*co*-AAm) layer, the layer expands due to swelling as the PNIPAm layer simultaneously shrinks and undergoes a volume phase transition. This process is reversible and can be used to prepare hydrogel actuators that function in open air and can grasp a heated object (hydrogels used in air are coated with oil to prevent evaporation of internal water, **Figure 20**a).

A distinct opportunity in preparing composite hydrogels is the ability to introduce sequential, stepwise actuation. The most conventional approach to incorporate sequential deformation in a hydrogel is via the preparation of material bimorphs with differing LCSTs and UCSTs. So and Hayward demonstrate sequential deformation of a PNIPAm hydrogel by varying segment concentrations of acrylic acid (AAc) or methyl acrylate (MA) to tune the UCST in ionic liquid media.[462] The UCST of the PNIPAm homopolymer is measured at 41 °C (PNIPAm only displays a UCST in ionic liquids). Conversely, the UCST of PNIPAm containing

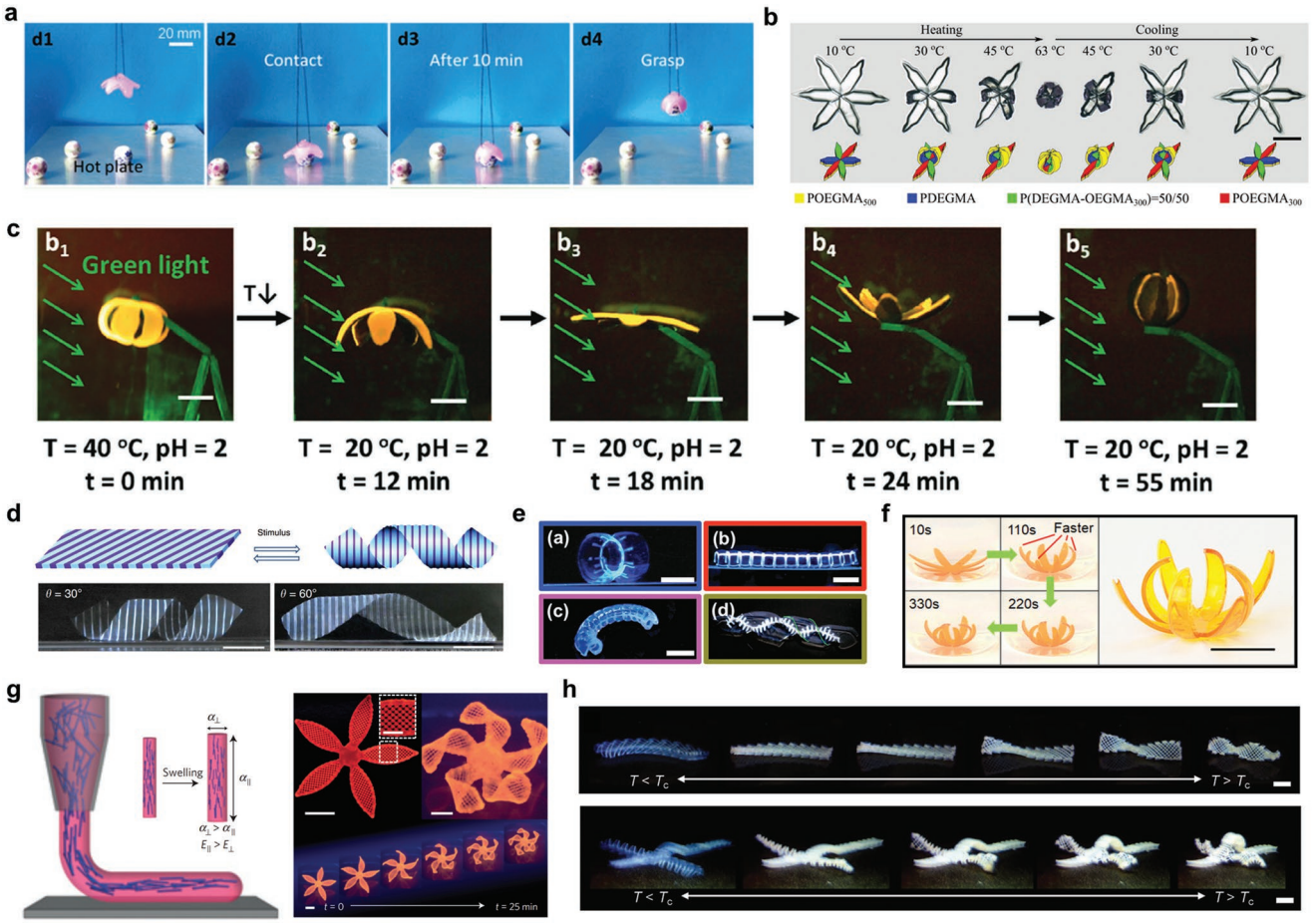

Figure 20. Programmed anisotropy in hydrogels. a) A lower/upper critical solution temperature (LCST/UCST) bilayer gripper capable of grasping heated objects in non-aqueous environments. Reproduced with permission.[469] Copyright 2018, RSC. b) Sequential folding in a bilayer gripper with LCST variation across the arms. Reproduced with permission.[470] Copyright 2018, Wiley-VCH. c) Multi response flower-like hydrogel exhibiting temperature induced folding and pH induced fluorescence. Reproduced with permission.[471] Copyright 2017, Wiley-VCH. d) Sequential photopolymerizations generate patterned modulations in hydrogel swelling ratios resulting in twisted deformations under temperature or ionic media. Reproduced with permission.[474] Copyright 2013, Springer Nature. e) Increasingly complex 2D photomasking generating rolling and twisting in hydrogels. Reproduced with permission.[475] Copyright 2015, RSC. f) DLP printing of hydrophilic and hydrophobic bilayers displaying sequential folding at elevated temperatures. Reproduced with permission.[479] Copyright 2018, American Chemical Society. g) 3D printing via direct ink writing (DIW) of acrylamide-based hydrogels with shear aligned cellulose fibers resulting in anisotropic parallel and perpendicular swelling ratios. Reproduced with permission.[480] Copyright 2016, Springer Nature. h) DIW of thermally responsive poly(*N*-isopropylacrylamide) hydrogel containing non-responsive poly(ethylene glycol) (PEG) components facilitating patterned uniaxial contraction. Reproduced with permission.[482] Copyright 2015, RSC.

6 mol% of the hydrogen-bonding-capable AAc increased the UCST to 75 °C, and inclusion of 10 mol% of the non-hydrogen-bonding MA decreased the UCST to 32 °C. Sequential folding of the composite hydrogel is regulated by the UCSTs of the materials. Gracias and co-workers demonstrated similar sequential folding over a narrower temperature range in bilayers of poly[oligo (ethylene glycol) methyl ether methacrylate] (POEGMA) with a tunable LCST.[470] The LCST is tuned from 18 to 50 °C by varying the concentration and side chain length of the ethylene glycol units in three separate gels. Actuators are prepared via sequential photopolymerizations with the use of a photomask to prepare a gripper with bilayer arms displaying different volume transition temperatures (Figure 20b). When the temperature is raised, the arms sequentially close in the order of their LCSTs. Such actuation can be cycled reversibly over 20 times.

Chen and co-workers reported on multistimuli, sequential response in a hydrogel bilayer prepared from a thermally responsive graphene-oxide/PNIPAm (GO-PNIPAm) layer and a pH-responsive perylene bisimide-functionalized hyperbranched polyethylenimine (PBI-HPEI).[471] In low-temperature water (below the LCST of the GO-PNIPAm film) a flower-like bilayer gel deforms to a closed state. Upon heating, the hydrogel deswells and unfolds. When the flower is "open", green light exposure induces a fluorescence response in the PBI layer. This response is enhanced in acidic conditions. The fluorescence response can be sequentially deactivated by turning off the light, or by cooling the pNIPAM layer, closing the flower via reswelling, and preventing light penetration into the interior of the flower (Figure 20c).

Unique macroscopic responses in bilayers can also be achieved by asymmetric assembly of the individual bilayers.

For example, Zhao and co-workers reported a supramolecular approach for preparing asymmetric hydrogels that utilizes the guest–host interactions of ferrocene and β-cyclodextrin as a "lego" like assembly mechanism.[472] A β-cyclodextrin-containing, responsive hydrogel based on an acrylamide/carboxylic acid copolymer is linked to a nonresponsive hydrogel (also containing β-cyclodextrin) via a nonresponsive, ferrocene containing hydrogel.[472] A β-cyclodextrin-containing, responsive hydrogel (red) based on an acrylamide/carboxylic acid copolymer is linked to a nonresponsive hydrogel (blue, also containing β-cyclodextrin) via a nonresponsive, ferrocene containing hydrogel (orange/brown). By simply pressing the responsive and nonresponsive gels together with an intermediate ferrocene gel, unique architectures are created that display buckling and out-of-plane deformation. Chu and co-workers used a similar approach where bilayers of p(NIPAm-*co*-AAm) are prepared containing various concentrations of clay nanosheets.[473] Intermolecular hydrogen bonding interactions between the hydrogel layers stabilize the resultant materials. Layers containing increased nanosheet concentrations display a decreased volume phase transition relative to a noncomposite p(NIPAm-*co*-AAm) hydrogel at comparative temperatures, resulting in anisotropic shape change and swelling when constructed in asymmetric geometries.

8.2.3. Multimaterial Monoliths

Shape programming in hydrogels can be realized in bilayers, patterned composites, and printed elements. By spatially localizing the bilayer, nonuniform swelling stresses may be achieved resulting in complex deformations. Kumacheva and co-workers presented a means to impart prescribed, 3D shape change by the inclusion of small-scale but distinct modulations in a hydrogel material (Figure 20d).[474] Here, a PNIPAm hydrogel sheet is swollen with 2-acrylamido-2-methylpropane sulphonic acid (AMPS) and a diacrylamide diacrylate prior to UV photopolymerization through a photomask. By controlling the width and angle of a series of AMPS containing lines, the PNIPAm gel curls into a helix when heated or exposed to an ionic aqueous solution as the PNIPAm gel shrinks and the AMPS lines remain swollen (Figure 20e).[475] Hong and co-workers utilized similar patterns in pH responsive bilayers to achieve reversible switching between left and right handed helices,[476] and Zhu and Wang utilized an evaporative method to create high modulus contrast bilayers that display rapid and reversible helix formation.[477]

Sequential photopolymerizations have also been used to achieve large-scale patterning in bilayer hydrogels. Wang et al. utilized photomasking and preswelling to control the deformation direction of hydrogel strips prepared with high-swelling, p(NIPAm-*co*-AMPS) disks, embedded in a PNIPAm gel.[478] By using a mask and exposing alternating sides of the hydrogel to water, a series of directional bends can be achieved due to the induction of a through-thickness swelling gradient. By immersing in an ionic solution, the swelling mismatch between the p(NIPAm-*co*-AMPS) disks and the pNIPAM gel is reduced, and then reversibly amplified by reimmersion in pure water. A single strip can be repatterned via controlled water exposure using the masking technique to generate a range of bending geometries. Fang and co-workers utilized a DLP process to rapidly prepare large-scale bilayers of alternating chemistries that display origami-like folding and sequential deformation.[479] First, a swellable poly(ethylene glycol) diacrylate (PEGDA) is polymerized in a series of patterns and then reassembled into a closed cell of defined thickness. A hydrophobic poly(propylene glycol) dimethacrylate (PPGDMA) is then infilled and polymerized to create a monolithic material. When placed in water, the PEGDA layer swells, and the materials bend towards the PPGDMA layer. By controlling the thickness and location of the PEDGA layers, complex folding geometries can be achieved along with sequential deformation in appropriately structured materials (Figure 20f).

Direct ink writing (DIW) has also been used to prepare patterned hydrogel actuators. Lewis and co-workers introduced anisotropy into acrylamide-based hydrogels by the inclusion of cellulose fibers.[480] The rigid cellulose fibers shear align parallel to the print direction, leading to anisotropic swelling in the hydrogel composite as a function of modulus mismatch in the parallel versus perpendicular axes ($E_{\parallel} > E_{\perp}$). Consequently, bilayers are prepared with the swelling anisotropy precisely specified in the xy plane resulting in complex curvature and bending in 3D geometries (Figure 20g). Similarly, DIW has been used to prepare bilayer hydrogel hinges in controlled geometries for reversible thermally, induced bending. Spinks and co-workers demonstrated that the rheological properties needed for controlled printing are accessible through the inclusion of high molecular weight polymer materials.[481] Yum recently utilized a similar approach by DIW printing of isotropic PNIPAm hydrogels reinforced with poly(ethylene glycol) (PEG) polymer chains.[482] By use of a fugitive carrier (a shear-thinning material that can be selectively removed from the polymerized hydrogel matrix), a series of homogeneous, multilayer hydrogels are prepared from low molecular precursors. As the PEG regions are not thermally responsive, PNIPAm-based swelling in the direction of the PEG filaments is resisted, resulting in perpendicular uniaxial contraction. When prepared in anisotropic layers, the swelling directionality allows for the programming of thermally responsive bends and twists (Figure 20h).

9. Liquid Crystal Elastomers and Networks

The polymerization of liquid crystalline monomers is a facile approach to prepare liquid crystalline polymer networks (LCNs) and elastomers (LCEs). When subjected to surface-enforced, field-assisted, rheological (shear), or mechanical alignment LCNs or LCEs become oriented and accordingly, exhibit mechanical anisotropy. This anisotropy is evident in the moduli difference in these materials. The modulus measured along the director axis (for nematic materials) is considerably larger than the modulus measured perpendicular to the director axis. Further, subjecting these aligned materials to stimuli (such as heat or light) can generate directional strain. Preparing these materials with local variation in the director orientation[483,484] is an emerging route to realizing shape programmable

elements,[483,485,486] topographical surface features, and material actuators.[487,488]

Liquid crystalline polymeric materials were first prepared nearly 100 years ago.[489,490] Within a historical context, current efforts focused on generating mechanical adaptivity in liquid crystalline polymer networks and elastomers are founded upon materials examinations reported in the 1980s. The pioneering efforts of Finkelmann realized the synthesis of LCEs consisting of lightly crosslinked polymer networks with side-chain or main-chain mesogenic units. Finkelmann's sustained efforts in nearly all cases prepared LCEs from polysiloxane compositions.[491–494] Almost concurrently, the reports of Broer et al. detailed the preparation of LCNs from the photopolymerization of multifunctional liquid crystalline monomers.[495–498] Comparatively, LCEs exhibit larger deformations associated with order disruption, achieving macroscopic contractions of 75%.[499] Conversely, the highly crosslinked nature of LCNs limits the influence of stimulus exposure on order and generates appreciable but comparatively limited directional strain. However, the stiffness of LCNs can generate greater work outputs in certain implementations. Accordingly, both LCEs and LCNs have been widely examined for potential use in actuation as well as soft robotics.

9.1. Materials and Mechanism of Transformation

9.1.1. Alignment of Liquid Crystals

Introducing, enforcing, or directing macroscopic alignment of the nematic phase within LCEs and LCNs is key to assessing and realizing large directional strains that largely motivate the burgeoning interest in these materials as actuators and robotic elements. Generally speaking, there are two primary means of introducing alignment: 1) mechanical (rheological) programming or 2) surface (field) alignment. Mechanical orientation of LCEs is most often associated with the platinum-catalyzed reaction of alkene-terminated LC mesogens with the Si—H bond of polysiloxane monomers (and polymers). The so-called "Finkelmann" method of mechanical programming prepares these materials in a two-stage reaction. The material is partially polymerized and then subjected to load to align the director axes of the mesogens in the materials. The reaction is completed with the material subjected to load.[499–501] This route enabled the initial preparation of LCE with single-crystal or monodomain orientation in film or fiber geometries. Yakacki and co-workers reported a two-stage reaction that emulates this method but employs a more accessible synthetic approach.[502] These authors prepare a lightly crosslinked network via a nucleophile catalyzed thiol-Michael click reaction. Subsequent mechanical programming introduces alignment to the material. Photoinitiated polymerization of excess acrylate groups completes the reaction and allows the LCE to retain the aligned state.[502,503]

Another related approach to mechanically align LCE is enabled by dynamic covalent chemistry.[504–507] Most frequently, transesterification or disulfide exchange is utilized to break and reform bonds via thermal, base, or radical catalyzed pathways. The restructuring of these dynamic linkages is central to the reconfigurations enabled by these formulations. In 2014, Pei and co-workers described a pioneering approach for incorporating these transesterifying chemistries into thermally triggered DCCs in LCE systems.[505,508] Thermally induced bond exchange has been further implemented by Kessler and co-workers, who prepared a multifunctional LCE epoxy network that allows for recycling and reprogramming of the LCE through disulfide bond exchange.[509] Bowman and co-workers have described a strategy using reversible addition fragmentation chain transfer (RAFT)-based DCC to induce stress relaxation in LCN films via an allyl sulfide bond exchange mechanism.[510] This is of particular relevance to LCEs that generate internal stress when heated, since the photoinduced plasticity afforded by the allyl sulfide bond exchange can relax stress, reorganize the polymer network, and stabilize different LCE conformations.

Surface-enforced alignment is widely applied to induce uniform orientation in low molar mass liquid crystals. Several review articles detail the fundamentals of surface-enforced alignment of liquid crystals.[511–513] Most commonly, polymeric materials (polyvinyl alcohol, polyamide, polyimide) are cast onto substrates (typically glass) and mechanically rubbed. The rubbing of these alignment layers introduce grooves that orient the near surface liquid crystals (anchored).[514–516] The enforcement of alignment at the surfaces is translated across the bulk associated with intermolecular interactions of liquid crystals. Similar approaches can be employed to generate homeotropic orientation through the cell thickness.[517] An increasingly popular approach to introduce surface-enforced alignment of liquid crystals is photoalignment.[513,518,519] Photoalignment layers are spin cast onto a rigid substrate and are typically composed of small photochromic molecules such as azobenzene and cinnamates. The dichroic nature of these materials makes them sensitive to polarized light, which can be used to induce uniform orientation of the dye molecules. Patterned exposure to linearly polarized light is a facile means of complexly patterning local variation in the director orientation. Not all polymerizable compositions of liquid crystal monomers are amenable to surface-enforced alignment. The liquid crystalline monomers, such as those of Broer, can be surface aligned both by polymeric and photoalignment surfaces. Arbitrary patterns of complex director profiles have been imprinted into LCNs[485,486] and LCEs.[483]

9.1.2. Stimuli-Response of LCEs and LCNs

The mechanical anisotropy of LCEs and LCNs as well as the stimuli-generated directional strain results in uniaxial or shape transformative mechanical responses. The mechanical response of LCEs is associated with stimuli-induced disorganization of the mesogen and polymer chain orientation. Most commonly, heat is used to induce thermotropic disruption of order in LCE. The mechanical anisotropy and directional strain of a uniaxially aligned LCE are associated with prolate (or oblate) orientations of the LC mesogens. Physically, this can be described as anisotropy in the radius of gyration of these materials in the parallel ($R_{\parallel}$) and perpendicular ($R_{\perp}$) axes. Polymer chains within main-chain LCEs adopt a prolate conformation and are elongated parallel to the nematic director, such that $R_{\parallel} > R_{\perp}$.[499,524] Heating

the material disrupts this anisotropy and the polymer networks approaches an isotropic state in which the polymer chains adopt a spherical, random-coil conformation (e.g., $R_{\parallel} \approx R_{\perp}$). Accordingly, an LCE exhibits macroscopic contraction along the nematic director.[520] Removing the order-disrupting stimuli (in this case, by cooling) reverses the strain response and the network memory of the material recovers the original order and orientation.

As densely crosslinked materials, the polymer network of LCNs maintains orientation and alignment when heated. Accordingly, mechanical deformation of LCN can be described by anisotropic thermal expansion, characterized by the coefficient of thermal expansion (α). When heated, the LCN expands perpendicular to the director orientation due to an increase in intermolecular distance between mesogens within the polymer networks.[521] Depending on materials composition, α in the parallel direction is near zero below the T_g of the LCN and becomes negative above T_g. The magnitude of the thermal expansion coefficients (and the resulting strains) can be enhanced by tilt of the mesogens. In a uniaxially aligned LCN, modest changes in length can be observed (3–10%). As will be discussed, adjusting the hierarchical orientation of LCNs in twisted or splay orientations can realize large deformations despite the limited strain.[522,523]

Photoinduced mechanical effects in LCE and LCN are also subject to intense interest. Commonly, absorbing materials (such as guest dye molecules or nanoinclusions) are embedded in LCE or LCN to allow for optical generation of heat (photothermal effects).[524] Photochemical processes have also been widely examined. Photochemical mechanisms employ chromophores (typically azobenzene) that undergo light-induced transformation capable of disrupting order in LCE. The phototropic nature of azobenzene-functionalized LCE is attributable to the isomerization of azobenzene from the "rod-like" trans isomer into the bent cis isomer. The photoisomerization of azobenzene disrupts intermolecular interactions in these materials and reduces or disrupts order.[525] In this sense, the phototropic reduction in order in an azobenzene-functionalized LCE is similar to the thermotropic mechanism described above.[526,527] Photochemical approaches to generate mechanical responses in azobenzene-functionalized LCNs are also widely reported. Two methods have been explored: 1) photoisomerization[499,528] or 2) orientation by exposure to linearly polarized light (Weigert effect).[529–531] Mechanically, prior reports have used light to induce bending in LCN,[530,532] twisting,[533,534] and even photoinduced motility[532,535–537] Other chromophores have been examined as approaches to realize photomechanical effects in LCN.[538]

Electromechanical effects in LCE have also been examined. Commonly, Joule heating of LCE by flexible or printed electrodes transduces electrical input into deformation. True electromechanical coupling has been explored via two mechanisms. The first is associated with the inherent dielectric anisotropy of liquid crystals ($\Delta\varepsilon = \varepsilon_{\parallel} - \varepsilon_{\perp}$; ε, dielectric constant). Application of an electric field of sufficient strength can distort the orientation of the mesogens to align parallel (positive $\Delta\varepsilon$) or perpendicular (negative $\Delta\varepsilon$) to the direction of the field. The reorientation of the mesogens in the LCE generates strain. However, the field strength required to introduce electromechanical effects in LCE via reorientation is large.[539–541] Accordingly, most examinations have focused on electromechanical effects that soften the materials by forming liquid crystal gels.[542–544] The inclusion of carbon nanotubes (CNT) to form LCE nanocomposites has also been explored as an approach to realize electromechanical effects in a related mechanism.[545,546] Very recently, the mechanical anisotropy of LCEs has been explored as dielectric elastomers where deformation is caused by directional differences in Maxwell stress.[547] An LCE with ionic liquid inclusions has been shown with similar bidirectional deformation as IEAP, as described in Section 5.[548]

9.2. Structural Motifs Enabling Function

9.2.1. Uniaxial Films and Fibers

Mechanical deformation of uniaxially aligned LCEs and LCNs has been widely explored in films or fibers.[499–503] Finkelmann first reported mechanical deformation of aligned LCEs under load.[549] A subsequent examination by Ikeda reported polarization-controlled bending in LCNs.[528] Since these seminal contributions, films have become the most commonly used form factors among LCN and LCE actuators, with countless compelling actuators developed therefrom. Giant lateral ferrostriction,[93] photomobility,[537] weight-lifting,[488] and all optical control of shape[550] are just a few examples of the vast functional outcomes of which these materials are capable. In 2004, Shelley and co-workers demonstrated a fast dye doped liquid crystal elastomer film that "swims" away from a point illumination source in water due to the force that its deformation exerts on the surrounding water.[551] In 2017, Priimagi and co-workers described an LCE-based flytrap device in which a light-responsive LCE film is mounted to an optical fiber. The optical feedback that results from an object entering the field of view of the LCE (such as a fly) increases light absorption into the LCE film and its subsequent folding from an open to a closed state.[552]

Fiber-based LCEs have been utilized in numerous actuation systems that can perform cyclical work cycles as well as contexts that have been inspired by biological machinery.[553–555] In 2003, Ratna and co-workers reported a nematic elastomer fiber actuator that is prepared by drawing out the fiber with tweezers from a bead of melted polymer and an isocyanate crosslinker, MDI. The mechanical drawing process yields fibers that are strongly birefringent and show lower viscoelastic losses and a maximum retractive force of 274 kPa.[556] In 2009, Broer and co-workers reported all-polymer microdevices based on LCE fibers that are prepared via photolithography by selectively patterning thin films of LCEs.[553] Later, this protocol was modified to prepare LCE fiber arrays in which drawn fibers are aligned perpendicular to their substrate. In the latter case, LCE fiber arrays are prepared by drop-casting bead arrays of oligomer solutions in between glass slides, then slowly separating the slides to draw out the fibers before fully polymerizing them. Arrays of anisotropic fibers prepared with this method are responsive and of similar scale to the cilia that propel motion in numerous biological systems.[557] In 2017, Parmeggiani and co-workers prepared LCE fibers from LCE polymeric precursors that are drawn out into their desired shape before being crosslinked. When attached to a mirror, the anisotropy of the aligned LCE fibers facilitates

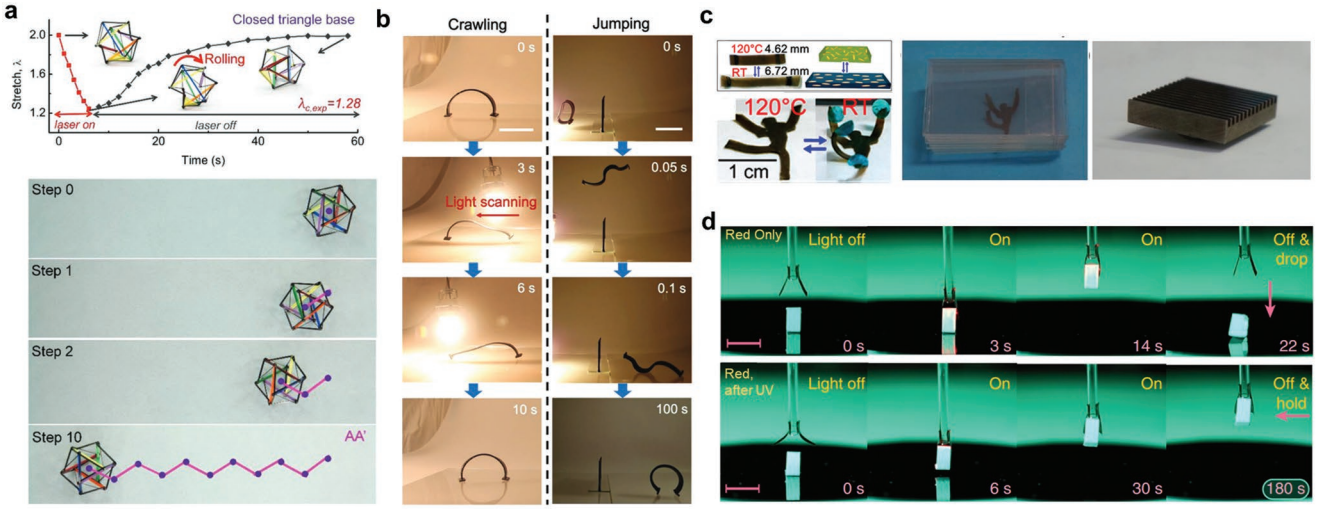

Figure 21. Uniaxial deformation in monodomain liquid crystal elastomers (LCE) and liquid crystal networks (LCNs). a) Photothermally induced fiber contraction generates rolling in a tensegrity robot. Reproduced with permission.[562] Copyright 2019, Wiley-VCH. b) Bioinspired crawling and jumping motions in carbon nanotube (CNT)-filled monodomain LCE. Reproduced with permission.[563] Copyright 2019, Wiley-VCH. c) Light-reprocessable monodomain actuator. Reproduced with permission.[564] Copyright 2016, ACS Publications. d) Reprogrammable photoresponsive gripper. Reproduced under the terms of the CC-BY Creative Commons Attribution License (https://creativecommons.org/licenses/by/4.0/).[566] Copyright 2018, The Authors, published by Springer Nature.

rotation and contraction under selective light stimulus, which allows the LCE to change the mirror orientation and operate as a remote beam steerer unit.[558] The following year, Sharma and Lagerwall reported preparation of core–sheath LCE fibers through electrospinning that can undergo irreversible contraction due to the stiffness of the passive sheath polymer.[559] More recently, Qi and co-workers harnessed the thiol-Michael reaction to extrude LCE fibers to emulate muscle fiber.[560] By weaving fibers together, the force in an arm-like actuator increases with fiber count. Another very recent example is the exploration of LCE fibers by Hayward and co-workers. These authors prepared mechanically aligned LCE fibers with inclusion of photothermal heaters[561] that are locally swollen with a gold salt solution followed by a photochemical reduction of Au^{3+} to Au^0. Photothermal heating of the fiber is induced with 532 nm laser exposure, which induces bend and repositions the waveguided light.

LCE fibers have been incorporated into soft robotics. In one example, Cai and co-workers prepared a carbon nanotube (CNT) LCE composite tensegrity robot and realized locomotion through a photothermal mechanism.[562] LCE nanocomposite fibers can be drawn into and placed as active elements in a series of plexiglass struts to prepare an icosahedron (12 open isosceles triangles and 8 closed equilateral triangles, **Figure 21**a). The tensegrity strain in the mechanical system is adjusted by actuation of the local LCE nanocomposite fibers. Local irradiation with NIR light induces directed motility across both smooth and uneven surfaces. This same group prepared a mechanically aligned, CNT–LCE composite[563] and subjected this system to magnetic stimuli to induce bioinspired deformations, including crawling and jumping (Figure 21b)

Ji and co-workers prepared a dynamic covalent network consisting of an ester-containing LCE.[564] Upon infrared light irradiation, a photothermal transesterification reaction is triggered to enable mold-less reprocessability. The use of light affords spatial and temporal control over the alignment process and can be used to generate a macroscopic deformation. By careful adjustment of the light intensity, a temperature gradient is generated through the thickness of the film resulting in a bending deformation. Further, the spatial control over alignment afforded by the light-induced programming facilitates the preparation of dynamic 3D structures. A lifting element prepared in this way is able to lift 1000× its weight (Figure 21c). Light-induced dynamic reprocessing was also utilized by Bowman and co-workers in the form of a photoinitiated, radically-mediated, addition–fragmentation process to reversibly fold and unfold origami.[565] Priimagi utilized a multi-wavelength process in an azobenzene LCE to photochemically trap, and then photothermally release, strain in a uniaxially aligned LCE to tune deformations. Under a combination of sequential UV, blue, and red light exposures, a reconfigurable gripper was realized (Figure 21d).[566]

9.2.2. Bending through Strain Gradients

A variety of approaches have been explored to induce bending responses attributable to heterogeneity in either the magnitude or directionality of strain across the material thickness. Early demonstrations from Ikeda and co-workers,[528] Tabiryan et al.,[529] and White[530] explored bending of uniaxially aligned LCN to UV and blue-green light. The considerable absorption of light by the azobenzene chromophores resulted in nonuniform light intensity across the material thicknesses, which causes bending. At higher intensities, White and co-workers induced oscillation through a self-shadowing effect in the deflection of cantilevers.[366,567,568]

A unique aspect of LCEs and LCNs is the ability to prepare polymer networks with through-thickness variation in mechanical properties. Two geometries have been examined—twisted nematic and splay. The nematic director of LCEs or LCNs

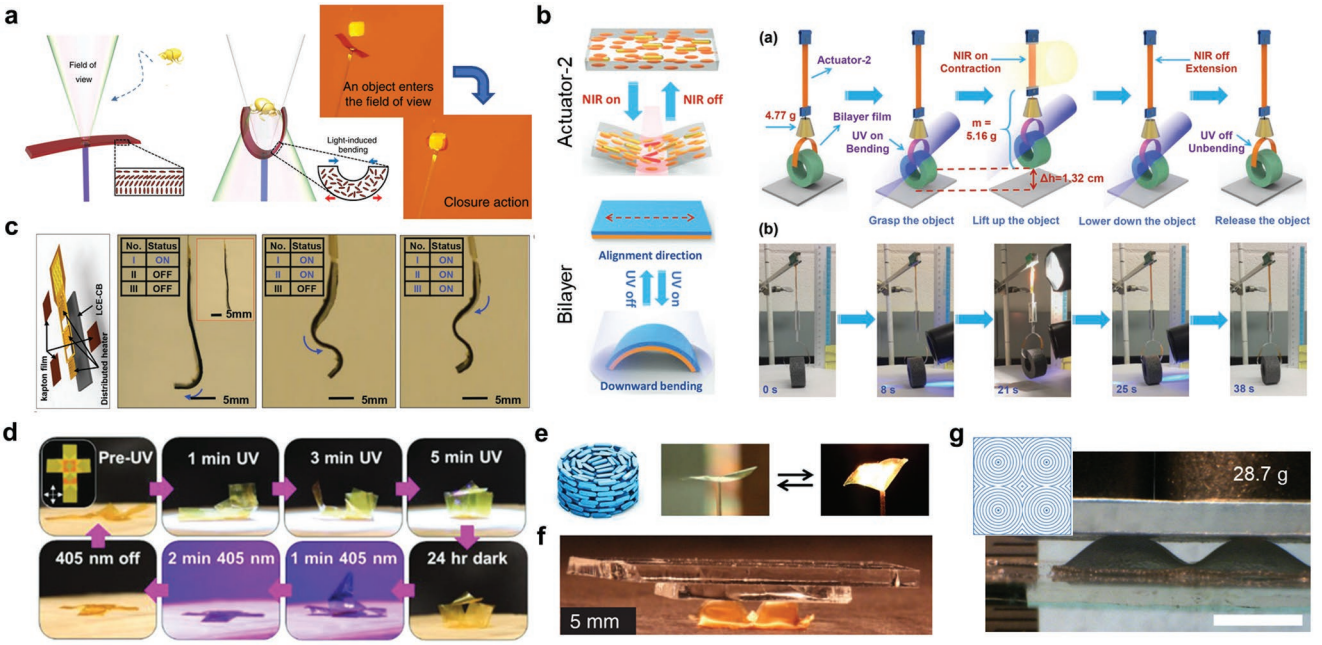

Figure 22. Surface aligned and bilayer material systems based on liquid crystal elastomers (LCEs) or polymer networks (LCN). a) Splay-aligned artificial flytrap capable of sensing-based actuation. Reproduced with permission.[552] Reproduced under the terms of the CC-BY Creative Commons Attribution License (https://creativecommons.org/licenses/by/4.0/). Copyright 2017, The Authors, published by Springer Nature. b) Photothermal and photochemical bilayer composite crane actuator. Reproduced with permission.[573] Copyright 2018, Wiley-VCH. c) Sequential deformation in a monodomain LCE containing three individually controlled Joule heating elements. Reproduced with permission.[574] Copyright 2018, Wiley-VCH. d) All-optical folding of an origami box with programmed director profile. Reproduced with permission.[550] Copyright 2019, Wiley-VCH. e) Orientation and deformation of a +1 azimuthal defect in LCN. Reproduced with permission.[485] Copyright 2012, Wiley-VCH. f) 3 × 3 array of azimuthal +1 defect deforming under load with a stroke of greater than 3000%. Reproduced with permission.[483] Copyright 2015, AAAS. g) Lamination of programmed LCE enable deformation under load more than 1100× the film weight. Reproduced with permission.[488] Reproduced under the terms of the CC-BY Creative Commons Attribution License (https://creativecommons.org/licenses/by/4.0/). Copyright 2018, The Authors, published by Springer Nature.

prepared with a splay orientation twist from planar on one surface to normal (homeotropic) on the other surface. This geometry is particularly conducive to bending. Upon exposure to a stimulus, the film contracts along the planar axis and expands along the homeotropic side. These mechanical responses are cooperative and enhance the magnitude of deflection in the direction of the planar oriented surface when compared to uniaxially aligned or twisted nematic LCE or LCN. This deformation is particularly suited to prepare grippers and walkers in robotic implementations. Broer and co-workers document the photoinduced motility achieved in a splay aligned LCN prepared with rapidly relaxing push-pull azobenzene chromophores.[569] Irradiation conditions produce a self-shadowing effect to generate wave-like motion. Harnessing the wave-like motion in a rigid frame enables motility. Further, Schenning and co-workers demonstrated a simple robotic actuator prepared as a composite of a photoresponsive splay aligned LCN gripper and magnetic strip of PDMS.[570] Under visible light exposure, the gripper opens via a photothermal mechanism. The magnetic PDMS element allows the gripper to be moved and rotated. Priimagi and co-workers utilized splay alignment to prepare a number of LCN soft robotic actuators. In an earlier example, autonomous activation was demonstrated in a light-driven artificial flytrap.[552] By utilizing a optical fiber as the anchor for a splay aligned LCN, optical feedback in the form of scattered light or heated air (through strong light absorption of a targeted object) results in a photochemical or photothermally induced bend and closing of the film as it approaches a target (**Figure 22**a). Priimagi and co-workers also harnessed visible light heating in an azobenzene LCE to produce caterpillar inspired locomotion.[571] Here three segments of splay alignment can be patterned to induce opposite bending deformations along the length of the film. When the light source is modulated over the sample, the LCE reversibly flattens and crawls.

Stimuli-induced and regulated bending has also been achieved in LCE and LCN bimorph. As described hereto, a bimorph typically is composed of a monodomain LCE laminated with another material. This geometry was explored recently by Zhao and co-workers to prepare a photothermal LCE actuator. In this examination, the bimorph is prepared by sequential polymerization to form an element with one side polymerized in the monodomain state (directional strain) and the other polymerized in the polydomain state.[572] When irritated with light, the actuating side contracts along the nematic director causing the bimorph to bend. These authors realized motility through scanned laser irradiation. This group also reported a bimorph composite with layers containing gold nanorods or azobenzene chromophores to enable differentiated photothermal and photochemical deformation.[573] Concurrent irradiation (UV and NIR) allows the material to realize simultaneous or sequential motions including grasping/releasing and lifting/lowering of an object (Figure 22b).

Bending can also be observed in bimorphs through Joule heating. For example, Yu and co-workers prepared a uniaxially aligned LCE with an integrated polyimide–Au heater.[574] When doped with carbon-black to improve the thermal conductivity, the directionality of deformation of the Kapton/LCE composite is controlled by an electric field. The inclusion of additional heaters and localization of Kapton films enables the preparation of a composite material system capable of motility (Figure 22c). Zhao and co-workers also employed Joule-heating to prepare to a series of LCN actuators.[575] These authors assimilated shape memory processing of a glassy LCN via compression molding to realize a reversible gripper, walkers, and a conveyor.

9.2.3. Twisting and Folding

LCE and LCN in the twisted nematic orientation have a continuous 90° rotation of their director profile through the thickness of the material. Inclusion of small concentration of chiral additive homogenizes the twist (right-handed or left-handed). An initial demonstration from Broer and co-workers demonstrated twisting.[532] Later, Urayama and co-workers systematically characterized the geometrical considerations of twisting in LCN with twisted nematic orientation to form either spiral ribbons or helicoids.[576] Wie et al.[577] as well as Katsonis et al.[534] extended on these initial works to photoinduce and regulate twisting.

Twisted nematic patterning in liquid crystals has also been employed to impart folding of LCE or LCN sheets, as a twisted nematic film contracts through the thickness (z) when exposed to a disorganizing stimulus. In liquid crystals, multiple folds may be patterned; however, the thickness contraction in the twisted nematic hinge also generates orthogonal strain in x and y, which can generate deleterious mechanical response. A research team at the Air Force Research Laboratory prepared twisted nematic hinges guided by mechanical design to realize self-folding of an origami box.[578] White and co-workers employed this same pattern to all-optically regulate formation of a folded box and recovery of the flat state.[550] Due to the long-life time of the azobenzene chromophore utilized in this examination, the closed-box deformation remains stable for up to 24 h. Upon visible light exposure, the *cis*→*trans* isomerization releases the photoinduced strain, the box opens and returns to its flat state (Figure 22d).

9.2.4. Curvature

Modes et al. predicted that variation of the director orientation described by topological defects would form elements of Gaussian curvature such as cones or anticones.[579,580] These patterns can be realized by various photoalignment approaches. A number of these activities have focused on the +1 azimuthal defect. This topology is such that the nematic director rotates concentrically around a central point. Subjecting LCNs or LCEs to stimuli generates directional strain, such that the film contracts in the azimuthal direction and extends in the radial direction. Accordingly, the stimuli-response of these materials results in the conversion of a flat sheet into a cone with the strain distribution centered at the defect. Initial experiments from Broer and co-workers document the experimental confirmation of the deformation of these topological director profiles into the expected cone and anticone (Figure 22e).[485] White and McConney prepared azobenzene-functionalized LCNs over a range of charge strengths (±10) and examined the differentiated mechanical response. Later, Ware et al. prepared arrays of +1 azimuthal defects enabled by the realization of synthetic approaches to prepare LCEs amenable to photoalignment.[483] Heating the patterned LCE generates nearly 2 J kg^{-1} of specific work at a stroke of 3000% (Figure 22f). Similar response can be realized in azobenzene-functionalized LCEs.[550,581] A recent demonstration extending upon these efforts realized a specific work of 20 J kg^{-1} by laminating LCE to prepare actuating materials capable of lifting 2500× their own weight (Figure 22g, 4 × 4 lifting 1100× film weight).[488] Wei and Lavrentovich have reported on the preparation of patterned topologies via plasmonic masks.[582]

9.2.5. 3D Printed Elements

Very recently, LCE and LCN have been prepared via additive manufacturing methods. Wiersma and co-workers documented a microscale 3D printed LCE actuator[583] in which the photoresponsive LCE elements are printed via direct laser write printing (DLW) and adjoined to high modulus substrates. Motility was observed to light exposure. White and co-workers used similar methods to prepare hybrid actuators via multimaterial compositions in LCEs.[584] The cationic epoxy polymerization used by these authors is particularly suited for printing high-resolution structures in oxygen-rich environments.

LCEs are commonly aligned by mechanical or rheological forces. 3D printing methods, such as DIW have been shown as facile methods to print LCE films and fibers (**Figure 23**a).[585] Spatial control of the orientation by flow directionality enables the preparation of complex topologies similar to those realized via photoalignment. Ware and co-workers first reported 3D printing of LCEs[587] via DIW and utilized oligomers prepared via aza-Michael reactions of a commercially available liquid crystalline monomer. These authors demonstrated mechanical reconfiguration of LCEs. Thermomechanical deformation of the 3D printed LCE prepared with a +1 topological defect also forms the cone predicted by Warner and Modes (Figure 23b).[587] Enabled by printing, adjacent regions of positive and negative Gaussian curvature generate elastic instabilities (snap-through) that these authors employed to catapult an object. Almost concurrently to this report, Lewis et al.[585] and Sánchez-Somolinos et al.[588] documented similar results. Lewis and co-workers examined the deformation of these printed objects under load, illustrating that printed LCE can lift 1000× their own weight and up to 70 g loads.[585] Very recently, Lewis and co-workers have extended on this examination to realize thermally driven rolling of an origami robot.[589] Sánchez-Somolinos and co-workers integrated printed LCE actuators with nonactuating materials.[588] When a printed LCE ring is embedded asymmetrically into a PDMS block, the thermal contraction of the LCE ring causes a lensing effect as the PDMS deforms into a convex structure. Qi and co-workers explored printing of a thiol-Michael LCE

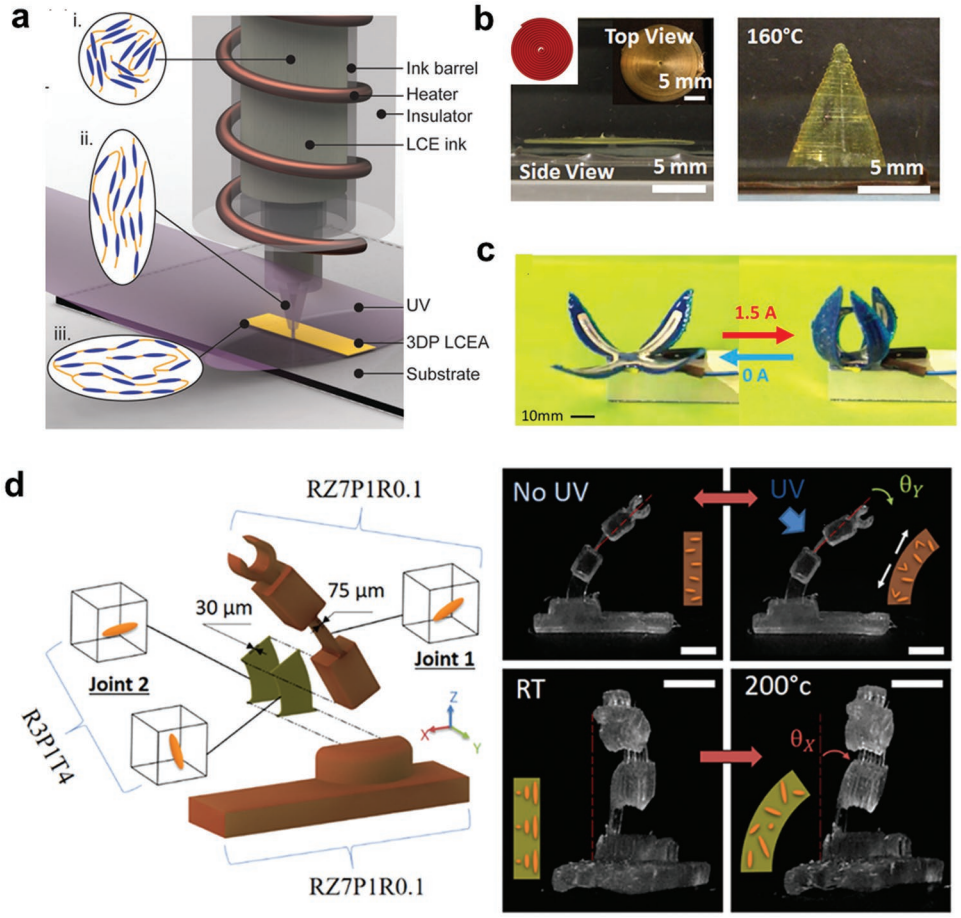

Figure 23. 3D printing of liquid crystal elastomer (LCE) actuators. a) Shear alignment via direct ink writing (DIW) of LCEs. Reproduced with permission.[585] Copyright 2018, Wiley-VCH. b) Print path and deformation behavior of +1 azimuthal defect. Reproduced with permission.[587] Copyright 2017, ACS Publications. c) Composite 3D printed LCE gripped remotely active via Joule heating. Reproduced with permission.[590] Copyright 2018, IOP Publishing. d) Voxel printing of LCE arm displaying sequential deformations. Reproduced with permission.[592] Copyright 2019, ACS.

ink with a comparatively lower nematic to isotropic transition temperature than these previous works.[590] The ink was subsequently used to generate composite actuators from a printed LCE and Joule heating components, displaying reversible actuation of complex geometries (Figure 23c). Ware and co-workers have also reported on a thiol-ene composition that further reduces the temperature required to induce mechanical response.[591] Recently, Ware and Shankar developed a new methodology for the preparation of oriented voxels in 3D printing LCEs.[593] Using a rotating magnet, the LC director can be selectively reoriented in multiple layers of the build. These authors 3D printed a robotic arm capable of two independent motions—a light triggered bending and thermally triggered bending (Figure 23d).

10. Outlook

What looms over the horizon for stimuli-responsive materials and their potential as material machines? The tremendous performance and advances detailed in this comprehensive review are indicative of a bright future. However, we expect the sustained growth of this subset of materials research will be correlated to the value proposition these materials can offer to mechanical systems and specifically to the engineers that design or manufacture them. It remains to be seen whether responsive materials will disrupt the design of machines, specifically in enabling monolithic or multimaterial material elements that are tailored for use and enable function.

As we look forward, it is important to assess the competition. To compete with standard materials and well-established mechanisms, material machines must advance functional performance beyond that achievable with conventional systems in any number of metrics: weight, simplicity of manufacture, or ruggedness. Performance attributes will also be critical—actuation force, cyclability, frequency, response time, environmental regulations, and optical properties. In some instances, for example SMAs—the maturity and commercial availability of the materials, coupled to the achievable energy density have enabled widespread integration in end use. On the other extreme, while the programmability of mechanical response in LCE/LCNs are compelling, sustained and focused research efforts must demonstrate robust and repeatable responses ideally with commercially available materials systems that are amenable to scalable

processing methods (to include layer by layer processing or 3D printing).

Design criteria and system constraints will ultimately dictate which responsive material is best suited for a particular implementation. In that sense, we prefer to take a holistic view of the materials discussed hereto. Performance gains attributable to stimuli-responsive materials in robotic systems will likely be associated with a distinctive balance at the nexus of power requirements, weight, and force–displacement characteristics. Approaches to retain mechanical output while reducing density will naturally realize performance gains in microscale implementations. The properties of the stimuli itself are also important. Thermomechanical effects in responsive materials are commonly utilized in a number of the material classes described. The energy efficiency of thermal inputs are well defined and understood, and simply distill to maximizing response over minimal temperature change. However, realizing stimuli-response across a narrow temperature window can also have tradeoffs, for example, further sensitizing the material system to environmental conditions. Light is a compelling stimulus, in that it can remotely and wirelessly trigger mechanical effects in many of these materials. Accordingly, the power source of photoresponsive robotic elements can be off boarded. However, complicated mechanical deformation will naturally introduce shadowing effects that may be difficult to circumvent. Although the power source for robotic implementations employing wired optical systems would also be offboard, the integrated fiber optics within the material would tether the robot to the power supply similar to pneumatic or electrically driven mechanical systems.

A emerging frontier that is unique to stimuli-responsive materials when compared to standard materials and mechanisms is the prospect of introducing autonomic operation to material machines. The term "smart" material has been widely used in the prior literature, often as synonymous with responsive materials. A responsive material is only "smart" when it is designed, tailored, or integrated to make decisions. In this sense, the material itself must have embedded intelligence to sense, react, and respond appropriately to a given obstacle or undertake a desired task. Correll has asked the question: "will robots be bodies with brains or brains with bodies?"[595] Emerging research detailed in this review details material systems with embodied intelligence enabled largely by various approaches to enabling materials state awareness through feedback mechanisms. Integrating sensory aptitude and computational function into responsive materials will be needed merge the intelligence of Coeus with the body of Hercules in robotics.

Acknowledgements

The authors acknowledge support from the Defense Advanced Research Projects Agency (DARPA) and the Army Research Office (ARO). The authors also recognize prior support from the Air Force Research Laboratory and the Air Force Office of Scientific Research.

Note: The website cited in ref. [4] was corrected on May 20, 2020, after initial publication online.

Conflict of Interest

The authors declare no conflict of interest.

Keywords

actuators, liquid crystalline elastomers, robotics, shape memory alloys, stimuli-responsive materials

Received: October 7, 2019
Revised: November 19, 2019
Published online: March 4, 2020

[1] K. Bhattacharya, R. D. James, *Science* **2005**, *307*, 53.
[2] Y. Bar-Cohen, C. Breazeal, *Proc. SPIE* **2003**, *5051*, 14.
[3] G. Kovacs, P. Lochmatter, M. Wissler, *Smart Mater. Struct.* **2007**, *16*, S306.
[4] Boston Dynamics: Atlas, https://www.bostondynamics.com/atlas (accessed: October 2019).
[5] K. Jayaram, N. T. Jafferis, N. Doshi, B. Goldberg, R. J. Wood, *Smart Mater. Struct.* **2018**, *27*, 065028.
[6] L. N. Awad, J. Bae, K. O'Donnell, S. M. M. De Rossi, K. Hendron, L. H. Sloot, P. Kudzia, S. Allen, K. G. Holt, T. D. Ellis, C. J. Walsh, *Sci. Transl. Med.* **2017**, *9*, eaai9084.
[7] Soft Robotics, https://www.softroboticsinc.com/mgrip (accessed: September 2019).
[8] N. Kellaris, V. Gopaluni Venkata, G. M. Smith, S. K. Mitchell, C. Keplinger, *Sci. Rob.* **2018**, *3*, eaar3276.
[9] D. Stoeckel, *Mater. Des.* **1990**, *11*, 302.
[10] R. G. Loewy, *Smart Mater. Struct.* **1997**, *6*, R11.
[11] K. Gath, C. Maranville, J. Tardiff, *Proc. SPIE* **2018**, 5, *1060202*.
[12] M. Ferraioli, D. Nuzzo, A. Concilio, S. Ameduri, *Proc. SPIE* **2019**, *10970*, 109701M.
[13] J. M. Jani, M. Leary, A. Subic, M. A. Gibson, *Mater. Des.* **2014**, *56*, 1078.
[14] A. Concilio, L. Lecce, in *Shape Memory Alloy Engineering* (Eds: L. Lecce, A. Concilio), Elsevier, **2015**, pp. 3–30.
[15] A. Ölander, *J. Am. Chem. Soc.* **1932**, *54*, 3819.
[16] F. Falk, *Acta Metall.* **1980**, *28*, 1773.
[17] K. Enami, A. Nagasawa, S. Nenno, *Scr. Metall.* **1975**, *9*, 941.
[18] L. M. Schetky, *Sci. Am.* **1979**, *241*, 74.
[19] K. Otsuka, X. Ren, *Intermetallics* **1999**, *7*, 511.
[20] K. Otsuka, X. Ren, *Prog. Mater. Sci.* **2005**, *50*, 511.
[21] W. J. Buehler, F. E. Wang, *Ocean Eng.* **1968**, *1*, 105.
[22] G. B. Kauffman, I. Mayo, *Chem. Educ.* **1997**, *2*, 1.
[23] R. H. Bricknell, K. N. Melton, O. Mercier, *Metall. Trans. A* **1979**, *10*, 693.
[24] G. F. Andreasen, R. E. Morrow, *Am. J. Orthod.* **1978**, *73*, 142.
[25] S. Civjan, E. F. Huget, L. B. Desimon, *J. Dent. Res.* **1975**, *54*, 89.
[26] N. Pandis, C. P. Bourauel, *Semin. Orthod.* **2010**, *16*, 249.
[27] W. M. Huang, Z. Ding, C. C. Wang, J. Wei, Y. Zhao, H. Purnawali, *Mater. Today* **2010**, *13*, 54.
[28] R. Dasgupta, *J. Mater. Res.* **2014**, *29*, 1681.
[29] L. Sun, W. M. M. Huang, Z. Ding, Y. Zhao, C. C. C. Wang, H. Purnawali, C. Tang, *Mater. Des.* **2012**, *33*, 577.
[30] T. Duerig, A. Pelton, D. Stöckel, *Mater. Sci. Eng., A* **1999**, *273-275*, 149.
[31] H. Qian, H. Li, G. Song, W. Guo, *Math. Probl. Eng.* **2013**, *2013*.
[32] Y. Zhang, S. Zhu, *J. Eng. Mech.* **2008**, *134*, 240.
[33] D. J. Miller, L. A. Fahnestock, M. R. Eatherton, *Eng. Struct.* **2012**, *40*, 288.
[34] D. J. Hartl, D. C. Lagoudas, *Proc. Inst. Mech. Eng., Part G* **2007**, *221*, 535.
[35] P. K. Kumar, in *Shape Memory Alloys: Modeling and Engineering Applications* (Ed: C. D. Lagoudas), Springer US, New York **2008**, pp. 1–16.
[36] J. Sohn, G.-W. Kim, S.-B. Choi, *Appl. Sci.* **2018**, *8*, 1928.
[37] X. Gao, W. Huang, *Proc. SPIE* **2003**, *4946*, 183.

[38] S. Barbarino, E. I. Saavedra Flores, R. M. Ajaj, I. Dayyani, M. I. Friswell, *Smart Mater. Struct.* **2014**, *23*, 063001.
[39] X. Zhang, J. Hu, S. Mao, E. Dong, J. Yang, *Smart Mater. Struct.* **2014**, *23*, 125004.
[40] J. Leng, X. Yan, X. Zhang, D. Huang, Z. Gao, *Smart Mater. Struct.* **2016**, *25*, 025007.
[41] J. E. Shim, Y. J. Quan, W. Wang, H. Rodrigue, S. H. Song, S. H. Ahn, *Smart Mater. Struct.* **2015**, *24*, 125033.
[42] L. Flemming, S. Mascaro, *Smart Mater. Struct.* **2013**, *22*, 014015.
[43] E. A. Allen, L. D. Taylor, J. P. Swensen, *Smart Mater. Struct.* **2019**, *28*, 074007.
[44] M. Ashir, A. Nocke, C. Cherif, *J. Ind. Text.* **2019**, *48*, 1081.
[45] M. Kang, Y. Pyo, J. young Jang, Y. Park, Y.-H. Son, M. Choi, J. wan Ha, Y.-W. Chang, C. S. Lee, *Sens. Actuators A Phys.* **2018**, *283*, 187.
[46] X. Huang, K. Kumar, M. K. Jawed, A. Mohammadi Nasab, Z. Ye, W. Shan, C. Majidi, *Adv. Mater. Technol.* **2019**, *4*, 1800540.
[47] X. Huang, K. Kumar, M. K. Jawed, A. M. Nasab, Z. Ye, W. Shan, C. Majidi, *Sci. Rob.* **2018**, *3*, eaau7557.
[48] S. Akbari, A. H. Sakhaei, S. Panjwani, K. Kowsari, A. Serjouei, Q. Ge, *Sens. Actuators, A.* **2019**, *290*, 177.
[49] D. Tanaka, Y. Uchiumi, S. Kawamura, M. Takato, K. Saito, F. Uchikoba, *Artif. Life Rob.* **2017**, *22*, 380.
[50] H. T. Lin, G. G. Leisk, B. Trimmer, *Bioinspiration Biomimetics* **2011**, *6*, 026007.
[51] J. Sheng, J. P. Desai, *Smart Mater. Struct.* **2015**, *24*, 105005.
[52] H. Rodrigue, W. Wei, B. Bhandari, S. H. Ahn, *Smart Mater. Struct.* **2015**, *24*, 125003.
[53] L. M. Fonseca, G. V. Rodrigues, M. A. Savi, A. Paiva, *Chaos, Solitons Fractals* **2019**, *122*, 245.
[54] C. D. Onal, R. J. Wood, D. Rus, *IEEE/ASME Trans. Mechatronics* **2013**, *18*, 430.
[55] K. Kuribayashi, K. Tsuchiya, Z. You, D. Tomus, M. Umemoto, T. Ito, M. Sasaki, *Mater. Sci. Eng., A* **2006**, *419*, 131.
[56] S. J. Park, C. H. Park, *Sci. Rep.* **2019**, *9*, 9157.
[57] H. Yin, J. Zhou, J. Li, V. S. Joseph, *J. Mater. Eng. Perform.* **2018**, *27*, 3581.
[58] L. Margheri, C. Laschi, B. Mazzolai, *Bioinspiration Biomimetics* **2012**, *7*, 025004.
[59] B. Mazzolai, L. Margheri, M. Cianchetti, P. Dario, C. Laschi, *Bioinspiration Biomimetics* **2012**, *7*, 025005.
[60] S. Kim, C. Laschi, B. Trimmer, *Trends Biotechnol.* **2013**, *31*, 287.
[61] H. Yang, M. Xu, W. Li, S. Zhang, *IEEE Trans. Ind. Electron.* **2019**, *66*, 6108.
[62] Z. Zhakypov, F. Heremans, A. Billard, J. Paik, *IEEE Rob. Autom. Lett.* **2018**, *3*, 2894.
[63] *Thin Film Shape Memory Alloys: Fundamentals and Device Applications* (Eds: S. Miyazaki, Y. Q. Fu, W. M. Huang), Cambridge University Press, Cambridge, UK **2009**.
[64] C. R. Knick, G. L. Smith, C. J. Morris, H. A. Bruck, *Sens. Actuators, A* **2019**, *291*, 48.
[65] C. R. Knick, D. J. Sharar, A. A. Wilson, G. L. Smith, C. J. Morris, H. A. Bruck, *J. Micromech. Microeng.* **2019**, *29*, 075005.
[66] H.-T. Lee, M.-S. Kim, G.-Y. Lee, C.-S. Kim, S.-H. Ahn, *Small* **2018**, *14*, 1801023.
[67] J. J. Gill, D. T. Chang, L. A. Momoda, G. P. Carman, *Sens. Actuators, A* **2001**, *93*, 148.
[68] L. B. Kong, T. Li, H. H. Hng, F. Boey, T. Zhang, S. Li, *Waste Energy Harvesting: Mechanical and Thermal Energies*, Vol. *24*, Springer US, New York **2014**.
[69] R. C. Turner, P. A. Fuierer, R. E. Newnham, T. R. Shrout, *Appl. Acoust.* **1994**, *41*, 299.
[70] V. Dentan, Y. Levy, M. Dumont, P. Robin, E. Chastaing, J. P. Montheard, *Proc. SPIE* **1989**, *1126*, 2.
[71] R. B. Meyer, L. Liebert, L. Strzelecki, P. Keller, *J. Phys., Lett.* **1975**, *36*, 69.
[72] J. S. Pulskamp, R. G. Polcawich, R. Q. Rudy, S. S. Bedair, R. M. Proie, T. Ivanov, G. L. Smith, *MRS Bull.* **2012**, *37*, 1062.
[73] J. Yan, M. Liu, Y. G. Jeong, W. Kang, L. Li, Y. Zhao, N. Deng, B. Cheng, G. Yang, *Nano Energy* **2019**, *56*, 662.
[74] A. Benjeddou, *Int. J. Smart Nano Mater.* **2018**, *9*, 98.
[75] Y. Wan, Y. Wang, C. F. Guo, *Mater. Today Phys.* **2017**, *1*, 61.
[76] J. C. Gerdeen, H. W. Lord, R. A. L. Rorrer, *Engineering Design with Polymers and Composites*, CRC Press, Boca Raton, FL, USA **2005**, https://doi.org/10.1201/9781420056372.
[77] K. K. Sappati, S. Bhadra, *Sensors* **2018**, *18*, 3605.
[78] M. Lethiecq, F. Levassort, L. P. Tran-Huu-Hue, M. Alguero, L. Pardo, T. Bove, E. Ringgaard, W. Wolny, *Proc. - IEEE Ultrason. Symp.* **2004**, *2*, 1153.
[79] P. E. Bloornfield, *IEEE Trans. Ultrason. Ferroelectr. Freq. Control* **2000**, *47*, 1397.
[80] Y. Tajitsu, *Piezoelectric Polymers* (Eds: K. Asaka, H. Okuzaki), Soft Actuators, Springer, Tokyo, Japan **2014**.
[81] Y. Huan, Y. Liu, Y. Yang, Y. Wu, *J. Appl. Polym. Sci.* **2007**, *104*, 858.
[82] N. Soin, D. Boyer, K. Prashanthi, S. Sharma, A. A. Narasimulu, J. Luo, T. H. Shah, E. Siores, T. Thundat, *Chem. Commun.* **2015**, *51*, 8257.
[83] G. Gutiérrez-Sánchez, J. Hernando-García, V. Ruiz-Diez, O. J. Dura, M. A. López de la Torre, J. L. Sánchez-Rojas, *Proc. SPIE* **2017**, *10246*, 102460N.
[84] A. N. Arshad, M. H. M. Wahid, M. Rusop, W. H. A. Majid, R. H. Y. Subban, M. D. Rozana, *J. Nanomater.* **2019**, *2019*, 5961563.
[85] A. J. Paleo, C. Martínez-Boubeta, L. Balcells, C. M. Costa, V. Sencadas, S. Lanceros-Mendez, *Nanoscale Res. Lett.* **2011**, *6*, 257.
[86] F. Saaid, I. Rodi, T. Winie, *AIP Conf. Proc.* **2017**, *1877*, 020006.
[87] G. P. Kontoudis, M. Liarokapis, K. G. Vamvoudakis, T. Furukawa, *Front. Rob. AI* **2019**, *6*, 47.
[88] J. Han, D. Li, C. Zhao, X. Wang, J. Li, X. Wu, *Sensors* **2019**, *19*, s19040830.
[89] E. Pukada, *IEEE Trans. Ultrason. Ferroelectr. Freq. Control* **2000**, *47*, 1277.
[90] A. Jákli, I. C. Pintre, J. L. Serrano, M. B. Ros, M. R. De La Fuente, *Adv. Mater.* **2009**, *21*, 3784.
[91] E. R. Beckel, N. B. Cramer, A. W. Harant, C. N. Bowman, *Polym. Prepr. (Am. Chem. Soc., Div. Polym. Chem.)* **2002**, *43*, 530.
[92] H. Takezoe, Y. Takanishi, *Jpn. J. Appl. Phys.* **2006**, *45*, 597.
[93] W. Lehmann, H. Skupin, C. Tolksdorf, E. Gebhard, R. Zentel, P. Krüger, M. Lösche, F. Kremer, *Nature* **2001**, *410*, 447.
[94] T. Hattori, Y. Takahashi, M. Iijima, E. Fukada, *Jpn. J. Appl. Phys.* **1996**, *35*, 2199.
[95] J. Kim, Y. B. Seo, *Smart Mater. Struct.* **2002**, *11*, 355.
[96] S. Tuukkanen, S. Rajala, in *Piezoelectricity - Organic and Inorganic Materials and Applications* (Eds: S. G. Vassiliadis, D. Matsouka), InTech Open, London, UK **2018**.
[97] J. Kim, S. D. Deshpande, S. Yun, Q. Li, *Polym. J.* **2006**, *38*, 659.
[98] S. K. Mahadeva, K. Walus, B. Stoeber, *ACS Appl. Mater. Interfaces* **2015**, *7*, 8345.
[99] J. Kim, S. Y. Yang, G.-Y. Yun, S. Jang, K. Yun, *Proc. SPIE* **2009**, *7287*, 728710.
[100] J. F. Tressler, S. Alkoy, R. E. Newnham, *J. Electroceram.* **1998**, *2*, 257.
[101] N. T. Jafferis, M. Lok, N. Winey, G. Y. Wei, R. J. Wood, *Smart Mater. Struct.* **2016**, *25*, 055033.
[102] M. Sitti, D. Campolo, J. Yan, R. S. Fearing, T. Su, D. Taylor, T. D. Sands, in *IEEE Int. Conf. Robotics and Automation*, IEEE, Piscataway, NJ, USA **2001**, p. 3839.
[103] A. G. Dharmawan, H. H. Hariri, S. Foong, G. S. Soh, K. L. Wood, *Proc. - IEEE Int. Conf. on Robotics and Automation*, IEEE, Piscataway, NJ, USA **2017**, p. 6008.
[104] H. H. Hariri, G. S. Soh, S. Foong, K. Wood, *IEEE Trans. Rob.* **2017**, *33*, 742.
[105] H. Peng, J. Yang, X. Lu, P. Zhu, D. Wu, *IEEE Trans. Ind. Electron.* **2019**, *66*, 7852.

[106] S. A. Rios, A. J. Fleming, Y. K. Yong, *IEEE Rob. Autom. Lett.* **2016**, *2*, 337.
[107] H. H. Hariri, L. A. Prasetya, S. Foong, G. S. Soh, K. N. Otto, K. L. Wood, *Proc. - IEEE Int. Conf. Robot. Autom.* **2016**, p. 4743.
[108] A. G. Dharmawan, H. H. Hariri, G. S. Soh, S. Foong, K. L. Wood, *J. Mech. Rob.* **2018**, *10*, 021003.
[109] S. A. Rios, A. J. Fleming, Y. K. Yong, in *IEEE/ASME Int. Conf. on Advanced Intelligent Mechatronics, AIM*, IEEE, Piscataway, NJ, USA **2016**, p. 982.
[110] S. A. Rios, A. J. Fleming, Y. K. Yong, in *IEEE/ASME Int. Conf. on Advanced Intelligent Mechatronics, AIM*, IEEE, Piscataway, NJ, USA **2015**, p. 318.
[111] J. Qu, K. R. Oldham, in *Proc. ASME Des. Eng. Tech. Conf.* **2016**, *4*.
[112] G. Fischer, M. Gogola, E. Garcia, M. Goldfarb, *J. Micromechatronics* **2001**, *1*, 205.
[113] A. A. Yumaryanto, J. An, S. Lee, in *2006 IEEE Conf. on Robotics, Automation, and Mechatronics*, IEEE, Piscataway, NJ, USA **2006**.
[114] T. Ho, S. Lee, *Robotica* **2013**, *31*, 89.
[115] M. Rubenstein, C. Ahler, R. Nagpal, in *Proc. - IEEE Int. Conf. on Robotics and Automation*, IEEE, Piscataway, NJ, USA **2012**, p. 3293.
[116] P. Birkmeyer, K. Peterson, R. S. Fearing, in *IEEE/RSJ Int. Conf. on Intelligent Robotos and Systems IROS*, IEEE, Piscataway, NJ, USA **2009**, p. 2683.
[117] D. W. Haldane, R. S. Fearing, *Proc. - IEEE Int. Conf. on Robotics and Automation*, IEEE, Piscataway, NJ, USA **2015**, p. 4539.
[118] A. T. Baisch, O. Ozcan, B. Goldberg, D. Ithier, R. J. Wood, *Int. J. Rob. Res.* **2014**, *33*, 1063.
[119] D. Chen, X. Li, J. Jin, C. Ruan, *Rev. Sci. Instrum.* **2019**, *90*, 015003.
[120] J. Zhang, J. Sheng, C. T. O'Neill, C. J. Walsh, R. J. Wood, J. H. Ryu, J. P. Desai, M. C. Yip, *IEEE Trans. Rob.* **2019**, *35*, 761.
[121] S. D. de Rivaz, B. Goldberg, N. Doshi, K. Jayaram, J. Zhou, R. J. Wood, *Sci. Rob.* **2018**, *3*, eaau3038.
[122] Y. Chen, N. Doshi, B. Goldberg, H. Wang, R. J. Wood, *Nat. Commun.* **2018**, *9*, 2495.
[123] K. Y. Ma, P. Chirarattananon, S. B. Fuller, R. J. Wood, *Science* **2013**, *340*, 603.
[124] K. L. Hoffman, R. J. Wood, *Science* **2011**, *31*, 852LP.
[125] N. Doshi, K. Jayaram, S. Castellanos, S. Kuindersma, R. J. Wood, *Bioinspiration Biomimetics* **2019**, *331*, 852 LP.
[126] L. Hines, D. Campolo, M. Sitti, *IEEE Trans. Rob.* **2014**, *30*, 220.
[127] G. Kósa, M. Shoham, M. Zaaroor, *IEEE Trans. Rob.* **2007**, *23*, 137.
[128] N. T. Jafferis, E. F. Helbling, M. Karpelson, R. J. Wood, *Nature* **2019**, *570*, 491.
[129] M. Ha, S. Lim, J. Park, D.-S. Um, Y. Lee, H. Ko, *Adv. Funct. Mater.* **2015**, *25*, 2841.
[130] C. Pan, L. Dong, G. Zhu, S. Niu, R. Yu, Q. Yang, Y. Liu, Z. L. Wang, *Nat. Photonics* **2013**, *7*, 752.
[131] C. K. Jeong, C. Baek, A. I. Kingon, K.-I. Park, S.-H. Kim, *Small* **2018**, *14*, 1704022.
[132] J. H. Lee, H. J. Yoon, T. Y. Kim, M. K. Gupta, J. H. Lee, W. Seung, H. Ryu, S. W. Kim, *Adv. Funct. Mater.* **2015**, *25*, 3203.
[133] S. Gupta, F. Giacomozzi, H. Heidari, L. Lorenzelli, R. Dahiya, *Proc. Eng.* **2016**, *168*, 662.
[134] Y. B. Lee, J. K. Han, S. Noothongkaew, S. K. Kim, W. Song, S. Myung, S. S. Lee, J. Lim, S. D. Bu, K.-S. An, *Adv. Mater.* **2017**, *29*, 1604500.
[135] H. B. Lee, Y. W. Kim, J. Yoon, N. K. Lee, S.-H. Park, *Smart Mater. Struct.* **2017**, *26*, 045032.
[136] H. He, Y. Fu, W. Zang, Q. Wang, L. Xing, Y. Zhang, X. Xue, *Nano Energy* **2017**, *31*, 37.
[137] Z. Lou, S. Chen, L. Wang, K. Jiang, G. Shen, *Nano Energy* **2016**, *23*, 7.
[138] X. Chen, J. Shao, N. An, X. Li, H. Tian, C. Xu, Y. Ding, *J. Mater. Chem. C* **2015**, *3*, 11806.
[139] F. A. Viola, A. Spanu, P. C. Ricci, A. Bonfiglio, P. Cosseddu, *Sci. Rep.* **2018**, *8*, 8073.
[140] P. Xiao, N. Yi, T. Zhang, Y. Huang, H. Chang, Y. Yang, Y. Zhou, Y. Chen, *Adv. Sci.* **2016**, *3*, 1500438.
[141] Q. Zheng, H. Zhang, H. Mi, Z. Cai, Z. Ma, S. Gong, *Nano Energy* **2016**, *26*, 504.
[142] B. Wang, C. Liu, Y. Xiao, J. Zhong, W. Li, Y. Cheng, B. Hu, L. Huang, J. Zhou, *Nano Energy* **2017**, *32*, 42.
[143] K. Hosoda, Y. Tada, M. Asada, *Rob. Auton. Syst.* **2006**, *54*, 104.
[144] H. Tian, *Integr. Ferroelectr.* **2018**, *192*, 94.
[145] W. K. Yen, J. Guo, *Ocean Eng.* **2018**, *161*, 77.
[146] Y. Wu, J. K. Yim, J. Liang, Z. Shao, M. Qi, J. Zhong, Z. Luo, X. Yan, M. Zhang, X. Wang, R. S. Fearing, R. J. Full, L. Lin, *Sci. Rob.* **2019**, *4*, eaax1594.
[147] S. Ahmed, E. Arrojado, Z. Ounaies, in *ASME 2016 Conference on Smart Materials, Adaptive Structures and Intelligent Systems,* ASME, **2016**, V001T01A017; https://doi.org/10.1115/SMASIS2016-9202.
[148] N. Hu, D. Chen, D. Wang, S. Huang, I. Trase, H. M. Grover, X. Yu, J. X. J. Zhang, Z. Chen, *Phys. Rev. Appl.* **2018**, *9*, 21002.
[149] Y. Bar-Cohen, *J. Spacecr. Rockets* **2002**, *39*, 822.
[150] G. Y. Gu, J. Zhu, L. M. Zhu, X. Zhu, *Bioinspiration Biomimetics* **2017**, *12*, 011003.
[151] F. Carpi, I. Anderson, S. Bauer, G. Frediani, G. Gallone, M. Gei, C. Graaf, C. Jean-Mistral, W. Kaal, G. Kofod, M. Kollosche, R. Kornbluh, B. Lassen, M. Matysek, S. Michel, S. Nowak, B. O'Brien, Q. Pei, R. Pelrine, B. Rechenbach, S. Rosset, H. Shea, *Smart Mater. Struct.* **2015**, *24*, 105025.
[152] C. Keplinger, M. Kaltenbrunner, N. Arnold, S. Bauer, *Proc. Natl. Acad. Sci. USA* **2010**, *107*, 4505.
[153] R. Pelrine, R. Kornbluh, Q. Pei, J. Joseph, Pei, J. Joseph, *Science* **2000**, *287*, 836.
[154] R. Kornbluh, R. Pelrine, J. Eckerle, J. Joseph, *Proc. - IEEE Int. Conf. Robot. Autom.* **1998**, *3*, 2147.
[155] Z. Suo, *Acta Mech. Solida Sin.* **2010**, *23*, 549.
[156] X. Zhang, C. Löwe, M. Wissler, B. Jähne, G. Kovacs, *Adv. Eng. Mater.* **2005**, *7*, 361.
[157] X. Ji, A. El Haitami, F. Sorba, S. Rosset, G. T. M. Nguyen, C. Plesse, F. Vidal, H. R. Shea, S. Cantin, *Sens. Actuators, B* **2018**, *261*, 135.
[158] T. G. La, G. K. Lau, *Appl. Phys. Lett.* **2016**, *108*, 012903.
[159] T. N. Nguyen, K. Rohtlaid, C. Plesse, G. T. M. Nguyen, C. Soyer, S. Grondel, E. Cattan, J. D. W. Madden, F. Vidal, *Electrochim. Acta* **2018**, *265*, 670.
[160] P. Rothemund, X. P. Morelle, K. Jia, G. M. Whitesides, Z. Suo, *Adv. Funct. Mater.* **2018**, *28*, 1800653.
[161] C. Keplinger, J.-Y. Sun, C. C. Foo, P. Rothemund, G. M. Whitesides, Z. Suo, *Science* **2013**, *341*, 984.
[162] K. H. Stark, N. C. G. Garton, *Nature* **1955**, *176*, 1225.
[163] I. A. Anderson, T. A. Gisby, T. G. McKay, B. M. O'Brien, E. P. Calius, *J. Appl. Phys.* **2012**, *112*, 041101.
[164] M. Kollosche, J. Zhu, Z. Suo, G. Kofod, *Phys. Rev. E* **2012**, *85*, 051801.
[165] T. G. La, G. K. Lau, *Appl. Phys. Lett.* **2013**, *102*, 192905.
[166] M. Poikelispää, A. Shakun, A. Das, J. Vuorinen, *Polym. Adv. Technol.* **2017**, *28*, 130.
[167] C. Chiang Foo, S. Cai, S. Jin Adrian Koh, S. Bauer, Z. Suo, *J. Appl. Phys.* **2012**, *111*, 034102.
[168] W. Hong, *J. Mech. Phys. Solids* **2011**, *59*, 637.
[169] S. Michel, X. Q. Zhang, M. Wissler, C. Löwe, G. Kovacs, *Polym. Int.* **2010**, *59*, 391.
[170] M. H. Jomaa, K. Masenelli-Varlot, G. Diguet, L. Seveyrat, L. Lebrun, K. Wongtimnoi, C. Vechambre, J. M. Chenal, J. Y. Cavaillé, *Polymer* **2015**, *62*, 139.
[171] X. Wang, Z. Li, Z. Chen, L. Zeng, L. Sun, *Adv. Ind. Eng. Polym. Res.* **2018**, *1*, 111.
[172] K. Wongtimnoi, B. Guiffard, A. Bogner-Van de Moortèle, L. Seveyrat, C. Gauthier, J. Y. Cavaillé, *Compos. Sci. Technol.* **2011**, *71*, 885.
[173] Ardimas, C. Putson, N. Muensit, *Compos. Sci. Technol.* **2018**, *158*, 164.

[174] F. Carpi, D. De Rossi, *IEEE Trans. Dielectr. Electr. Insul.* **2005**, *12*, 835.
[175] X. Sui, W. Zhou, L. Dong, Z. Wang, X. Liu, A. Zhou, J. Cai, Q. Chen, *Adv. Polym. Technol.* **2018**, *37*, 1507.
[176] Y. Y. Zhang, G. L. Wang, J. Zhang, K. H. Ding, Z. F. Wang, M. Zhang, *Polym. Compos.* **2019**, *40*, E62.
[177] Y. Zhao, J. W. Zha, L. J. Yin, Z. S. Gao, Y. Q. Wen, Z. M. Dang, *Polymer* **2018**, *137*, 269.
[178] K. Jung, J. C. Koo, J. Do Nam, Y. K. Lee, H. R. Choi, *Bioinspiration Biomimetics* **2007**, *2*, S42.
[179] C. T. Nguyen, H. Phung, T. D. Nguyen, C. Lee, U. Kim, D. Lee, H. Moon, J. Koo, J. Do Nam, H. R. Choi, *Smart Mater. Struct.* **2014**, *23*, 065005.
[180] M. Cianchetti, V. Mattoli, B. Mazzolai, C. Laschi, P. Dario, *Sens. Actuators, B* **2009**, *142*, 288.
[181] G. Haghiashtiani, E. Habtour, S.-H. Park, F. Gardea, M. C. McAlpine, *Extreme Mech. Lett.* **2018**, *21*, 1.
[182] N. Hosoya, H. Masuda, S. Maeda, *Appl. Acoust.* **2019**, *148*, 238.
[183] L. Qin, Y. Tang, U. Gupta, J. Zhu, *Smart Mater. Struct.* **2018**, *27*, 045017.
[184] I. A. Anderson, T. Hale, T. Gisby, T. Inamura, T. McKay, B. O'Brien, S. Walbran, E. P. Calius, *Appl. Phys. A* **2010**, *98*, 75.
[185] A. Minaminosono, H. Shigemune, Y. Okuno, T. Katsumata, N. Hosoya, S. Maeda, *Front. Rob. AI* **2019**, *6*, 1.
[186] R. D. Kornbluh, R. Pelrine, Q. Pei, R. Heydt, S. Stanford, S. Oh, J. Eckerle, **2002**, *4698*, 254.
[187] F. Carpi, G. Frediani, S. Turco, D. De Rossi, R. D. De, *Adv. Funct. Mater.* **2011**, *21*, 4152.
[188] H. S. Lee, H. Phung, D.-H. H. Lee, U. K. Kim, C. T. Nguyen, H. Moon, J. C. Koo, J. Do Nam, H. R. Choi, *Sens. Actuators, A* **2014**, *205*, 191.
[189] L. E. Knoop, J. Rossiter, *Electroact. Polym. Actuators Devices* **2014**, *9056*, 905610.
[190] J. Ashby, S. Rosset, E.-F. M. Henke, I. A. Anderson, *Proc. SPIE* **2019**, *10966*, L1.
[191] E.-F. M. Henke, K. E. Wilson, I. A. Anderson, *Proc. SPIE* **2017**, *10163*, 101631N1.
[192] M. Duduta, D. R. Clarke, R. J. Wood, in *Proc. - IEEE Int. Conf. on Robotics and Automation*, IEEE, Piscataway, NJ, USA **2017**, p. 4346.
[193] C. Christianson, N. N. Goldberg, D. D. Deheyn, S. Cai, M. T. Tolley, *Sci. Rob.* **2018**, *3*, eaat1893.
[194] P. Li, Y. Wang, U. Gupta, J. Liu, L. Zhang, D. Du, C. C. Foo, J. Ouyang, J. Zhu, *Adv. Funct. Mater.* **2019**, *29*, 1901908.
[195] J. Shintake, H. Shea, D. Floreano, *IEEE Int. Conf. on Intelligent Robotos and Systems*, IEEE, Piscataway, NJ, USA **2016**, p. 4957.
[196] Q. Pei, M. Rosenthal, S. Stanford, H. Prahlad, R. Pelrine, *Smart Mater. Struct.* **2004**, *13*, N86.
[197] W. B. Li, W. M. Zhang, H. X. Zou, Z. K. Peng, G. Meng, *Smart Mater. Struct.* **2018**, *27*, 115024.
[198] G. K. Lau, H. T. Lim, J. Y. Teo, Y. W. Chin, *Smart Mater. Struct.* **2014**, *23*, 025021.
[199] H. Zhao, A. M. Hussain, M. Duduta, D. M. Vogt, R. J. Wood, D. R. Clarke, *Adv. Funct. Mater.* **2018**, *28*, 1804328.
[200] E. Hajiesmaili, E. Khare, A. Chortos, J. Lewis, D. R. Clarke, *Extreme Mech. Lett.* **2019**, *30*, 100504.
[201] C. Cao, S. Burgess, A. T. Conn, *Front. Rob. AI* **2019**, *5*, 137.
[202] H. Godaba, J. Li, Y. Wang, J. Zhu, *IEEE Rob. Autom. Lett.* **2016**, *1*, 624.
[203] L. Calabrese, G. Frediani, M. Gei, D. De Rossi, F. Carpi, *IEEE/ASME Trans. Mechatronics* **2018**, *23*, 2328.
[204] J. Torop, A. Aabloo, E. W. H. Jager, *Carbon* **2014**, *80*, 387.
[205] Z. Wang, X. Liu, Q. Wang, *J. Intell. Mater. Syst. Struct.* **2017**, *28*, 2036.
[206] P. Brochu, Q. Pei, *Macromol. Rapid Commun.* **2010**, *31*, 10.
[207] R. Pelrine, R. Kornbluh, J. Joseph, R. Heydt, Q. Pei, S. Chiba, *Mater. Sci. Eng., C* **2000**, *11*, 89.
[208] M. Shahinpoor, *Electrochim. Acta* **2003**, *48*, 2343.
[209] Y. Bar-Cohen, *Proc. Inst. Mech. Eng., Part G* **2007**, *221*, 553.
[210] K. J. Kim, M. Shahinpoor, *Smart Mater. Struct.* **2003**, *12*, 65.
[211] Z. Liu, P. Calvert, *Adv. Mater.* **2000**, *12*, 288.
[212] H. Wang, Z. Wang, J. Yang, C. Xu, Q. Zhang, Z. Peng, *Macromol. Rapid Commun.* **2018**, *39*, 1800246.
[213] K. Asaka, K. Mukai, T. Sugino, K. Kiyohara, *Polym. Int.* **2013**, *62*, 1263.
[214] M. D. Bennett, D. J. Leo, *Sens. Actuators, A* **2004**, *115*, 79.
[215] K. Asaka, K. Oguro, Y. Nishimura, M. Mizuhata, H. Takenaka, *Polym. J.* **1995**, *27*, 436.
[216] A. Hunt, Z. Chen, X. Tan, M. Kruusmaa, *Smart Mater. Struct.* **2016**, *25*, 035016.
[217] L. Chang, Y. Liu, Q. Yang, L. Yu, J. Liu, Z. Zhu, P. Lu, Y. Wu, Y. Hu, *J. Bionic Eng.* **2018**, *15*, 765.
[218] Y. Liu, H. Cebeci, R. G. De, J. Lin, B. L. Wardle, Q. M. Z. High, W. Blackwell, C. Link, *Adv. Funct. Mater.* **2010**, *20*, 3266.
[219] J.-W. Lee, Y.-T. Yoo, J. Y. Lee, *ACS Appl. Mater. Interfaces* **2014**, *6*, 1266.
[220] J. H. Park, S. W. Lee, D. S. Song, J. Y. Jho, *ACS Appl. Mater. Interfaces* **2015**, *7*, 16659.
[221] H. S. Wang, J. Cho, D. S. Song, J. H. Jang, J. Y. Jho, J. H. Park, *ACS Appl. Mater. Interfaces* **2017**, *9*, 21998.
[222] I.-W. P. Chen, M.-C. Yang, C.-H. Yang, D.-X. Zhong, M.-C. Hsu, Y. Chen, *ACS Appl. Mater. Interfaces* **2017**, *9*, 5550.
[223] C. H. Rhee, H. K. Kim, H. Chang, J. S. Lee, *Chem. Mater.* **2005**, *17*, 1691.
[224] V. K. Nguyen, Y. Yoo, *Sens. Actuators, B* **2007**, *123*, 183.
[225] J. W. Lee, S. Yu, S. M. Hong, C. M. Koo, *J. Mater. Chem. C* **2013**, *1*, 3784.
[226] O. C. Yılmaz, I. Sen, B. O. Gurses, O. Ozdemir, L. Cetin, M. Sarıkanat, Y. Seki, K. Sever, E. Altinkaya, *Composites, Part B* **2019**, *165*, 747.
[227] D. Guo, Y. Han, J. Huang, E. Meng, L. Ma, H. Zhang, Y. Ding, *ACS Appl. Mater. Interfaces* **2019**, *11*, 2386.
[228] D. R. MacFarlane, N. Tachikawa, M. Forsyth, J. M. Pringle, P. C. Howlett, G. D. Elliott, J. H. Davis Jr., M. Watanabe, P. Simon, C. Austen Angell, *Energy Environ. Sci.* **2014**, *7*, 232.
[229] I. Must, V. Vunder, F. Kaasik, I. Põldsalu, U. Johanson, A. Punning, A. Aabloo, *Sens. Actuators, B* **2014**, *202*, 114.
[230] L. Lu, J. Liu, Y. Hu, Y. Zhang, W. Chen, *Adv. Mater.* **2013**, *25*, 1270.
[231] J. C. Dias, A. C. Lopes, B. Magalhães, G. Botelho, M. M. Silva, J. M. S. S. Esperança, S. Lanceros-Mendez, *Polym. Test.* **2015**, *48*, 199.
[232] K.-S. Kwon, T. Nga Ng, *Org. Electron.* **2014**, *15*, 294.
[233] J. Lu, S. G. Kim, S. Lee, I. K. Oh, *Adv. Funct. Mater.* **2008**, *18*, 1290.
[234] J. H. Jeon, R. K. Cheedarala, C. D. Kee, I. K. Oh, *Adv. Funct. Mater.* **2013**, *23*, 6007.
[235] X.-L. Wang, I.-K. Oh, L. Xu, *Sens. Actuators, B.* **2010**, *145*, 635.
[236] V. Panwar, C. Lee, S. Y. Ko, J. O. Park, S. Park, *Mater. Chem. Phys.* **2012**, *135*, 928.
[237] V. Panwar, K. Cha, J.-O. Park, S. Park, *Sens. Actuators, B* **2012**, *161*, 460.
[238] J. H. Park, M. J. Han, D. S. Song, J. Y. Jho, *ACS Appl. Mater. Interfaces* **2014**, *6*, 22847.
[239] J. Y. Lee, H. S. Wang, B. R. Yoon, M. J. Han, J. Y. Jho, *Macromol. Rapid Commun.* **2010**, *31*, 1897.
[240] T. Fukushima, K. Asaka, A. Kosaka, T. Aida, *Angew. Chem., Int. Ed.* **2005**, *44*, 2410.
[241] N. Kamamichi, T. Maeba, M. Yamakita, T. Mukai, *Adv. Rob.* **2010**, *24*, 1471.
[242] W. M. Winslow, *J. Appl. Phys.* **1949**, *20*, 1137.
[243] J. S. Oh, S. B. Choi, *J. King Saud Univ., Sci.* **2017**, *29*, 390.

[244] J. Nikitczuk, B. Weinberg, P. K. Canavan, C. Mavroidis, *IEEE/ASME Trans. Mechatronics* **2010**, *15*, 952.
[245] S. R. Kang, S. W. Cha, Y. H. Hwang, Y. S. Lee, S. B. Choi, *Sens. Actuators, A* **2018**, *279*, 649.
[246] J. S. Oh, S. H. Choi, S. B. Choi, *Smart Mater. Struct.* **2014**, *23*, 015010.
[247] R. Bansevicius, J. A. Virbalis, *Mechatronics* **2007**, *17*, 570.
[248] M. Agarwal, Y. Lvov, K. Varahramyan, *Nanotechnology* **2006**, *17*, 5319.
[249] J. Perelaer, C. E. Hendriks, A. W. M. De Laat, U. S. Schubert, *Nanotechnology* **2009**, *20*, 165303.
[250] L. Hu, J. W. Choi, Y. Yang, S. Jeong, F. La Mantia, L. F. Cui, Y. Cui, *Proc. Natl. Acad. Sci. USA* **2009**, *106*, 21490.
[251] L. Hu, G. Zheng, J. Yao, N. Liu, B. Weil, M. Eskilsson, E. Karabulut, Z. Ruan, S. Fan, J. T. Bloking, M. D. McGehee, L. Wågberg, Y. Cui, *Energy Environ. Sci.* **2013**, *6*, 513.
[252] W. Bao, A. D. Pickel, Q. Zhang, Y. Chen, Y. Yao, J. Wan, K. Fu, Y. Wang, J. Dai, H. Zhu, D. Drew, M. Fuhrer, C. Dames, L. Hu, *Adv. Mater.* **2016**, *28*, 4684.
[253] G. Yu, L. Hu, M. Vosgueritchian, H. Wang, X. Xie, J. R. McDonough, X. Cui, Y. Cui, Z. Bao, *Nano Lett.* **2011**, *11*, 2905.
[254] J. E. Mates, I. S. Bayer, M. Salerno, P. J. Carroll, Z. Jiang, L. Liu, C. M. Megaridis, *Carbon* **2015**, *87*, 163.
[255] C. Chen, C. Yang, S. Li, D. Li, *Carbohydr. Polym.* **2015**, *134*, 309.
[256] A. Razaq, M. H. Asif, R. Kalsoom, A. F. Khan, M. S. Awan, S. Ishrat, S. M. Ramay, *J. Appl. Polym. Sci.* **2015**, *132*, 3.
[257] H. Koga, M. Nogi, N. Komoda, T. T. Nge, T. Sugahara, K. Suganuma, *NPG Asia Mater.* **2014**, *6*, e93.
[258] M. Nogi, M. Karakawa, N. Komoda, H. Yagyu, T. T. Nge, *Sci. Rep.* **2015**, *5*, 17254.
[259] R.-Z. Li, A. Hu, T. Zhang, K. D. Oakes, *ACS Appl. Mater. Interfaces* **2014**, *6*, 21721.
[260] H. Wu, S. W. Chiang, W. Lin, C. Yang, Z. Li, J. Liu, X. Cui, F. Kang, C. P. Wong, *Sci. Rep.* **2015**, *4*, 6275.
[261] S. B. Bibikov, V. N. Gorshenev, R. S. Sharafiev, A. M. Kuznetsov, *Mater. Chem. Phys.* **2008**, *108*, 39.
[262] Y. Ming, Y. Yang, R. P. Fu, C. Lu, L. Zhao, Y. M. Hu, C. Li, Y. X. Wu, H. Liu, W. Chen, *Adv. Mater. Technol.* **2018**, *3*, 1800257.
[263] S. Saito, Y. Katoh, H. Kokubo, M. Watanabe, S. Maruo, *J. Micromech. Microeng.* **2009**, *19*, 035005.
[264] Z. Chen, P. Hou, Z. Ye, *ASME. J. Dyn. Sys., Meas., Control.* **2019**, *141*, 071001.
[265] M. Aureli, V. Kopman, M. Porfiri, *IEEE/ASME Trans. Mechatronics* **2010**, *15*, 603.
[266] S. W. Yeom, I. K. Oh, *Smart Mater. Struct.* **2009**, *18*, 85002.
[267] C. Yue, S. Guo, M. Li, Y. Li, in *IEEE Int. Conf. on Intelligent Robotos and Systems*, IEEE, Piscataway, NJ, USA **2015**, p. 171.
[268] A. Kodaira, K. Asaka, T. Horiuchi, G. Endo, H. Nabae, K. Suzumori, *IEEE Rob. Autom. Lett.* **2019**, *4*, 1335.
[269] J. D. Carrico, K. J. Kim, K. K. Leang, in *Proc. - IEEE Int. Conf. Robotos and Automation*, IEEE, Piscataway, NJ, USA **2017**, 4313.
[270] M. He, K. Zhang, G. Chen, J. Tian, B. Su, *ACS Appl. Mater. Interfaces* **2017**, *9*, 16466.
[271] K. Ahmed, N. Naga, M. Kawakami, H. Furukawa, *Macromol. Chem. Phys.* **2018**, *219*, 1870054.
[272] R. L. Truby, R. K. Katzschmann, J. A. Lewis, D. Rus, *RoboSoft 2019 - 2019 IEEE Int. Conf. on Soft Robotics*, IEEE, Piscataway, NJ, USA **2019**, p. 322.
[273] Q. Tian, J. Lou, A. Mikkola, *Mech. Mach. Theory* **2017**, *107*, 210.
[274] J. R. Davidson, H. I. Krebs, *IEEE/ASME Trans. Mechatronics* **2018**, *23*, 2156.
[275] A. Zatopa, S. Walker, Y. Menguc, *Soft Rob.* **2018**, *5*, 258.
[276] M. Wehner, M. T. Tolley, Y. Mengüç, Y.-L. Park, A. Mozeika, Y. Ding, C. Onal, R. F. Shepherd, G. M. Whitesides, R. J. Wood, *Soft Rob.* **2014**, *1*, 263.
[277] D. Sasaki, T. Noritsugu, M. Takaiwa, K. Fukui, *Proc. JSME Annu. Conf. Rob. Mechatronics* **2004**, *2004*, 178.
[278] A. T. Asbeck, K. Schmidt, C. J. Walsh, *Rob. Auton. Syst.* **2015**, *73*, 102.
[279] T. Tanaka, Y. Satoli, S. N. I. Kaneko, Y. Suzuki, N. Sakamoto, S. Seki, in *Int. Conf. on Control, Automation and SystEm*, ICCAS **2008**, p. 2002.
[280] M. Wehner, Y. L. Park, C. Walsh, R. Nagpal, R. J. Wood, T. Moore, E. Goldfield, *Proc. IEEE RAS EMBS Int. Conf. on Biomedical Robotics and Biomechatronics*, IEEE, Piscataway, NJ, USA **2012**, p. 1586.
[281] M. Wehner, B. Quinlivan, P. M. Aubin, E. Martinez-Villalpando, M. Baumann, L. Stirling, K. Holt, R. Wood, C. Walsh, in *Proc. - IEEE Int. Conf. on Robotics and Automation*, IEEE, Piscataway, NJ, USA **2013**, p. 3362.
[282] S. V Krichel, O. Sawodny, A. Hildebrandt, in *Am. Control Conf.* **2010**, *2010*, 4385.
[283] B. Wang, A. McDaid, M. Biglari-Abhari, T. Giffney, K. Aw, *Sens. Actuators, A* **2017**, *257*, 173.
[284] D. G. Caldwell, G. A. Medrano-Cerda, M. Goodwin, *Proc. - IEEE Int. Conf. on Robotics and Automation*, IEEE, Piscataway, NJ, USA **1994**, p. 3558.
[285] H. Al-Fahaam, S. Davis, S. Nefti-Meziani, *Rob. Auton. Syst.* **2018**, *99*, 63.
[286] H. Hingorani, Y.-F. Zhang, B. Zhang, A. Serjouei, Q. Ge, *Int. J. Smart Nano Mater.* **2019**, *10*, 225.
[287] M. S. Verma, A. Ainla, D. Yang, D. Harburg, G. M. Whitesides, *Soft Rob.* **2018**, *5*, 133.
[288] J. T. B. Overvelde, T. Kloek, J. J. A. D'haen, K. Bertoldi, *Proc. Natl. Acad. Sci. USA* **2015**, *112*, 10863.
[289] C. Majidi, in *Robotic Systems and Autonomous Platforms*, Woodhead Publishing, **2019**, pp. 425–448.
[290] G. Agarwal, N. Besuchet, B. Audergon, J. Paik, *Sci. Rep.* **2016**, *6*, 34224.
[291] A. Pourghodrat, C. A. Nelson, *ASME. J. Med. Devices.* **2017**, *11*, 011003.
[292] A. Chiolerio, M. B. Quadrelli, *Adv. Sci.* **2017**, *4*, 1700036.
[293] M. Wehner, R. L. Truby, D. J. Fitzgerald, B. Mosadegh, G. M. Whitesides, J. A. Lewis, R. J. Wood, *Nature* **2016**, *536*, 451.
[294] N. W. Bartlett, M. T. Tolley, J. T. B. Overvelde, J. C. Weaver, B. Mosadegh, K. Bertoldi, G. M. Whitesides, R. J. Wood, *Soft Robot.* **2015**, *349*, 161.
[295] Engineers Edge, https://www.engineersedge.com/ (accessed: September 2019).
[296] M. De Volder, D. Reynaerts, *J. Micromech. Microeng.* **2010**, *20*, 043001.
[297] K. Takashima, J. Rossiter, T. Mukai, *Sens. Actuators, A* **2010**, *164*, 116.
[298] S. D. Thomalla, J. D. Van De Ven, *IEEE Trans. Rob.* **2018**, *34*, 1593.
[299] T. Ranzani, M. Cianchetti, G. Gerboni, I. De Falco, A. Menciassi, *IEEE Trans. Rob.* **2016**, *32*, 187.
[300] B. Tondu, *J. Intell. Mater. Syst. Struct.* **2012**, *23*, 225.
[301] B. Tondu, P. Lopez, *Control Syst.* **2000**, *20*, 15.
[302] J. Yi, X. Chen, C. Song, Z. Wang, *Soft Rob.* **2018**, *5*, 81.
[303] S. Ganguly, A. Garg, A. Pasricha, S. K. Dwivedy, *Mechatronics* **2012**, *22*, 1135.
[304] H. Aschemann, D. Schindele, *IEEE Trans. Ind. Electron.* **2008**, *55*, 3855.
[305] W. Liu, C. R. Rahn, *J. Appl. Mech.* **2003**, *70*, 853.
[306] A. Al-Ibadi, S. Nefti-Meziani, S. Davis, *Syst. Sci. Control Eng.* **2018**, *6*, 80.
[307] L. Ge, L. Dong, D. Wang, Q. Ge, G. Gu, *Sens. Actuators, A Phys.* **2018**, *273*, 285.
[308] W. Felt, K. Y. Chin, C. D. Remy, *IEEE/ASME Trans. Mechatronics* **2016**, *21*, 1201.
[309] D. Sangian, S. Naficy, G. M. Spinks, *J. Intell. Mater. Syst. Struct.* **2016**, *27*, 2508.

[310] D. Sangian, J. Foroughi, S. Farajikhah, S. Naficy, G. M. Spinks, *Smart Mater. Struct.* **2017**, *26*, 015011.
[311] R. Morita, H. Nabae, G. Endo, K. Suzumori, *Adv. Rob.* **2018**, *32*, 511.
[312] A. A. M. Faudzi, G. Endo, S. Kurumaya, K. Suzumori, *IEEE Rob. Autom. Lett.* **2018**, *3*, 100.
[313] Y. Yamamoto, H. Nishi, Y. Torii, A. Takanishi, H. O. Lim, *Int. Conf. Control. Autom. Syst.* **2016**, 1132.
[314] T. Abe, S. Koizumi, H. Nabae, G. Endo, K. Suzumori, N. Sato, M. Adachi, F. Takamizawa, *IEEE Rob. Autom. Lett.* **2019**, *4*, 2532.
[315] G. Singh, C. Xiao, E. T. Hsiao-Wecksler, G. Krishnan, *Bioinspiration Biomimetics* **2018**, *13*, 036010.
[316] A. Kojima, M. Okui, I. Hisamichi, T. Tsuji, T. Nakamura, *IEEE Rob. Autom. Lett.* **2019**, *4*, 2592.
[317] F. Ilievski, A. D. Mazzeo, R. F. Shepherd, X. Chen, G. M. Whitesides, *Angew. Chem., Int. Ed.* **2011**, *50*, 1890.
[318] C. D. Onal, X. Chen, G. M. Whitesides, D. Rus, in *Springer Tracts in Advanced Robotics*, Vol. *100*, (Eds: H. Christensen, O. Khatib), Springer International Publishing, Switzerland **2017**, pp. 525–540.
[319] R. F. Shepherd, F. Ilievski, W. Choi, S. A. Morin, A. A. Stokes, A. D. Mazzeo, X. Chen, M. Wang, G. M. Whitesides, *Proc. Natl. Acad. Sci. USA* **2011**, *108*, 20400.
[320] P. Polygerinos, S. Lyne, Z. Wang, L. F. Nicolini, B. Mosadegh, G. M. Whitesides, C. J. Walsh, in *IEEE Int. Conf. on Intelligent Robotos and Systems*, IEEE, Piscataway, NJ, USA **2013**, p. 1512.
[321] K. Elgeneidy, N. Lohse, M. Jackson, *Mechatronics* **2018**, *50*, 234.
[322] L. Belding, B. Baytekin, H. T. Baytekin, P. Rothemund, M. S. Verma, A. Nemiroski, D. Sameoto, B. A. Grzybowski, G. M. Whitesides, *Adv. Mater.* **2018**, *30*, 1704446.
[323] N. R. Sinatra, T. Ranzani, J. J. Vlassak, K. K. Parker, R. J. Wood, *J. Micromech. Microeng.* **2018**, *28*, 084002.
[324] E. Acome, S. K. Mitchell, T. G. Morrissey, M. B. Emmett, C. Benjamin, M. King, M. Radakovitz, C. Keplinger, *Science* **2018**, *359*, 61.
[325] Y. Shapiro, A. Wolf, K. Gabor, *Sens. Actuators, A* **2011**, *167*, 484.
[326] A. A. Calderon, J. C. Ugalde, J. C. Zagal, N. O. Perez-Arancibia, *2016 IEEE Int. Conf. Robotics and Biomimetics, ROBIO*, IEEE, Piscataway, NJ, USA **2016**, p. 31.
[327] J. Z. Ge, A. A. Calderón, L. Chang, N. O. Pérez-Arancibia, *Bioinspiration Biomimetics* **2019**, *14*, 036004.
[328] D. Yang, M. S. Verma, J. H. So, B. Mosadegh, C. Keplinger, B. Lee, F. Khashai, E. Lossner, Z. Suo, G. M. Whitesides, *Adv. Mater. Technol.* **2016**, *1*, 1600055.
[329] S. A. Morin, S. W. Kwok, J. Lessing, J. Ting, R. F. Shepherd, A. A. Stokes, G. M. Whitesides, *Adv. Funct. Mater.* **2014**, *24*, 5541.
[330] A. Nemiroski, Y. Y. Shevchenko, A. A. Stokes, B. Unal, A. Ainla, S. Albert, G. Compton, E. MacDonald, Y. Schwab, C. Zellhofer, G. M. Whitesides, *Soft Rob.* **2017**, *4*, 183.
[331] D. J. Preston, H. J. Jiang, V. Sanchez, P. Rothemund, J. Rawson, M. P. Nemitz, W.-K. Lee, Z. Suo, C. J. Walsh, G. M. Whitesides, *Sci. Rob.* **2019**, *4*, eaaw5496.
[332] E. W. Hawkes, L. H. Blumenschein, J. D. Greer, A. M. Okamura, *Sci. Rob.* **2017**, *2*, eaan3028.
[333] B. A. Baydere, S. K. Talas, E. Samur, *Sens. Actuators, A* **2018**, *281*, 84.
[334] H.-Y. Chen, R. S. Diteesawat, A. Haynes, A. J. Partridge, M. F. Simons, E. Werner, M. Garrad, J. Rossiter, A. T. Conn, *Front. Rob. AI* **2019**, *6*, 52.
[335] Z. Wang, S. Hirai, in *IEEE/SICE Int. Symp. System Integration*, IEEE, Piscataway, NJ, USA **2016**, p. 629.
[336] R. Maccurdy, R. Katzschmann, Y. Kim, D. Rus, *Proc. - IEEE Int. Conf. Robotics and Automation*, IEEE, Piscataway, NJ, USA **2016**, p. 3878.
[337] L. Ge, L. Dong, D. Wang, Q. Ge, G. Gu, *Sens. Actuators, A.* **2018**, *273*, 285.
[338] J. Yi, X. Chen, C. Song, J. Zhou, Y. Liu, S. Liu, Z. Wang, *IEEE Trans. Rob.* **2019**, *35*, 114.
[339] M. Schaffner, J. A. Faber, L. Pianegonda, P. A. Rühs, F. Coulter, A. R. Studart, *Nat. Commun.* **2018**, *9*, 878.
[340] S. Hayashi, C. Giordano, N. Ishikawa, *J. Ind. Text.* **1993**, *23*, 74.
[341] Y. Zhang, X. Y. Yin, M. Zheng, C. Moorlag, J. Yang, Z. L. Wang, *J. Mater. Chem. A* **2019**, *7*, 6972.
[342] L. Montero De Espinosa, W. Meesorn, D. Moatsou, C. Weder, *Chem. Rev.* **2017**, *117*, 12851.
[343] Y. Liu, H. Du, L. Liu, J. Leng, *Smart Mater. Struct.* **2014**, *23*, 023001.
[344] I. K. Kuder, A. F. Arrieta, W. E. Raither, P. Ermanni, *Prog. Aeronaut. Sci.* **2013**, *63*, 33.
[345] D. Campbell, M. S. Lake, M. R. Scherbarth, E. Nelson, R. W. Six, *Collect. Tech. Pap.- AIAA/ASME/ASCE/AHS/ASC Struct. Struct. Dyn. Mater. Conf.* **2005**, *10*, 6735.
[346] P. R. Buckley, G. H. McKinley, T. S. Wilson, W. Small IV, W. J. Benett, J. P. Bearinger, M. W. McElfresh, D. J. Maitland, *IEEE Trans. Biomed. Eng.* **2006**, *53*, 2075.
[347] W. Sokolowski, A. Metcalfe, S. Hayashi, L. Yahia, J. Raymond, *Biomed. Mater.* **2007**, *2*, S23.
[348] A. Lendlein, M. Behl, B. Hiebl, C. Wischke, *Expert Rev. Med. Devices* **2010**, *7*, 357.
[349] A. Cohades, V. Michaud, *Adv. Ind. Eng. Polym. Res.* **2018**, *1*, 66.
[350] W. Voit, T. Ware, R. R. Dasari, P. Smith, L. Danz, D. Simon, S. Barlow, S. R. Marder, K. Gall, *Adv. Funct. Mater.* **2010**, *20*, 162.
[351] W. M. Huang, B. Yang, Y. Q. Fu, *Polyurethane Shape Memory Polymers*, Taylor & Francis **2011**.
[352] H. Wu, P. Chen, C. Yan, C. Cai, Y. Shi, *Mater. Des.* **2019**, *171*, 107704.
[353] Y. Han, J. Hu, X. Chen, *Mater. Chem. Front.* **2019**, *3*, 1128.
[354] P. T. Knight, K. M. Lee, T. Chung, P. T. Mather, *Macromolecules* **2009**, *42*, 6596.
[355] L. Peponi, I. Navarro-Baena, J. M. Kenny, in *Smart Polymers and their Applications* (Eds: M. R. Aguilar, J. S. Román), Woodhead Publishing, **2014**, pp. 204–236.
[356] H. Ren, Z. Mei, S. Chen, H. Zhuo, S. Chen, H. Yang, J. Zuo, Z. Ge, *J. Mater. Sci.* **2016**, *51*, 9131.
[357] S. K. Lee, S. H. Yoon, I. Chung, A. Hartwig, B. K. Kim, *J. Polym. Sci., Part A: Polym. Chem.* **2011**, *49*, 634.
[358] C. Liu, H. Qin, P. T. Mather, *J. Mater. Chem.* **2007**, *17*, 1543.
[359] M. D. Hager, S. Bode, C. Weber, U. S. Schubert, *Prog. Polym. Sci.* **2015**, *49-50*, 3.
[360] F. L. Ji, Y. Zhu, J. L. Hu, Y. Liu, L. Y. Yeung, G. D. Ye, *Smart Mater. Struct.* **2006**, *15*, 1547.
[361] Y. Yu, T. Ikeda, *Macromol. Chem. Phys.* **2005**, *206*, 1705.
[362] S. Mukherjee, J. J. Cash, B. S. Sumerlin, in *Dynamic Covalent Chemistry: Principles, Reactions, and Applications* (Eds: W. Zhang, Y. Jin), Wiley **2017**, pp. 321–358.
[363] Q. Zhao, H. J. Qi, T. Xie, *Prog. Polym. Sci.* **2015**, *49–50*, 79.
[364] A. Lendlein, H. Jiang, O. Jünger, R. Langer, *Nature* **2005**, *434*, 879.
[365] K. M. Lee, D. H. Wang, H. Koerner, R. A. Vaia, L. S. Tan, T. J. White, *Angew. Chem., Int. Ed.* **2012**, *51*, 4117.
[366] K. M. Lee, H. Koerner, R. A. Vaia, T. J. Bunning, T. J. White, *Soft Matter* **2011**, *7*, 4318.
[367] S. K. Ahn, P. Deshmukh, R. M. Kasi, *Macromolecules* **2010**, *43*, 7330.
[368] S. K. Ahn, P. Deshmukh, M. Gopinadhan, C. O. Osuji, R. M. Kasi, *ACS Nano* **2011**, *5*, 3085.
[369] H. Meng, G. Li, *Polymer* **2013**, *54*, 2199.
[370] J. R. Kumpfer, S. J. Rowan, *J. Am. Chem. Soc.* **2011**, *133*, 12866.
[371] M. Burnworth, L. Tang, J. R. Kumpfer, A. J. Duncan, F. L. Beyer, G. L. Fiore, S. J. Rowan, C. Weder, *Nature* **2011**, *472*, 334.
[372] Q. Yang, W. Zheng, W. Zhao, C. Peng, J. Ren, Q. Yu, Y. Hu, X. Zhang, *Polym. Chem.* **2019**, *10*, 718.

[373] S. Chen, H. Yuan, S. Chen, H. Yang, Z. Ge, H. Zhuo, J. Liu, *J. Mater. Chem. A* **2014**, *2*, 10169.
[374] J. Ban, L. Mu, J. Yang, S. Chen, H. Zhuo, *J. Mater. Chem. A* **2017**, *5*, 14514.
[375] J. Zhou, H. Cao, R. Chang, G. Shan, Y. Bao, P. Pan, *ACS Macro Lett.* **2018**, *7*, 233.
[376] M. Bodaghi, A. R. Damanpack, W. H. Liao, *Smart Mater. Struct.* **2018**, *27*, 065010.
[377] Y. Bai, X. Zhang, Q. Wang, T. Wang, *J. Mater. Chem. A* **2014**, *2*, 4771.
[378] L. Wang, X. Yang, H. Chen, T. Gong, W. Li, G. Yang, S. Zhou, *ACS Appl. Mater. Interfaces* **2013**, *5*, 10520.
[379] Y. Luo, Y. Guo, X. Gao, B. G. Li, T. Xie, *Adv. Mater.* **2013**, *25*, 743.
[380] J. Li, T. Liu, S. Xia, Y. Pan, Z. Zheng, X. Ding, Y. Peng, *J. Mater. Chem.* **2011**, *21*, 12213.
[381] I. A. Rousseau, P. T. Mather, *JACS* **2003**, *125*, 15300.
[382] L. Lu, G. Li, *ACS Appl. Mater. Interfaces* **2016**, *8*, 14812.
[383] T. Chung, A. Romo-Uribe, P. T. Mather, *Macromolecules* **2008**, *41*, 184.
[384] K. Wang, X. X. Zhu, *ACS Biomater. Sci. Eng.* **2018**, *4*, 3099.
[385] L. Fang, T. Fang, X. Liu, Y. Ni, C. Lu, Z. Xu, *Compos. Sci. Technol.* **2017**, *152*, 190.
[386] E. T. Thostenson, T.-W. Chou, *J. Phys. D: Appl. Phys.* **2002**, *35*, L77.
[387] H. Hou, J. J. Ge, J. Zeng, Q. Li, D. H. Reneker, A. Greiner, S. Z. D. Cheng, *Chem. Mater.* **2005**, *17*, 967.
[388] J. Kwon, H. Kim, *J. Polym. Sci., Part A: Polym. Chem.* **2005**, *43*, 3973.
[389] J. Leng, H. Lu, Y. Liu, S. Du, *APL* **2007**, *6931*, 693109.
[390] H. Lv, J. Leng, S. Du, *Proc SPIE* **2008**, *6929*, 69291L.
[391] W. Chen, X. Tao, *Macromol. Rapid Commun.* **2005**, *26*, 1763.
[392] S. Mondal, *Mini-Rev. Org. Chem.* **2009**, *6*, 114.
[393] J. Leng, H. Lv, Y. Liu, S. Du, *Appl. Phys. Lett.* **2007**, *91*, 144105.
[394] J. S. Park, Y. C. Chung, S. Do Lee, J. W. Cho, B. C. Chun, *Fibers Polym.* **2008**, *9*, 661.
[395] S. Kyung Lee, S. H. Yoon, I. Chung, A. Hartwig, B. Kyu Kim, *J. Polym. Sci., Part A: Polym. Chem.* **2010**, *49*, 634.
[396] A. Kausar, *J. Plast. Film Sheeting* **2019**, https://doi.org/10.1177/8756087919865296.
[397] Y. Wang, T. Ma, W. Tian, J. Ye, X. Wang, X. Jiang, *Pigm. Resin Technol.* **2018**, *47*, 72.
[398] H. Zhou, H. Luo, Y. Yao, H. Wang, G. Yi, W. Lin, Y. Gu, *Mater. Lett.* **2019**, *252*, 76.
[399] C. Qian, Y. Zhu, Y. Dong, Y. Fu, *J. Intell. Mater. Syst. Struct.* **2017**, *28*, 2749.
[400] H. Lu, X. Wang, Y. Yao, J. Gou, D. Hui, B. Xu, Y. Q. Fu, *Composites, Part B* **2015**, *80*, 1.
[401] Z. Yang, X. Han, H. K. Lee, G. C. Phan-Quang, C. S. L. Koh, C. L. Lay, Y. H. Lee, Y. E. Miao, T. Liu, I. Y. Phang, X. Y. Ling, *Nanoscale* **2018**, *10*, 16005.
[402] M. K. Hassanzadeh-Aghdam, R. Ansari, *Composites, Part B* **2019**, *162*, 167.
[403] E. Wang, Y. Dong, M. Z. Islam, L. Yu, F. Liu, S. Chen, X. Qi, Y. Zhu, Y. Fu, Z. Xu, N. Hu, *Compos. Sci. Technol.* **2019**, *169*, 209.
[404] H. Yang, W. R. Leow, T. Wang, J. Wang, J. Yu, K. He, D. Qi, C. Wan, X. Chen, *Adv. Mater.* **2017**, *29*, 1701627.
[405] M. Zhang, K. R. Atkinson, R. H. Baughman, *Science* **2004**, *306*, 1358.
[406] W. Xu, D. H. Gracias, *ACS Nano* **2019**, *13*, 4883.
[407] G. Zhang, Q. Zhao, L. Yang, W. Zou, X. Xi, T. Xie, *ACS Macro Lett.* **2016**, *5*, 805.
[408] E. Havens, E. A. Snyder, T. H. Tong, *Smart Struct. Mater. 2005 Ind. Commer. Appl. Smart Struct. Technol.* **2005**, *5762*, 48.
[409] K. M. Lee, D. H. Wang, H. Koerner, R. A. Vaia, L. S. Tan, T. J. White, *Macromol. Chem. Phys.* **2013**, *214*, 1189.
[410] H. Zou, Y. Lu, W. Yuan, S. Wang, *Polym. Chem.* **2017**, *8*, 661.
[411] H. Y. Zhong, L. Chen, X. F. Liu, R. Yang, Y. Z. Wang, *J. Mater. Chem. C* **2017**, *5*, 9702.
[412] Z. Bin Wen, D. Liu, X. Y. Li, C. H. Zhu, R. F. Shao, R. Visvanathan, N. A. Clark, K. K. Yang, Y. Z. Wang, *ACS Appl. Mater. Interfaces* **2017**, *9*, 24947.
[413] T. Fang, L. Cao, S. Chen, J. Fang, J. Zhou, L. Fang, C. Lu, Z. Xu, *Mater. Des.* **2018**, *144*, 129.
[414] S. Chen, J. Ban, L. Mu, H. Zhuo, *Polym. Chem.* **2018**, *9*, 576.
[415] Y. J. Yu, K. Hearon, T. S. Wilson, D. J. Maitland, *Smart Mater. Struct.* **2011**, *20*, 085010.
[416] Y. Chae Jung, H. Hwa So, J. Whan Cho, *J. Macromol. Sci., Part B* **2006**, *45*, 453.
[417] X.-J. J. Han, Z.-Q. Q. Dong, M.-M. M. Fan, Y. Liu, J.-H. H. Li, Y.-F. F. Wang, Q.-J. J. Yuan, B.-J. J. Li, S. Zhang, *Macromol. Rapid Commun.* **2012**, *33*, 1055.
[418] M. Behl, K. Kratz, J. Zotzmann, U. Nöchel, A. Lendlein, *Adv. Mater.* **2013**, *25*, 4466.
[419] X. Ning, X. Wang, Y. Zhang, X. Yu, D. Choi, N. Zheng, D. S. Kim, Y. Huang, Y. Zhang, J. A. Rogers, *Adv. Mater. Interfaces* **2018**, *5*, 1800284.
[420] T. Chen, O. R. Bilal, R. Lang, C. Daraio, K. Shea, *Phys. Rev. Appl.* **2019**, *11*, 64069.
[421] J. E. M. Teoh, J. An, X. Feng, Y. Zhao, C. K. Chua, Y. Liu, *Materials* **2018**, *11*, 376.
[422] D. H. Wang, L. S. Tan, *ACS Macro Lett.* **2019**, *21*, 546.
[423] Y. Liu, W. Zhang, F. Zhang, X. Lan, J. Leng, S. Liu, X. Jia, C. Cotton, B. Sun, B. Gu, T.-W. Chou, *Composites, Part B* **2018**, *153*, 233.
[424] G. Li, S. Wang, Z. Liu, Z. Liu, H. Xia, C. Zhang, X. Lu, J. Jiang, Y. Zhao, *ACS Appl. Mater. Interfaces* **2018**, *10*, 40189.
[425] L. C. Wang, W. L. Song, D. Fang, *ACS Appl. Mater. Interfaces* **2019**, *11*, 3450.
[426] M. K. McBride, M. Podgorski, S. Chatani, B. T. Worrell, C. N. Bowman, *ACS Appl. Mater. Interfaces* **2018**, *10*, 22739.
[427] J. Cui, J. G. M. Adams, Y. Zhu, *Smart Mater. Struct.* **2018**, *27*, 055009.
[428] Q. Zhang, T. Rudolph, A. J. Benitez, O. E. C. Gould, M. Behl, K. Kratz, A. Lendlein, *Smart Mater. Struct.* **2019**, *28*, 055037.
[429] H. Birjandi Nejad, J. M. Robertson, P. T. Mather, *MRS Commun.* **2015**, *5*, 211.
[430] H. Wei, X. Cauchy, I. O. Navas, Y. Abderrafai, K. Chizari, U. Sundararaj, Y. Liu, J. Leng, D. Therriault, *ACS Appl. Mater. Interfaces* **2019**, *11*, 24523.
[431] M. Bodaghi, A. R. Damanpack, W. H. Liao, *Mater. Des.* **2017**, *135*, 26.
[432] M. Bodaghi, A. R. Damanpack, W. H. Liao, *Smart Mater. Struct.* **2016**, *25*, 105034.
[433] Y. Mao, Z. Ding, C. Yuan, S. Ai, M. Isakov, J. Wu, T. Wang, M. L. Dunn, H. J. Qi, *Sci. Rep.* **2016**, *6*, 24761.
[434] Q. Ge, A. H. Sakhaei, H. Lee, C. K. Dunn, N. X. Fang, M. L. Dunn, *Sci. Rep.* **2016**, *6*, 31110.
[435] R. Suriano, R. Bernasconi, L. Magagnin, M. Levi, *J. Electrochem. Soc.* **2019**, *166*, B3274.
[436] K. Chen, X. Kuang, V. Li, G. Kang, H. J. Qi, *Soft Matter* **2018**, *14*, 1879.
[437] H. Wei, Q. Zhang, Y. Yao, L. Liu, Y. Liu, J. Leng, *ACS Appl. Mater. Interfaces* **2017**, *9*, 876.
[438] J. Kopeček, *Biomaterials* **2007**, *28*, 5185.
[439] J. Kopeček, J. Yang, *Polym. Int.* **2007**, *56*, 1078.
[440] H. L. Lim, Y. Hwang, M. Kar, S. Varghese, *Biomater. Sci.* **2014**, *2*, 603.
[441] E. M. Ahmed, *J. Adv. Res.* **2015**, *6*, 105.
[442] A. S. Hoffman, *Adv. Drug Delivery Rev.* **2012**, *64*, 18.
[443] S. J. Buwalda, K. W. M. Boere, P. J. Dijkstra, J. Feijen, T. Vermonden, W. E. Hennink, *J. Controlled Release* **2014**, *190*, 254.
[444] O. Wichterle, D. Lím, *Nature* **1960**, *185*, 117.

[445] K. Otake, H. Inomata, M. Konno, S. Saito, *Macromolecules* **1990**, *23*, 283.
[446] S. J. Jeon, A. W. Hauser, R. C. Hayward, *Acc. Chem. Res.* **2017**, *50*, 161.
[447] X. Peng, H. Wang, *J. Polym. Sci., Part B: Polym. Phys.* **2018**, *56*, 1314.
[448] X. Le, W. Lu, J. Zhang, T. Chen, *Adv. Sci.* **2019**, *6*, 1801584.
[449] J. Shang, X. Le, J. Zhang, T. Chen, P. Theato, *Polym. Chem.* **2019**, *10*, 1036.
[450] O. Erol, A. Pantula, W. Liu, D. H. Gracias, *Adv. Mater. Technol.* **2019**, *4*, 1900043.
[451] P. Calvert, *Adv. Mater.* **2009**, *21*, 743.
[452] L. Ionov, *Adv. Funct. Mater.* **2013**, *23*, 4555.
[453] A. Kumar, A. Srivastava, I. Y. Galaev, B. Mattiasson, *Prog. Polym. Sci.* **2007**, *32*, 1205.
[454] M. Heskins, J. E. Guillet, *J. Macromol. Sci.: Part A: Chem.* **1968**, *2*, 1441.
[455] S. K. Ahn, R. M. Kasi, S. C. Kim, N. Sharma, Y. Zhou, *Soft Matter* **2008**, *4*, 1151.
[456] I. Tokarev, S. Minko, *Soft Matter* **2009**, *5*, 511.
[457] H. L. Lim, J. C. Chuang, T. Tran, A. Aung, G. Arya, S. Varghese, *Adv. Funct. Mater.* **2011**, *21*, 55.
[458] D. Morales, E. Palleau, M. D. Dickey, O. D. Velev, *Soft Matter* **2014**, *10*, 1337.
[459] Y. Klein, E. Efrati, E. Sharon, *Science* **2007**, *315*, 1116.
[460] E. Sharon, E. Efrati, *Soft Matter* **2010**, *6*, 5693.
[461] J. Kim, J. A. Hanna, M. Byun, C. D. Santangelo, R. C. Hayward, *Science* **2012**, *335*, 1201.
[462] S. So, R. C. Hayward, *ACS Appl. Mater. Interfaces* **2017**, *9*, 15785.
[463] A. Nojoomi, H. Arslan, K. Lee, K. Yum, *Nat. Commun.* **2018**, *9*, 3705.
[464] L. Huang, R. Jiang, J. Wu, J. Song, H. Bai, B. Li, Q. Zhao, T. Xie, *Adv. Mater.* **2017**, *29*, 1605390.
[465] R. Luo, J. Wu, N. D. Dinh, C. H. Chen, *Adv. Funct. Mater.* **2015**, *25*, 7272.
[466] H. Kim, J. H. Kang, Y. Zhou, A. S. Kuenstler, Y. Kim, C. Chen, T. Emrick, R. C. Hayward, *Adv. Mater.* **2019**, *31*, 1900932.
[467] C. Yang, W. Wang, C. Yao, R. Xie, X. J. Ju, Z. Liu, L. Y. Chu, *Sci. Rep.* **2015**, *5*, 13622.
[468] D. Han, C. Farino, C. Yang, T. Scott, D. Browe, W. Choi, J. W. Freeman, H. Lee, *ACS Appl. Mater. Interfaces* **2018**, *10*, 17512.
[469] J. Zheng, P. Xiao, X. Le, W. Lu, P. Théato, C. Ma, B. Du, J. Zhang, Y. Huang, T. Chen, *J. Mater. Chem. C* **2018**, *6*, 1320.
[470] K. Kobayashi, S. H. Oh, C. K. Yoon, D. H. Gracias, *Macromol. Rapid Commun.* **2018**, *39*, 1700692.
[471] C. Ma, W. Lu, X. Yang, J. He, X. Le, L. Wang, J. Zhang, M. J. Serpe, Y. Huang, T. Chen, *Adv. Funct. Mater.* **2018**, *28*, 1704568.
[472] C. Ma, T. Li, Q. Zhao, X. Yang, J. Wu, Y. Luo, T. Xie, *Adv. Mater.* **2014**, *26*, 5665.
[473] C. Yao, Z. Liu, C. Yang, W. Wang, X. J. Ju, R. Xie, L. Y. Chu, *ACS Appl. Mater. Interfaces* **2016**, *8*, 21721.
[474] Z. L. Wu, M. Moshe, J. Greener, H. Therien-Aubin, Z. Nie, E. Sharon, E. Kumacheva, *Nat. Commun.* **2013**, *4*, 1586.
[475] H. Thérien-Aubin, M. Moshe, E. Sharon, E. Kumacheva, *Soft Matter* **2015**, *11*, 4600.
[476] Z. J. Wang, C. N. Zhu, W. Hong, Z. L. Wu, Q. Zheng, *J. Mater. Chem. B* **2016**, *4*, 7075.
[477] J. Wang, J. Wang, Z. Chen, S. Fang, Y. Zhu, R. H. Baughman, L. Jiang, *Chem. Mater.* **2017**, *29*, 9793.
[478] Z. J. Wang, W. Hong, Z. L. Wu, Q. Zheng, *Angew. Chem., Int. Ed.* **2017**, *56*, 15974.
[479] Z. Zhao, X. Kuang, C. Yuan, H. J. Qi, D. Fang, *ACS Appl. Mater. Interfaces* **2018**, *10*, 19932.
[480] A. Sydney Gladman, E. A. Matsumoto, R. G. Nuzzo, L. Mahadevan, J. A. Lewis, *Nat. Mater.* **2016**, *15*, 413.
[481] S. Naficy, R. Gately, R. Gorkin III, H. Xin, G. M. Spinks, *Macromol. Mater. Eng.* **2017**, *302*, 1600212.
[482] H. Arslan, A. Nojoomi, J. Jeon, K. Yum, *Adv. Sci.* **2019**, *6*, 1800703.
[483] T. H. Ware, M. E. McConney, J. J. Wie, V. P. Tondiglia, T. J. White, *Science* **2015**, *347*, 982.
[484] T. J. White, D. J. Broer, *Nat. Mater.* **2015**, *14*, 1087.
[485] L. T. De Haan, C. Sánchez-Somolinos, C. M. W. Bastiaansen, A. P. H. J. Schenning, D. J. Broer, *Angew. Chem., Int. Ed.* **2012**, *51*, 12469.
[486] M. E. McConney, A. Martinez, V. P. Tondiglia, K. M. Lee, D. Langley, I. I. Smalyukh, T. J. White, *Adv. Mater.* **2013**, *25*, 5880.
[487] D. Liu, D. J. Broer, *Angew. Chem., Int. Ed.* **2014**, *53*, 4542.
[488] T. Guin, M. J. Settle, B. A. Kowalski, A. D. Auguste, R. V Beblo, G. W. Reich, T. J. White, *Nat. Commun.* **2018**, *9*, 2531.
[489] D. Vorlander, *Z. Phys. Chem.* **1923**, *105*, 211.
[490] W. J. Jackson, H. F. Kuhfuss, *J. Polym. Sci., Part A: Polym. Chem.* **1996**, *34*, 3031.
[491] H. Finkelmann, H.-J. Kock, G. Rehage, *Makromol. Chem., Rapid Commun.* **1981**, *2*, 317.
[492] M. Portugall, H. Ringsdorf, R. Zentel, *Makromol. Chem.* **1982**, *183*, 2311.
[493] H. Ringsdorf, R. Zentel, *Makromol. Chem.* **1982**, *183*, 1245.
[494] J. Küpfer, H. Finkelmann, *Makromol. Chem., Rapid Commun.* **1991**, *12*, 717.
[495] D. J. Broer, H. Finkelmann, K. Kondo, *Makromol. Chem.* **1988**, *189*, 185.
[496] D. J. Broer, G. N. Mol, G. Challa, *Makromol. Chem.* **1989**, *190*, 19.
[497] D. J. Broer, J. Boven, G. N. Mol, G. Challa, *Makromol. Chem.* **1989**, *190*, 2255.
[498] D. Broer, R. Hikmet, G. Challa, *Makromol. Chem.* **1989**, *190*, 3201.
[499] H. Wermter, H. Finkelmann, *e-Polym.* **2001**, *1*, 21974586.
[500] G. H. E. Bergmann, H. Finkelmann, V. Percec, M. Zhao, *Macromol. Rapid Commun.* **1997**, *18*, 353.
[501] B. Donnio, H. Wermter, H. Finkelmann, *Macromolecules* **2000**, *33*, 7724.
[502] C. M. Yakacki, M. Saed, D. P. Nair, T. Gong, S. M. Reed, C. N. Bowman, *RSC Adv.* **2015**, *5*, 18997.
[503] M. O. Saed, A. H. Torbati, C. A. Starr, R. Visvanathan, N. A. Clark, C. M. Yakacki, *J. Polym. Sci., Part B: Polym. Phys.* **2017**, *55*, 157.
[504] Y. Jin, C. Yu, R. J. Denman, W. Zhang, *Chem. Soc. Rev.* **2013**, *42*, 6634.
[505] Z. Pei, Y. Yang, Q. Chen, E. M. Terentjev, Y. Wei, Y. Ji, *Nat. Mater.* **2014**, *13*, 36.
[506] D. W. Hanzon, N. A. Traugutt, M. K. McBride, C. N. Bowman, C. M. Yakacki, K. Yu, *Soft Matter* **2018**, *14*, 951.
[507] G. Feio, J. L. Figueirinhas, A. R. Tajbakhsh, E. M. Terentjev, *Phys. Rev. B* **2008**, *78*, 020201.
[508] Z. Pei, Y. Yang, Q. Chen, Y. Wei, Y. Ji, *Adv. Mater.* **2016**, *28*, 156.
[509] Y. Li, Y. Zhang, O. Rios, J. K. Keum, M. R. Kessler, *RSC Adv.* **2017**, *7*, 37248.
[510] M. K. McBride, M. Hendrikx, D. Liu, B. T. Worrell, D. J. Broer, C. N. Bowman, *Adv. Mater.* **2017**, *29*, 1606509.
[511] L. T. De Haan, A. P. H. J. Schenning, D. J. Broer, *Polymer* **2014**, *55*, 5885.
[512] Y. Xia, A. Honglawan, S. Yang, *Liq. Cryst. Rev.* **2019**, *7*, 30.
[513] B. A. Kowalski, T. C. Guin, A. D. Auguste, N. P. Godman, T. J. White, *ACS Macro Lett.* **2017**, *6*, 436.
[514] D. W. Berreman, *Phys. Rev. Lett.* **1972**, *28*, 1683.
[515] A. J. Pidduck, S. D. Haslam, G. P. Bryan-Brown, R. Bannister, I. D. Kitely, *Appl. Phys. Lett.* **1997**, *71*, 2907.
[516] L. T. Creagh, A. R. Kmetz, *Mol. Cryst. Liq. Cryst.* **1973**, *24*, 59.
[517] A. D. Auguste, J. W. Ward, J. O. Hardin, B. A. Kowalski, T. C. Guin, J. D. Berrigan, T. J. White, *Adv. Mater.* **2018**, *30*, 1802438.
[518] O. Yaroshchuk, Y. Reznikov, *J. Mater. Chem.* **2012**, *22*, 286.

[519] T. Seki, S. Nagano, M. Hara, *Polymer* **2013**, *54*, 6053.
[520] C. Ohm, M. Brehmer, R. Zentel, *Adv. Mater.* **2010**, *22*, 3366.
[521] D. J. Broer, G. N. Mol, *Polym. Eng. Sci.* **1991**, *31*, 625.
[522] G. N. Mol, K. D. Harris, C. W. M. Bastiaansen, D. J. Broer, *Adv. Funct. Mater.* **2005**, *15*, 1155.
[523] K. D. Harris, C. W. M. Bastiaansen, J. Lub, D. J. Broer, *Nano Lett.* **2005**, *5*, 1857.
[524] L. Dong, Y. Zhao, *Mater. Chem. Front.* **2018**, *2*, 1932.
[525] G. S. Kumar, D. C. Neckers, *Chem. Rev.* **1989**, *89*, 1915.
[526] H. Finkelmann, E. Nishikawa, G. G. Pereira, M. Warner, *Phys. Rev. Lett.* **2001**, *87*, 015501.
[527] J. Cviklinski, A. R. Tajbakhsh, E. M. Terentjev, *Eur. Phys. J. E* **2002**, *9*, 427.
[528] Y. Yu, M. Nakano, T. Ikeda, *Nature* **2003**, *425*, 145.
[529] N. Tabiryan, S. Serak, X.-M. Dai, T. J. Bunning, *Opt. Express* **2005**, *17*, 40.
[530] T. J. White, S. V. Serak, N. V. Tabiryan, R. A. Vaia, T. J. Bunning, *J. Mater. Chem.* **2009**, *19*, 1080.
[531] H. M. van der Kooij, S. A. Semerdzhiev, J. Buijs, D. J. Broer, D. Liu, J. Sprakel, *Nat. Commun.* **2019**, *10*, 3501.
[532] K. D. Harris, R. Cuypers, P. Scheibe, C. L. Van Oosten, C. W. M. Bastiaansen, J. Lub, D. J. Broer, *J. Mater. Chem.* **2005**, *15*, 5043.
[533] J. J. Wie, K. M. Lee, M. L. Smith, R. A. Vaia, T. J. White, *Soft Matter* **2013**, *9*, 9303.
[534] S. Iamsaard, S. J. Aßhoff, B. Matt, T. Kudernac, J. J. L. M. Cornelissen, S. P. Fletcher, N. Katsonis, *Nat. Chem.* **2014**, *6*, 229.
[535] T. Ube, T. Ikeda, *Adv. Opt. Mater.* **2019**, *7*, 1900380.
[536] Y. Shang, J. Wang, T. Ikeda, L. Jiang, *J. Mater. Chem. C* **2019**, *7*, 3413.
[537] M. Yamada, M. Kondo, R. Miyasato, Y. Naka, J. I. Mamiya, M. Kinoshita, A. Shishido, Y. Yu, C. J. Barrett, T. Ikeda, *J. Mater. Chem.* **2009**, *19*, 60.
[538] H. K. Bisoyi, Q. Li, *Chem. Rev.* **2016**, *116*, 15089.
[539] C. M. Spillmann, B. R. Ratna, J. Naciri, *Appl. Phys. Lett.* **2007**, *90*, 021911.
[540] P. Papadopoulos, P. Heinze, H. Finkelmann, F. Kremer, *Macromolecules* **2010**, *43*, 6666.
[541] T. Okamoto, K. Urayama, T. Takigawa, *Soft Matter* **2011**, *7*, 10585.
[542] Y. Yusuf, J. H. Huh, P. E. Cladis, H. R. Brand, H. Finkelmann, S. Kai, *Phys. Rev. E* **2005**, *71*, 061702.
[543] K. Urayama, H. Kondo, Y. O. Arai, T. Takigawa, *Phys. Rev. E* **2005**, *71*, 051713.
[544] S. Hashimoto, Y. Yusuf, S. Krause, H. Finkelmann, P. E. Cladis, H. R. Brand, S. Kai, *Appl. Phys. Lett.* **2008**, *92*, 181902.
[545] S. Courty, J. Mine, A. R. Tajbakhsh, E. M. Terentjev, *Europhys. Lett.* **2003**, *64*, 654.
[546] T. Guin, B. A. Kowalski, R. Rao, A. D. Auguste, C. A. Grabowski, P. F. Lloyd, V. P. Tondiglia, B. Maruyama, R. A. Vaia, T. J. White, *ACS Appl. Mater. Interfaces* **2018**, *10*, 1187.
[547] Z. S. Davidson, H. Shahsavan, A. Aghakhani, Y. Guo, L. Hines, Y. Xia, S. Yang, M. Sitti, *Sci. Adv.* **2019**, *5*, eaay0855.
[548] C. Feng, C. P. H. Rajapaksha, J. M. Cedillo, C. Piedrahita, J. Cao, V. Kaphle, B. Lüssem, T. Kyu, A. Jákli, *Macromol. Rapid Commun.* **2019**, *40*, 1900299.
[549] H. Finkelmann, A. Greve, M. Warner, *Eur. Phys. J. E* **2001**, *5*, 281.
[550] B. R. Donovan, V. M. Matavulj, S. K. Ahn, T. Guin, T. J. White, *Adv. Mater.* **2019**, *31*, 1805750.
[551] M. Camacho-Lopez, H. Finkelmann, P. Palffy-Muhoray, M. Shelley, *Nat. Mater.* **2004**, *3*, 307.
[552] O. M. Wani, H. Zeng, A. Priimagi, *Nat. Commun.* **2017**, *8*, 15546.
[553] C. L. Van Oosten, C. W. M. M. Bastiaansen, D. J. Broer, *Nat. Mater.* **2009**, *8*, 677.
[554] D. K. Kim, M. Hwang, J. P. F. Lagerwall, *J. Polym. Sci., Part B: Polym. Phys.* **2013**, *51*, 855.
[555] R. Stannarius, A. Eremin, K. Harth, M. Morys, A. Demiglio, C. Ohm, R. Zentel, *Soft Matter* **2012**, *8*, 1858.
[556] J. Naciri, A. Srinivasan, H. Jeon, N. Nikolov, P. Keller, B. R. Ratna, *Macromolecules* **2003**, *36*, 8499.
[557] A. H. Gelebart, M. Mc Bride, A. P. H. J. Schenning, C. N. Bowman, D. J. Broer, *Adv. Funct. Mater.* **2016**, *26*, 5322.
[558] S. Nocentini, D. Martella, D. S. Wiersma, C. Parmeggiani, *Soft Matter* **2017**, *13*, 8590.
[559] A. Sharma, J. P. F. Lagerwall, *Materials* **2018**, *11*, 393.
[560] D. J. Roach, C. Yuan, X. Kuang, V. C. F. Li, P. Blake, M. L. Romero, I. Hammel, K. Yu, H. J. Qi, *ACS Appl. Mater. Interfaces* **2019**, *11*, 19514.
[561] A. S. Kuenstler, H. Kim, R. C. Hayward, *Adv. Mater.* **2019**, *31*, 1901216.
[562] Z. Wang, K. Li, Q. He, S. Cai, *Adv. Mater.* **2019**, *31*, 1806849.
[563] C. Ahn, X. Liang, S. Cai, *Adv. Mater. Technol.* **2019**, *4*, 1900185.
[564] Y. Yang, Z. Pei, Z. Li, Y. Wei, Y. Ji, *J. Am. Chem. Soc.* **2016**, *138*, 2118.
[565] M. K. McBride, A. M. Martinez, L. Cox, M. Alim, K. Childress, M. Beiswinger, M. Podgorski, B. T. Worrell, J. Killgore, C. N. Bowman, *Sci. Adv.* **2018**, *4*, eaat4634.
[566] M. Lahikainen, H. Zeng, A. Priimagi, *Nat. Commun.* **2018**, *9*, 4148.
[567] K. M. Lee, M. L. Smith, H. Koerner, N. Tabiryan, R. A. Vaia, T. J. Bunning, T. J. White, *Adv. Funct. Mater.* **2011**, *21*, 2913.
[568] T. J. White, N. V. Tabiryan, S. V. Serak, U. A. Hrozhyk, V. P. Tondiglia, H. Koerner, R. A. Vaia, T. J. Bunning, *Soft Matter* **2008**, *4*, 1796.
[569] A. H. Gelebart, D. Jan Mulder, M. Varga, A. Konya, G. Vantomme, E. W. Meijer, R. L. B. Selinger, D. J. Broer, *Nature* **2017**, *546*, 632.
[570] M. Pilz da Cunha, Y. Foelen, R. J. H. van Raak, J. N. Murphy, T. A. P. Engels, M. G. Debije, A. P. H. J. Schenning, *Adv. Opt. Mater.* **2019**, *7*, 1801643.
[571] H. Zeng, O. M. Wani, P. Wasylczyk, A. Priimagi, *Macromol. Rapid Commun.* **2018**, *39*, 1700224.
[572] F. Ge, R. Yang, X. Tong, F. Camerel, Y. Zhao, *Angew. Chem., Int. Ed.* **2018**, *57*, 11758.
[573] X. Lu, H. Zhang, G. Fei, B. Yu, X. Tong, H. Xia, Y. Zhao, *Adv. Mater.* **2018**, *30*, 1706597.
[574] C. Wang, K. Sim, J. Chen, H. Kim, Z. Rao, Y. Li, W. Chen, J. Song, R. Verduzco, C. Yu, *Adv. Mater.* **2018**, *30*, 1706695.
[575] Y. Guo, M. Jiang, C. Peng, K. Sun, O. Yaroshchuk, O. D. Lavrentovich, Q. H. Wei, *Crystals* **2017**, *7*, 8.
[576] Y. Sawa, F. Ye, K. Urayama, T. Takigawa, V. Gimenez-Pinto, R. L. B. Selinger, J. V. Selinger, *Proc. Natl. Acad. Sci. USA* **2011**, *108*, 6364.
[577] G. Wei, C. Zhao, J. Hollingsworth, Z. Zhou, F. Jin, Z. Zhang, H. Cheng, C. C. Han, *Soft Matter* **2013**, *9*, 9924.
[578] K. Fuchi, T. H. Ware, P. R. Buskohl, G. W. Reich, R. A. Vaia, J. White, J. J. Joo, *Soft Matter* **2015**, *11*, 7288.
[579] C. D. Modes, K. Bhattacharya, M. Warner, *Proc. R. Soc. A* **2011**, *467*, 1121.
[580] C. D. Modes, K. Bhattacharya, M. Warner, *Phys. Rev. E* **2010**, *81*, 060701.
[581] S. K. Ahn, T. H. Ware, K. M. Lee, V. P. Tondiglia, T. J. White, *Adv. Funct. Mater.* **2016**, *26*, 5819.
[582] Y.-Y. Xiao, Z.-C. Jiang, X. Tong, Y. Zhao, *Adv. Mater.* **2019**, *31*, 1903452.
[583] D. Martella, H. Zeng, P. Wasylczyk, M. Burresi, C. Parmeggiani, D. S. Wiersma, D. Martella, M. Burresi, D. S. Wiersma, *Adv. Mater.* **2015**, *27*, 3883.
[584] J. M. McCracken, V. P. Tondiglia, A. D. Auguste, N. P. Godman, B. R. Donovan, B. N. Bagnall, H. E. Fowler, C. M. Baxter, V. Matavulj, J. D. Berrigan, T. J. White, *Adv. Funct. Mater.* **2019**, *29*, 1970274.
[585] A. Kotikian, R. L. Truby, J. W. Boley, T. J. White, J. A. Lewis, *Adv. Mater.* **2018**, *30*, 1706164.

[586] C. P. Ambulo, J. J. Burroughs, J. M. Boothby, H. Kim, M. R. Shankar, T. H. Ware, *ACS Appl. Mater. Interfaces* **2017**, *9*, 37332.
[587] C. D. Modes, K. Bhattacharya, M. Warner, *Phys. Rev. E - Stat. Nonlinear, Soft Matter Phys.* **2010**, 81.
[588] M. López-Valdeolivas, D. Liu, D. J. Broer, C. Sánchez-Somolinos, *Macromol. Rapid Commun.* **2018**, *39*, 1700710.
[589] A. Kotikian, C. McMahan, E. C. Davidson, J. M. Muhammad, R. D. Weeks, C. Daraio, J. A. Lewis, *Sci. Rob.* **2019**, *4*, eaax7044.
[590] D. J. Roach, X. Kuang, C. Yuan, K. Chen, H. J. Qi, *Smart Mater. Struct.* **2018**, *27*, 125011.
[591] M. O. Saed, C. P. Ambulo, H. Kim, R. De, V. Raval, K. Searles, D. A. Siddiqui, J. M. O. Cue, M. C. Stefan, M. R. Shankar, T. H. Ware, *Adv. Funct. Mater.* **2019**, *29*, 1806412.
[592] M. Tabrizi, T. H. Ware, M. R. Shankar, *ACS Appl. Mater. Interfaces* **2019**, *11*, 28236.
[593] F. Ali, W. Raza, X. Li, H. Gul, K.-H. Kim, *Nano Energy* **2019**, *57*, 879.
[594] N. Choudhary, D. Kaur, *Sens. Actuators, A* **2016**, *242*, 162.
[595] McEvoy, M. Andrew, N. Correll, *Science* **2015**, *347*, 1261689.